Mid-range frequency low-temperature pulse-tube refrigerator

Klaasse Bos, C.G.

Award date:
2006

Eindhoven University of Technology
Department of Applied Physics
Low-temperature Physics

Mid-range frequency low-temperature pulse-tube refrigerator

Cor Klaasse Bos

February 2006, Eindhoven

Prof.dr. A.T.A.M. de Waele
Dr.ir. I. A. Tanaeva

Project funded by STW

Table of contents

List of symbols

	Symbols
a	Grain size (m)
A	Surface area (m^2)
c	Specific heat capacity ($J\ K^{-1}\ kg^{-1}$) Mechanical damping coefficient ($N\ s\ m^{-1}$)
C	Flow conductance ($m^3\ s^{-1}\ Pa^{-1}$) Volumetric heat capacity ($J\ m^{-3}\ K^{-1}$)
C_v	Molar heat capacity at constant volume ($J\ K^{-1}\ mol^{-1}$)
C_p	Molar heat capacity at constant pressure ($J\ K^{-1}\ mol^{-1}$)
d	Diameter (m)
f	Frequency (s^{-1}) Factor
F	Force (N) Temperature time dependency prefactor (K m)
g	Geometrical factor
j	Molar flow rate density ($mol\ s^{-1}\ m^{-2}$)
k	Spring constant ($N\ m^{-1}$)
L,l	Length (m)
m	Mass (kg)
n	Amount of gas (mol), mesh density (m^{-1})
p	Pressure ($N\ m^{-2}$)
r	Radius (m)
P	Power ($J\ s^{-1}$)
$\dot{Q}$	Heat flow ($J\ s^{-1}$)
R	Molar ideal gas constant ($J\ K^{-1}\ mol^{-1}$)
R_x	Ratio of quantity x
S	Entropy ($J\ K^{-1}$)
t	Time (s)
T	Temperature (K)
U	Internal energy (J)
v	Velocity ($m\ s^{-1}$)
V	Volume (m^3)
x	Position (m)
z	Flow impedance factor (m^{-2})
Z	Flow impedance (m^{-3})
α	Pulse-tube velocity ratio Volumetric thermal expansion coefficient (K^{-1})
β	Volumetric heat exchange parameter ($J\ s^{-1}\ K^{-1}\ m^{-3}$)
γ	Poisson constant equal to C_p/C_v
δ	Depth, size, diameter (m)
Δ	Difference
η	Viscosity ($J\ s\ m^{-3}$)
κ	Thermal conductivity ($J\ s^{-1}\ m^{-1}\ K^{-1}$)
ρ	Density ($kg\ m^{-3}$)
χ	Heat capacity ratio correction factor
ω	Angular frequency (s^{-1})

	Subscripts
0	Time-averaged
1	Amplitude, first orifice, stage 1
2	Double inlet, stage 2
3	Stage 3
b	Buffer
c	Compressor, compression, conduction, cycle
C	Heat capacity, Carnot
CD	Conduction degradation (factor)
e	Exchange (of heat)
f	Filling (factor)
g	Gas
H	High, hot end
He	Helium
i	Irreversible, inlet
L	Low, cold end
m	Molar, motor
n	Normal
p	Pressure, piston
r	Regenerator, resonance
s	Spring
t	Tube
te	Effective tube (volume)
T	Thermal
v,V	Volume, volumetric
x	Cosine time dependency prefactor
y	Sine time dependency prefactor
z	Flow impedance
β	Volumetric heat exchange parameter

	Superscripts
V	Volumetric

	Abbreviations
COP	Coefficient of performance
PTR	Pulse-tube refrigerator
GM	Gifford-McMahon
DC	Direct current
J-T	Joule-Thomson

1 Introduction

State of the art research and technology are relying increasingly on special physical characteristics of materials at low temperatures. Therefore, it is not surprising that the application area of low temperature physics has expanded rapidly in the past decade. Cryogenics deals with the production of low temperatures, typically below 120 K. In this chapter some examples of cryogenic applications are discussed. A short overview of common four-kelvin cryocoolers is presented. The benefits of a pulse-tube refrigerator (PTR) are explained briefly, as well as why the PTR is likely to become the new 'working horse' of four-kelvin temperature-range cryogenics. Finally, a general description of the content of this Master's thesis is given.

The field of application of cryogenics is very broad. Nowadays, various types of detectors used for medical, military, environmental, and scientific purposes exploit the reduction of thermal noise in electronics at low temperatures in order to obtain more sensitive equipment. The liquefaction, transport and storage of gases, cryosurgery, agriculture, and biology are other examples of fields in which low temperatures are used extensively. Furthermore, low temperatures can be used to condense gases in order obtain ultra high vacuum (the so-called cryopumping). Moreover, interesting physical phenomena such as superconductivity, superfluidity, and Bose-Einstein condensation only occur at very low temperatures. Superconducting magnets have extended the application area of cryocooling with, for example, the introduction of Magnetic Resonance Imaging (MRI) and SQUID detectors in hospitals. Many of the applications mentioned above operate in the four-kelvin temperature region. It is important that cryocoolers are low cost and efficient with a high reliability and a long lifetime. Furthermore, in many applications with sensitive equipment, mechanical or magnetic interference should be avoided.

A brief introduction to cryocoolers, commonly used in the four-kelvin temperature region, is given below. In many cases helium is the working fluid[1]. Additional introductorily information about cryocoolers can be found in ref. [1] and [2].

The Joule-Thomson (J-T) expansion coolers are simple, fast, and potentially small coolers without moving parts. The cooling object is cooled by expansion of gas flowing from high- to low pressure through a flow resistance. In an open-cycle mode the cooler can run only for a short time, depending on the amount of the compressed gas available. Continuous closed-cycle operation of the cooler requires a compressor. The purity of the compressed gas is of great importance to avoid plugging of the expansion orifice. J-T coolers are often found in combination with a Gifford-McMahon (GM) or Stirling-type precooling stage in order to reach 4 K. Stirling cryocoolers are widely used, efficient, and potentially small. In the fundamental cooling cycle, the working gas is compressed, displaced, and expanded in an expansion space by two pistons moving with a phase-difference. One piston is located at the hot end of the expansion space, and one piston is located at the cold end. By rejecting the heat, generated during compression, to the

[1] Strictly speaking, helium in many cryocoolers is in its fluid phase. However, it is often called a 'gas'.

surroundings, the expansion leads to a net cooling effect. The main disadvantage of the Stirling cryocooler is the moving piston in the cold part of the refrigerator. The cold-end piston increases wear and, therefore, shortens the cryocooler's lifetime. The moving piston at the cold end also causes additional thermal losses and induces vibrations and magnetic interference at the cold end. The Gifford-McMahon cryocooler is a highly reliable cooler, due to the low operating frequencies and the small pressure drop over the displacer [1]. Its cooling principle is comparable to the cooling principle of the Stirling cryocooler. As with the Stirling-type cooler, the displacer at the cold end induces mechanic and magnetic interference. The efficiency of the GM-type compressor is low compared to the Stirling compressor. Furthermore, the GM-type compressor needs lubrication (oil). The oil residue has to be removed from the gas before it can be used in the actual cryocooler. In case of a pulse-tube refrigerator (PTR) the moving displacer at the cold end of the Stirling cryocooler is removed. The hot end of the tube is connected to a buffer by an orifice (see Figure 1-1). The absence of moving parts at the cold-end significantly reduces vibrations, avoids losses due to heat conduction in the displacer, and increases the lifetime of the cryocooler. As is the case with a Stirling cryocooler, the cooling mechanism relies on the compression, displacement, and expansion of the gas in the tube. The details of the cooling mechanism as well as the components of a PTR are discussed in chapter 2. In 1984 the orifice PTR was invented by Mikulin *et al.* [3]. R. Radebaugh was able to decrease the cold-end temperature of 60 K for a single-stage PTR [4]. For several years, the Low Temperature Group of the Eindhoven University of Technology set the record for the lowest PTR temperature at 1.78 K, using a three-stage ^{3}He PTR [5]. In 2003 this record was broken by the group of G. Thummes from the Giessen University, who obtained a cold-end temperature of 1.27 K using a hybrid ^{3}He/^{4}He PTR [6]. During the last decades, the efficiency of PTRs is improved significantly. PTRs are now amongst the most efficient cryocoolers available.

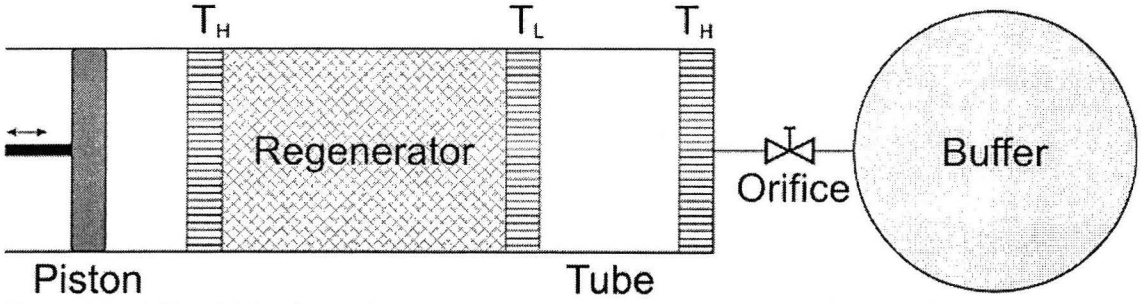

Figure 1-1. Orifice PTR with a piston compressor to generate pressure oscillations. The regenerator pre-cools the gas before it reaches the cold-end heat exchanger at temperature T_L. This is where an object can be cooled. The actual expansion and compression take place in the (pulse) tube. The components marked with T_H are the hot-end heat exchangers, where heat is rejected to the surroundings. The orifice and buffer induce a gas flow at the hot-end of the tube.

The pressure oscillations in a PTR can be generated using a piston (Stirling-type compressor), or by a GM-type compressor in combination with a rotary valve. Both methods are shown in Figure 1-2. The rotary valve alternately connects the PTR to the high- and the low-pressure sides of the compressor. Generally, GM-type PTRs are operated at low frequencies, typically 1 – 2 Hz. The operating frequency of Stirling-type PTRs is typically 50 – 60 Hz. Currently, temperatures below 4 K can mainly be obtained

using low-frequency GM-type PTRs. Unfortunately, the efficiency of the GM-type compressor in combination with the rotary valve is low; typically 25 %. Furthermore, the compressor is susceptible to wear, and needs oil for lubrication. This oil needs to be removed from the helium before it enters the PTR. The efficiency of a Stirling-type compressor is in the order of 80 %. Current Stirling-type compressors do not need lubrication and are highly reliable due to the application of, for example, so-called flexure bearings [7]. Therefore, it can be very beneficial to generate the pressure oscillations using a Stirling-type compressor, even for the four-kelvin region. However, in this case the operating frequency of the PTR needs to be increased by an order of magnitude.

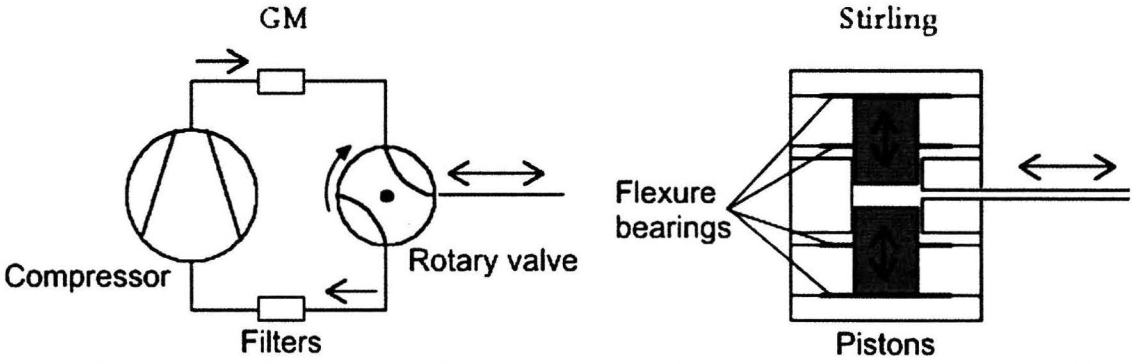

Figure 1-2. Generation of pressure oscillations by means of a GM-type compressor and a rotary valve (left). Also shown are the filters necessary to protect the rotary valve (and the PTR) from oil residue. Stirling-type compressor using two opposing pistons (right). Each piston is supported by two flexure bearings. The arrows indicate the motion of the gas flow, the rotation of the rotary valve, or the motion of the pistons.

Building an efficient and reliable four-kelvin PTR, driven by a Stirling-type compressor, is the ultimate goal of this project. The purpose of this work in particular is to increase the operating frequency of an existing three-stage GM-type PTR, operating at 1.8 Hz, to frequencies where the Stirling-type compressor can replace the GM-type compressor – rotary valve combination. At the same time, the cold-end temperature should be kept below 4 K. Design criteria for a new four-kelvin PTR, suitable to be driven by a Stirling-type compressor, are derived. The feasibility of this technology is already demonstrated by Olsen *et al.* [8]. The changing dynamics of the PTR, the coupling to a completely different compressor, the interplay between the various system parameters and design criteria make this task extremely challenging. However, the potential of the new cryocooler, together with the lively interest and active support of industrial companies such as Stirling Cryogenics & Refrigeration B.V., make it also a very rewarding task.

The theoretical background for this work is given in chapter 2. The operation principle of the PTR, its components, and the parameters governing its performance are treated. In chapter 3 more details about the setup are presented. This chapter focuses on the frequency dependency of both the generation of pressure oscillations and the optimization of the PTR. In chapter 4 the results are presented and discussed. The results of the optimization only by adjusting the orifices are followed by the results of the modifications to the PTR components. The conclusions as well as the recommendations for future work are given in chapter 5.

2 Theory

In this chapter the theoretical aspects of the PTR are treated. The general operation principle of a PTR as well as the PTR components are discussed. Expressions for the cooling power and the coefficient of performance (COP) are derived. For more details, see ref. [9] and [11].

2.1 The operation principle of the PTR

The cooling of many refrigerators, including the PTR, is based on the adiabatic and reversible expansion of a gas. The general expression for the molar entropy S_m (J K^{-1}) of a homogeneous substance is [11]

$$T\mathrm{d}S_m = C_p\mathrm{d}T - T\alpha_V V_m \mathrm{d}p, \tag{2-1}$$

with T (K) the temperature, V_m (m^3 mol^{-1}) the molar volume, C_p (J K^{-1} mol^{-1}) the molar heat capacity at constant pressure and p (Pa) the pressure. The volumetric thermal expansion coefficient α_V (K^{-1}) is

$$\alpha_V = \frac{1}{V_m}\left(\frac{\partial V_m}{\partial T}\right)_p. \tag{2-2}$$

With S_m constant, the expression for the temperature change is given by

$$\mathrm{d}T = \frac{T\alpha_V V_m}{C_p}\mathrm{d}p. \tag{2-3}$$

Generally, α_V has a positive value. For an ideal gas, $T{\cdot}\alpha_V$ equals one. It can be seen that compression leads to warming up and expansion leads to cooling down.

The operation principle is explained using the orifice PTR as an example, schematically shown in Figure 2-1. The PTR components shown in Figure 2-1 are now discussed briefly. In §2.2 these components and their functions are discussed in more detail.

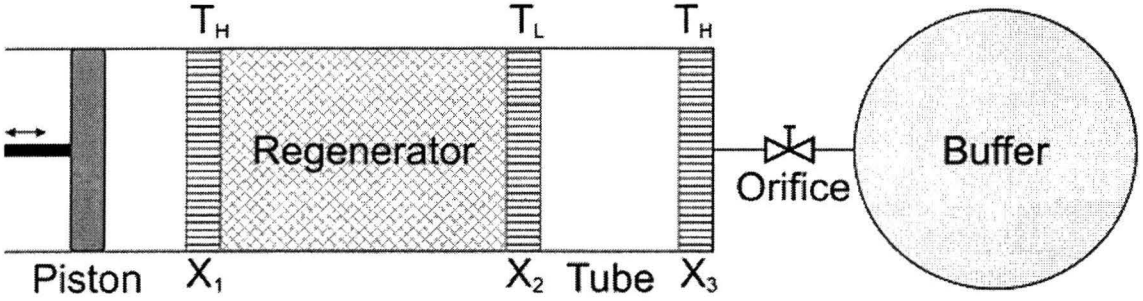

Figure 2-1. Stirling-type orifice PTR with, from left to right, the piston compressor, regenerator hot-end heat exchanger, the regenerator, the regenerator cold-end heat exchanger, the (pulse) tube, the pulse-tube hot-end heat exchanger, the (first) orifice, and the buffer.

The piston moves back and forth, generating an oscillating pressure at the inlet of the PTR (X_1). X_1 is the hot-end heat exchanger which is at room temperature T_H. At X_1 heat is rejected to the surroundings (cooling water). The regenerator's purpose is to store heat, and to precool gas that flows to the cold-end heat exchanger X_2. It consists of a porous material with a high heat capacity. X_2 is the cold-end heat exchanger at temperature T_L, where the actual cooling takes place. The gas in the (pulse) tube is expanded and compressed due to the pressure oscillations generated by the moving piston. At hot-end heat exchanger X_3 the heat that was extracted at X_2 is rejected to the surroundings at room temperature T_H. Through an orifice the gas can enter a large volume; the buffer. The pressure in the buffer is practically constant. All components are considered ideal[2].

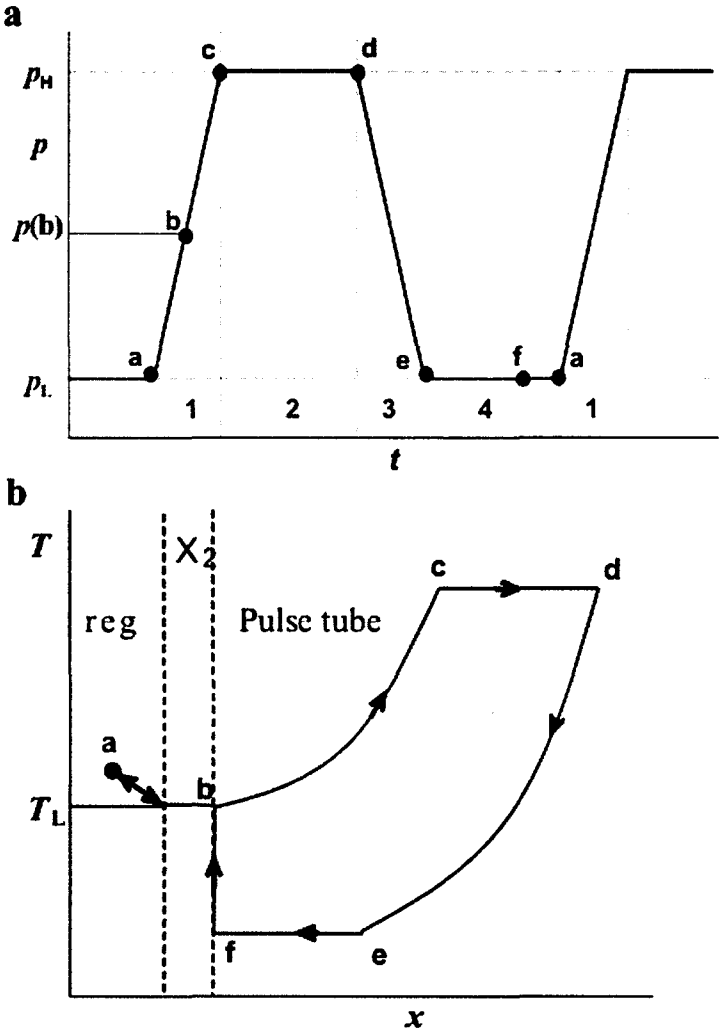

Figure 2-2. **a)** The pressure in the pulse tube as a function of the time. During compression (from a to c) the pressure rises from the low pressure p_L to the high pressure p_H. During expansion (form d to e) the pressure decreases from p_H to p_L. **b)** The temperature as a function of the position of an element of gas that travels back and forth between the regenerator (left), the cold-end heat exchanger X_2 (area between the dashed lines), and the pulse tube (right).

[2] The properties of the ideal components are discussed in §2.2.

Figure 2-2a shows the pressure in the pulse tube as a function of the time, for an idealized cycle. Figure 2-2b shows the temperature of the gas element as a function of its position for one cycle. This cycle is divided into four steps.

Consider a gas element in the regenerator near the cold-end heat exchanger X_2, traveling back and forth between the regenerator, X_2, and the pulse tube.

1. From a to c via b; the compression step. The orifice is closed as the piston moves to the right. The pressure rises. As the pressure rises, the gas element moves through the regenerator, being precooled by it, towards X_2, where it arrives at the cold-end at temperature T_L. The gas leaves X_2 at position b, and enters the pulse tube. The gas element continues to be compressed, now adiabatically because in the pulse tube it is thermally isolated from its surroundings. Therefore, the temperature of the gas element rises (equation 2-3).
2. From c to d. The orifice opens at time c. The gas inside the pulse tube is now at high pressure p_H, which is higher than the pressure in the buffer p_b, being the cycle-averaged pressure. The gas starts flowing from the pulse tube to the buffer. At the same time the piston is still moving to the right, keeping the pressure in the pulse tube constant at p_H.
3. From d to e; the expansion step. At d the piston is in its far-right position and starts moving back. The orifice is closed. The pressure decreases and the gas moves back towards X_2. This expansion is adiabatic, so the temperature decreases together with the pressure. When the pressure reaches p_L (at time e) the temperature of the gas element is below T_L.
4. From e back to a via f. The orifice is open. Because the pressure in the pulse tube is lower than p_b, gas flows from the buffer into the pulse tube. The piston continues to move to the left, keeping the pressure constant at p_L. The gas moves towards X_2 and enters X_2 at point f. Because the temperature of the gas element is below T_L, it extracts heat from the cold-end heat exchanger, effectively cooling it. The amount of heat that is extracted is discussed in §2.3. From f the gas element moves back to its original position (a) inside the regenerator.

2.2 PTR components

In this work, the so called GM-type double-inlet PTR is used. In a GM-type PTR the pressure oscillations are generated using a combination of a Gifford-McMahon (GM) compressor and a rotating valve (RV). The double inlet is an extra connection between the hot end of the regenerator and the hot end of the pulse tube. The minor orifice connects the buffer either to the high- or to the low-pressure side of the compressor. In Figure 2-3 a scheme of a single-stage GM-type double-inlet PTR is shown. This figure is used to explain the functions of the basic components of the PTR, which is done in this section. Later, in chapter 3, the practical details of the *three-stage* version used in this work are discussed.

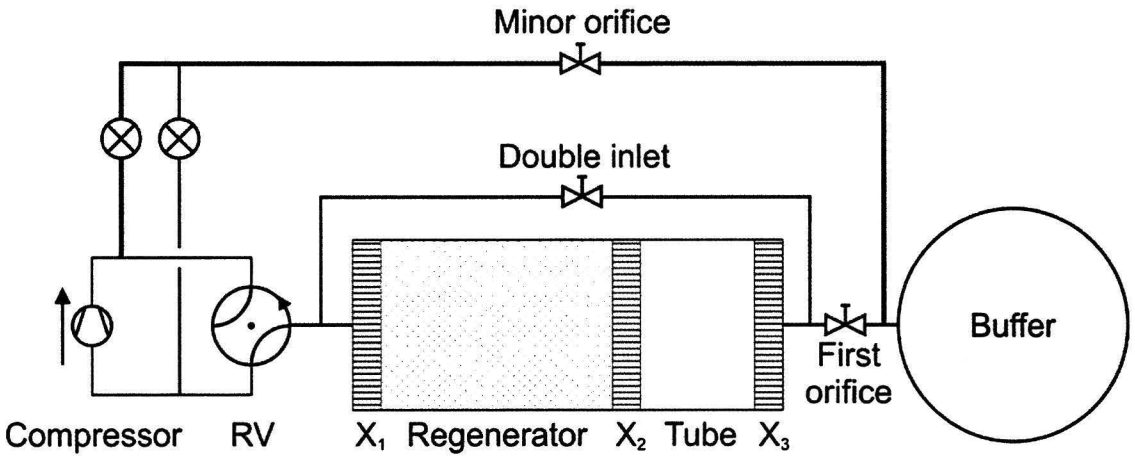

Figure 2-3. Diagram of a single-stage PTR with first orifice, double inlet, and minor orifice. Also shown are the GM-type compressor, the rotary valve (RV), the heat exchangers ($X_{1,2,3}$), the regenerator, the (pulse) tube, and the buffer.

2.2.1 Generation of pressure oscillations

In order to generate pressure oscillations at the cold end of the pulse tube, a large volume flow is needed at the regenerator hot end due to the difference in the density of the gas. For a cold-end temperature of 20 K the ratio between the volume flow at room temperature and the volume flow at 20 K is 15, for 2 K this ratio can become as high as 70. Generally, a GM-type compressor is capable of maintaining a large volume flow, which is the main reason why most low-temperature PTRs are GM-type nowadays. The compressor generates a constant flow which is led to a rotary valve. The rotary valve connects the rest of the system alternately to the high- and the low-pressure side of the compressor. This generates an oscillating pressure in the PTR. By changing the rotation speed of the rotary valve, the oscillation frequency can be adjusted, typically between 1 and 20 Hz. As already mentioned, the main disadvantage of the GM-type compressor – rotary valve combination is that the efficiency is only 25 %. Furthermore, it is less reliable and has a shorter lifetime compared to the Stirling compressor, which is discussed below. Also, a GM-type compressor needs lubrication, from which the residue has to be removed from the gas before it can be fed to the rotary valve. Moreover, for the GM-type compressor cooling water is needed. Therefore, a GM-type PTR is unsuitable for space application.
In the example of §2.1 the pressure oscillations are generated by a moving piston. In principle, the piston can be forced to oscillate at any frequency, but driving it at the resonance frequency increases the efficiency significantly. This is done in a so-called Stirling-type compressor, with a typical efficiency of 80 % (compare to 25 % for the GM-type). A high efficiency generally leads to a lightweight, more compact compressor. Also, less cooling water (or none at all) is needed. Therefore, it would be beneficial to develop a low-temperature PTR driven by a Stirling-type compressor.

The frequency of the pressure oscillations is equal to the frequency of the motion of the piston. The frequency is an important parameter for both the compressor and the cooling system connected to it. In the following, an expression for the resonance frequency of a typical Stirling-type compressor is derived. Consider a system as shown in Figure 2-4. A

piston with radius r_p (m) and mass m_p (kg) moves with a stroke amplitude Δx (m). The piston movement generates a time dependent pressure p_c in the compression space with volume V_c. At the back side of the piston a buffer volume V_b at pressure p_b is present. A spring with stiffness k_s (N m^{-1}) is placed at the back of the piston. Also, friction with damping coefficient c (N s m^{-1}) is present (not shown in the figure). The time-averaged pressure in the buffer and in the compressor is p_0. Linear motors apply a (time dependent) force F_m (N) on the piston.

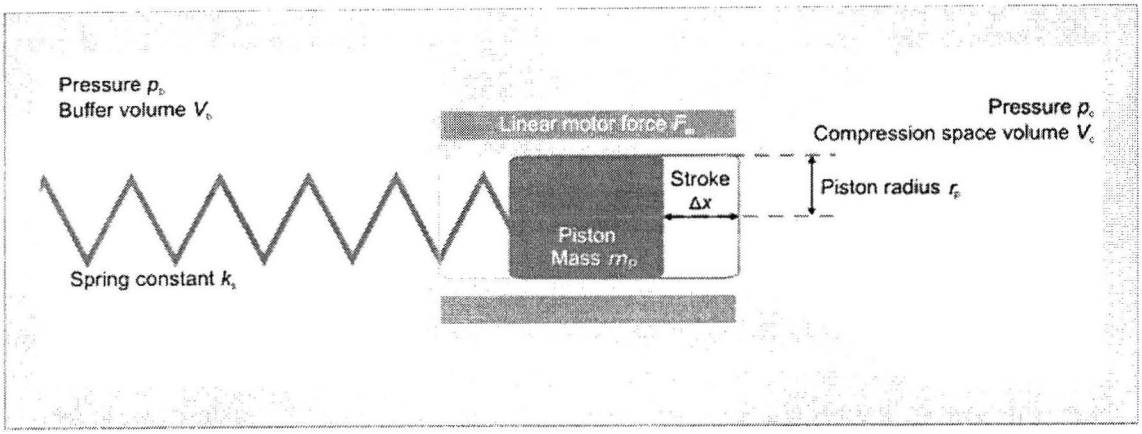

Figure 2-4. Diagram of a piston compressor.

The differential equation describing the dynamic behavior of this system is [10]

$$m_p\ddot{x} + c\dot{x} + k_s x + \pi r_p^2 (p_c - p_b) = F_m, \tag{2-4}$$

with x (m) the location, $\dot{x}$ (m s^{-1}) the velocity, and $\ddot{x}$ (m s^{-2}) the acceleration of the piston. In the compression space and the buffer the gas is thermally isolated from the wall, so adiabatic compression and expansion can be assumed. Assuming an ideal gas, Poisson's law can be used to find the pressure change due to a change in volume

$$pV^\gamma = \text{constant}. \tag{2-5}$$

Here, the Poisson constant γ is equal to C_p/C_v, and C_v (J K^{-1} mol^{-1}) is the molar heat capacity at constant volume. The compression space volume V_c and buffer volume V_b are

$$V_c = V_{c0} - \pi r_p^2 x, \text{ and} \tag{2-6a}$$

$$V_b = V_{b0} + \pi r_p^2 x, \tag{2-6b}$$

with V_{c0} and V_{b0} the volume of the compression space and buffer, respectively, at equilibrium (x=0). In principle, motor force F_m can be chosen in such a way, that the time t (s) dependency of the position of the piston x is sinusoidal.

$$x = \Delta x \cos(\omega t). \tag{2-7}$$

Here, ω is the angular frequency (s^{-1}). Combining equations 2-5, 2-6, and 2-7, the pressures in the compression space and in the buffer are

$$p_c = \frac{p_0 V_{c0}^{\gamma}}{\left[V_{c0} - \pi r_p^2 \Delta x \cos(\omega t)\right]^{\gamma}}, \text{ and} \tag{2-8a}$$

$$p_b = \frac{p_0 V_{b0}^{\gamma}}{\left[V_{b0} + \pi r_p^2 \Delta x \cos(\omega t)\right]^{\gamma}}. \tag{2-8b}$$

For a typical Stirling compressor, the displaced volume amplitude ($\pi r_p^2 \Delta x$) is small compared to the equilibrium compression space volume V_{c0} and the equilibrium buffer volume V_{b0}. Therefore, p_c and p_b can be approximated by

$$p_c = p_0 + \gamma \frac{p_0 \pi r_p^2 \Delta x}{V_{c0}} \cos(\omega t), \text{ and} \tag{2-9a}$$

$$p_b = p_0 - \gamma \frac{p_0 \pi r_p^2 \Delta x}{V_{b0}} \cos(\omega t). \tag{2-9b}$$

Combining equations 2-4 and 2-9, the equation for Δx is obtained:

$$\Delta x = \frac{\hat{F}_m}{\sqrt{\left[k_s + \gamma p_0 \pi^2 r_p^4 \left(\frac{1}{V_{c0}} + \frac{1}{V_{b0}}\right) - m_p \omega^2\right]^2 + c^2 \omega^2}}, \tag{2-10}$$

with ^ indicating the amplitude of the motor force. Using this equation, it can be shown that the resonance frequency f_r (s^{-1}) is approximately

$$f_r \approx \frac{1}{2\pi} \sqrt{\frac{k_s}{m_p} + \frac{\gamma p_0 \pi^2 r_p^4}{m_p} \left(\frac{1}{V_{c0}} + \frac{1}{V_{b0}}\right)}, \tag{2-11}$$

where the damping factor c is assumed small. Typical resonance frequencies of a Stirling compressor range from 20 to 50 Hz. For low frequencies, a thin, heavy piston, a weaker spring, a low filling pressure, and/or larger volumes should be used. In practice, only few of these parameters (or none at all) can be chosen freely due to design limitations or demands of the cooling system attached to the compressor. Below ~7 Hz it can be increasingly difficult to stabilize the piston against changes in pressure or gravity [9]. Due to the same stability issues, Stirling-type compressors generally are not suited for compressing or expanding large amounts of gas. The pressure amplitude at the coldest part of the PTR can become small due to this effect. Because the cooling power (§2.3) is

proportional to the square of the pressure amplitude, this can severely degrade the cooling power of the PTR. It should be noted that a smaller pressure amplitude can have positive effects as well. At low temperatures, nonideal gas effects become more and more important. The dissipative losses increase with increasing pressure amplitudes [12]. In this case, a smaller pressure amplitude decreases losses and improves the performance.

It can be seen that the time-dependent piston position and the pressure in the compression space are in phase (equations 2-7 and 2-9). In reality this is not the case. Pressure p_c also depends on the system that is attached to the compressor, introducing a phase difference between the piston's position and p_c. The relation between the parameters governing the dynamics of the PTR and the Stirling compressor can make the optimization of a combination of the two an extremely challenging task.

2.2.2 Heat exchangers

The heat exchangers shown in Figure 2-3 provide thermal contact between the gas and the surroundings. In case of X_1 and X_3 heat is released to the cooling water at room temperature. X_2 is in thermal contact with the object to be cooled. Generally, copper is used as heat exchanger material because of its high heat conductivity. An ideal heat exchanger has the following properties:

1. The thermal contact between the working gas and the surroundings is perfect.
2. The flow resistance is zero.

These requirements can be conflicting. Good thermal contact implies many small flow channels. However, this geometry generally increases the flow resistance.

2.2.3 Regenerator

The regenerator's purpose is to precool the gas before it enters the cold-end heat exchanger X_2, where the actual cooling takes place. The regenerator consists of a porous material that can store/release heat from/to the gas that is flowing through the material. An ideal regenerator has the following properties:

1. The heat capacity of the porous material is large.
2. The thermal contact between the porous material and the working gas is good.
3. The flow resistance of the porous material is zero.
4. The axial thermal conductivity is zero.

Some of these requirements are conflicting. E.g. good thermal contact between the gas and regenerator material (requirement 2) leads to an increased flow resistance (requirement 3). The material properties (i.e. heat capacity and thermal conductivity) are temperature dependent. Therefore, it can be beneficial to use different materials for different (parts of the) regenerators working at different temperature ranges. The choice of the regenerator material is often determined by the comparison of the volumetric heat capacity ρc [J K^{-1} m^{-3}] and thermal conductivity κ [J s^{-1} K^{-1} m^{-1}] of the material itself and the working gas, at the corresponding pressure and temperature range.

Requirement 2 demands a good thermal contact between the material and the working gas. In other words: all of the regenerator material must 'see' the working gas, and vice-versa. To quantify this, it is meaningful to use the thermal penetration depth δ_T (m)

$$\delta_T = \sqrt{\frac{\kappa}{\pi f \rho c}}, \tag{2-12}$$

where ρ (kg m^{-3}) is the density, and c (J K^{-1} kg^{-1}) the specific heat capacity. The thermal penetration depth also depends on the frequency f. The quantity $1/f$ is the time a certain temperature oscillation gets to propagate into the regenerator material. The thermal conductivity κ determines the speed at which energy can be transported through the regenerator material. The product ρc is a measure for the amount of energy needed to warm up a unit volume of regenerator material. In general, δ_T shows to which extent (depth) the material (or working gas) is capable of exchanging heat with its surroundings within a certain time. Therefore, it is also a good measure for the optimal diameter of the features (e.g. grain- or pore size) in the regenerator. The choice of the configuration of the regenerator is complicated by requirements 3 and 4, mentioned above. Losses caused by axial thermal conduction and flow resistance have to be taken into account also. In the §3.3.2 the choice of the regenerator material is discussed in detail.

2.2.4 Pulse tubes

In the pulse tubes the gas is thermally isolated from the surroundings, as opposed to the thermal environment of the gas in the regenerator. This allows adiabatic and reversible expansion and compression, which results in cooling down or warming up of the gas (see equation 2-3). An ideal pulse tube has the following properties:

1. No heat exchange between the tube-wall and the gas.
2. No thermal conduction.
3. No mixing or turbulence in the gas.

Figure 2-5 shows the temperature of a gas element that enters or leaves the pulse tube at the cold end (left) or the hot end (right) as a function of its location along the axis of the pulse tube. At the hot end, the gas moves towards the buffer if the pressure in the pulse tube p_t is higher than the pressure in the buffer p_b, during compression. On the other hand, gas enters the pulse tube if p_t is smaller than p_b, during expansion. The compressed gas is warmer than the expanded gas. Therefore, the gas that leaves the pulse tube is warmer than when it entered the pulse tube. This heat is rejected to the surroundings at heat exchanger X_3, which is kept at constant temperature T_H.

At the cold end the gas enters the pulse tube via X_2 at high pressure and T_L. The gas leaves the pulse tube via X_2 at low pressure, with a temperature $T < T_L$, extracting heat from X_2. This is how the actual cooling takes place. In fact, this process is similar to the mechanism explained in §2.1, but now the pressure and displacement of the gas is sinusoidal.

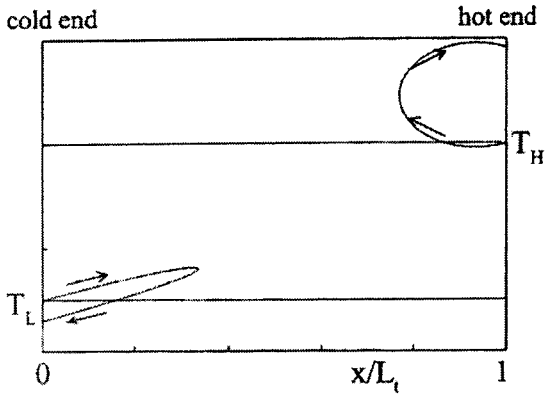

Figure 2-5. Temperature – location diagram of gas entering the pulse tube at the cold end (left) and gas entering the pulse tube at the hot end (right). L_t is the pulse-tube length. Also shown are the cold-end temperature T_L and hot-end temperature T_H.

In reality, the process explained above is more complicated. The gas flow at the cold end is related to the gas flow at the hot end. If the gas in the pulse tube is assumed adiabatic and caloric perfect, Poisson's law (equation 2-5) can be used to find this relation. The time derivative of Poisson's law is

$$\gamma p_t V_t^{\gamma-1} \frac{dV_t}{dt} + V_t^{\gamma} \frac{dp_t}{dt} = 0, \tag{2-13}$$

where γ is assumed constant. Volume V_t is the volume of the pulse tube and p_t is the pressure in the pulse tube. At the pulse-tube cold end and the hot end, a gas piston is moving in and out the pulse tube through a surface area A_t (m^2) with velocity v_L ($m\ s^{-1}$) and v_H, respectively. If one or both of these pistons move into the pulse tube, the gas inside the pulse tube that initially was in volume V_t is compressed to a volume smaller than V_t. Therefore, the change of the volume of the gas inside the pulse tube is given by

$$\frac{dV_t}{dt} = A_t(v_H - v_L). \tag{2-14}$$

Combining this with equation 2-13 gives

$$\gamma p_t \frac{A_t(v_H - v_L)}{V_t} + \frac{dp_t}{dt} = 0. \tag{2-15}$$

If the pressure changes are small compared to the time-averaged pressure p_0 in the pulse tube, this equation can be written as

$$v_L = v_H + \frac{C_v}{C_p} \frac{L_t}{p_0} \frac{dp_t}{dt}, \tag{2-16}$$

which is the relation between the velocity at the cold end of the pulse tube, the hot end of the pulse tube and the pressure in the pulse tube [14].

2.2.5 First orifice and buffer

The buffer is a sufficiently large volume so the pressure oscillations inside the buffer, caused by the gas flow through the first orifice, are negligible. The first orifice and buffer allow a gas flow at the hot end of the pulse tubes which is in phase with the pressure in the pulse tube. In case of an ideal PTR the performance is independent of the phase difference between the pressure and the velocity of the gas at the cold end of the pulse tube, represented by parameter α (discussed later). In case of a nonideal PTR the optimal performance can be reached when α is in the order one. For a PTR without double-inlet valve, the optimal velocity phase difference φ is 45° [14]. In practice, the optimal phase difference can deviate from this value.

2.2.6 Double-inlet valve

The double-inlet valve shunts the regenerator and the pulse tube, and acts as a 'shortcut' from the compressor to the pulse tube. This reduces the gas flow through the regenerator and the subsequent losses inside the regenerator. However, this also decreases the cooling power (equation 2-30). Moreover, the double-inlet valve itself also causes losses due to the pressure drop over the valve. In an optimal situation the reduction of the losses in the regenerator outweighs the increase of the other losses, increasing the overall performance of the system ([14], [19]). Note that the positive effect of the double-inlet valve relies entirely on a finite flow resistance of the regenerator.

2.2.7 Minor orifice

By opening the double inlet an internally closed circuit is created, running from the regenerator hot end, through the regenerator to the pulse tube and back to the regenerator hot end via the double inlet. A so-called DC flow can run in this internal circuit when the flow resistance of the gas going into the regenerator is different from the gas flowing back. This asymmetry can be caused by an asymmetric geometry of the orifices, the flow straighteners, or the regenerator. However, even in a perfectly symmetric system a DC flow can be present because the gas flowing through the double inlet is flowing in under high pressure (high density) and is flowing back under low pressure (low density). Due to this asymmetry, the amount of gas entering the system through the double inlet can be slightly larger than the amount of gas that is flowing back every cycle. The same principle is valid for the regenerator. If the asymmetry in the flow resistance of the regenerator would be equal to the asymmetry of the double-inlet valve, the time-averaged pressure in the pulse tube would be slightly higher, but no DC flow would occur. In reality, this is not the case. The geometries of the regenerator and the double inlet are completely different. Moreover, in the regenerator also a temperature profile (and therefore: gas-density profile) is present. The resulting DC-flow can cause a net enthalpy flow running from the pulse tube's hot end X_3 (or from the regenerator's hot end X_1, if the net gas flow is in the opposite direction) towards the cold end X_2. This reduces the performance of the system. In order to counteract this flow, the minor orifice connects the hot end of the pulse tube either to the high pressure side, or to the low pressure side of the compressor.

2.3 α parameter and cooling power

In this section an important characteristic α-parameter is introduced, representing the out-of-phase component of the flow at the cold end of the pulse tube, compared to the flow at the hot end. Next, the cooling power of a double inlet PTR is derived, based on the derivation in ref. [14].

The volumetric flow rate $\dot{V}$ [$m^3\ s^{-1}$] through a flow resistance with conductance C [$m^3\ s^{-1}\ Pa^{-1}$] can be calculated using

$$\dot{V} = C\,\Delta p, \tag{2-17}$$

with Δp the pressure difference over the flow conductance. For C the flow conductance of the first orifice C_1, the flow conductance of the double inlet C_2, or the effective flow conductance of the regenerator C_r can be used. The effective flow conductance C_r of a regenerator with length L_r (m) is defined as

$$C_r^{-1} = \frac{Z_r}{L_r}\int_0^{L_r} \eta \frac{T}{T_L}\mathrm{d}l \tag{2-18}$$

where Z_r (m^{-3}) the flow impedance factor of the regenerator. The effective flow conductance of the regenerator takes into account the density (of an ideal gas) and the viscosity η (J s m^{-3}). Now, the flow rate through the regenerator, double-inlet valve, and the first orifice can be calculated. The pulse tube pressure p_t, the time-averaged pressure p_0, and the compressor pressure p_c are used for determining Δp. The time dependence of p_t is assumed harmonic

$$p_t = p_0 + p_1\cos(\omega t), \tag{2-19}$$

with p_1 the amplitude of the pressure oscillations in the pulse tube. The α-parameter is defined for a single-orifice pulse tube [13], shown in Figure 2-1. Therefore, the velocity of the gas at the hot end of the pulse tube v_H is given by

$$v_H = \frac{C_1}{A_t}(p_t - p_b) = \frac{C_1 p_1}{A_t}\cos(\omega t), \tag{2-20}$$

with A_t the surface area of the pulse tube. The buffer is assumed sufficiently large, so pressure $p_b = p_0$. The velocity of the gas at the cold end of the pulse tube v_L can be calculated using equation 2-16.

$$v_L = \frac{C_1 p_1}{A_t}\left[\cos(\omega t) - \alpha\sin(\omega t)\right] \tag{2-21}$$

Here, the α-parameter is introduced:

$$\alpha = A_t \frac{C_v}{C_1 C_p} \frac{L_t}{p_0} \omega . \tag{2-22}$$

In ref. [13] it was shown that the optimal value for α equals one (45° phase shift) for an ideal single-orifice PTR. However, for a *double-inlet* PTR the situation is different. The velocity of the flow at hot-end of the pulse tube consists of two contributions with two different phase angles:

$$v_H = \frac{C_1}{A_t}(p_t - p_b) + \frac{C_2}{A_t}(p_t - p_c), \tag{2-23}$$

with p_c the compressor pressure, at the inlet of the PTR. The velocity at the cold en of the pulse tube is given by

$$v_L = \frac{C_r}{A_t}(p_c - p_t), \tag{2-24}$$

so

$$p_c - p_t = \frac{C_1}{C_2 + C_r} p_1 [\cos(\omega t) - \alpha \sin(\omega t)]. \tag{2-25}$$

Assuming an ideal gas the molar flow rate $\dot{n}$ can be calculated for the regenerator ($\dot{n}_r$), first orifice ($\dot{n}_1$), and the double inlet ($\dot{n}_2$).

$$\dot{n}_r = \frac{p_0}{RT_L} \frac{C_r C_1}{C_2 + C_r} p_1 [\cos(\omega t) - \alpha \sin(\omega t)] \tag{2-26}$$

$$\dot{n}_1 = \frac{p_0}{RT_H} C_1 p_1 \cos(\omega t) \tag{2-27}$$

$$\dot{n}_2 = \frac{p_0}{RT_H} \frac{C_2 C_1}{C_2 + C_r} p_1 [\cos(\omega t) - \alpha \sin(\omega t)] \tag{2-28}$$

Here, R (J K^{-1} mol^{-1}) is the molar ideal gas constant. The molar entropy S_m (J K^{-1}) is given by equation 2-1. Using the ideal gas law and the expression for α_V (equation 2-2), S_m is given by

$$S_m(p,T) = S_m(p_0,T_0) + \frac{C_p}{T}(T - T_0) - R\frac{p_1}{p_0}\cos(\omega t), \tag{2-29}$$

with T_0 (K) the time-averaged temperature of the gas.

For this linearization, the changes in temperature and pressure are assumed small compared to T_0 and p_0. Now, the average entropy flow rate can be calculated by integrating over a cycle and dividing by the cycle time t_c (=2π/ω). The cold-end temperature is assumed constant. The heat flow extracted at X_3 can be calculated, resulting in the cooling power.

$$\overline{\dot{Q}}_L = -T_L \frac{1}{t_c}\int_0^{t_c} S_m \dot{n}_r \mathrm{d}t = \frac{1}{2}\frac{C_r C_1}{C_2 + C_r} p_1^2 \tag{2-30}$$

Here, it can be seen that the cooling power is proportional to the square of the pressure amplitude in the pulse tube. The compressor pressure p_c and the compressor volumetric flow rate $\dot{V}_c$ can be calculated using conservation of mass and equations 2-17 – 2-28.

$$p_c = p_t + \frac{RT_L}{p_0}\frac{\dot{n}_r}{C_r} = p_0 + p_1\cos(\omega t) + \frac{C_1}{C_2 + C_r} p_1[\cos(\omega t) - \alpha\sin(\omega t)] \tag{2-31}$$

Using $\dot{n}_c = \dot{n}_r + \dot{n}_2$, the compressor flow rate is

$$\dot{V}_c = C_1 \frac{C_2 + C_r(T_H/T_L)}{C_2 + C_r} p_1[\cos(\omega t) - \alpha\sin(\omega t)]. \tag{2-32}$$

The coefficient of performance is defined as

$$COP = \frac{\overline{\dot{Q}}_L}{P}, \tag{2-33}$$

with P (J s^{-1}) the input power, equal to the work done by the compressor per second.

$$P = \frac{1}{t_c}\int_0^{t_c} p_c \dot{V}_c \mathrm{d}t \tag{2-34}$$

Using equations 2-30 – 2-34, the COP is

$$COP = \frac{C_r(C_2 + C_r)}{\left[C_2 + C_r(T_H/T_L)\right]\left[C_2 + C_r + (1+\alpha^2)C_1\right]}. \tag{2-35}$$

Optimizing the PTR means maximizing this equation by adjusting the flow conductances.

Using equation 2-22 it can be shown that the *COP* is optimal if $\alpha = 1$ or

$$C_{1,O} = A_t \frac{C_v}{C_p} \frac{L_t}{p_0} \omega, \tag{2-36}$$

the optimal conductance for first orifice, and

$$C_{2,O} = -C_r + \sqrt{\frac{2C_r C_{1,0}}{COP_C}}, \tag{2-37}$$

the optimal conductance for the double-inlet valve. The Carnot coefficient of performance COP_C can be derived from the general equation for the work done by the compressor, given by

$$P = \left(\frac{T_H}{T_L} - 1 \right) \overline{\dot{Q}}_L + T_H \overline{\dot{S}}_i, \tag{2-38}$$

which includes the entropy production $\overline{\dot{S}}_i$ due to irreversible losses in the PTR. These losses are discussed in detail later. If $\overline{\dot{S}}_i$ is zero, COP_C can be calculated.

$$COP_C = \frac{T_L}{T_H - T_L} \tag{2-39}$$

In practice, irreversible losses are present in the PTR, so the actual *COP* is smaller than the ideal COP_C.

3 Experiments

In the first part of this chapter the experimental setup is treated extensively. The PTR itself and the generation of pressure oscillations in particular are discussed. The second part of this chapter focuses on the frequency-dependent characteristics and optimization of the PTR.

3.1 Experimental setup

Figure 3-1 shows a diagram of the three-stage PTR as it is used in this work. The compressor and the rotary valve can be found in the top-right corner of the diagram.

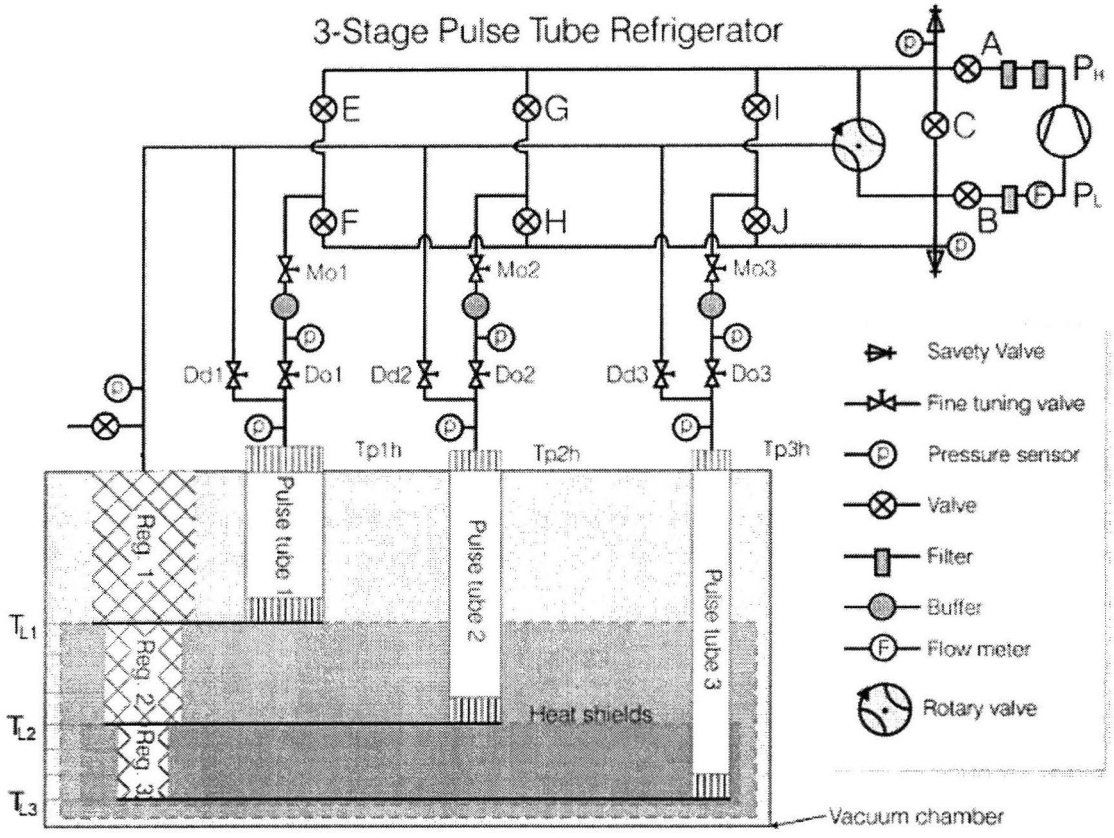

Figure 3-1. Diagram of the three-stage PTR. The top-right part of the diagram shows the compressor, rotary valve and valves A – J. The cooling system consists of the regenerators (Reg. 1, Reg. 2, and Reg. 3), the first orifices Do1, Do2, and Do3, the double-inlet valves (Dd1, Dd2, and Dd3), the minor orifices (Mo1, Mo2, and Mo3), the buffers and the pulse tubes. The hot- and cold-end heat exchangers can be found at the top and bottom of the pulse tubes, respectively. The locations where the temperatures are measured are shown in the top left corner. The second-stage and the third-stage cold ends are shielded by copper thermal-radiation shields attached to the first- and the second-stage pulse-tube cold end.

The 4.5 kW GM-type compressor runs at 50 Hz, continuously pumping the gas from the low-pressure side (p_L) to the high-pressure side (p_H). From the high-pressure side of the compressor, gas flows through two filters and valve A to the rotary valve. The first filter is a Headline Filters 0.24 l charcoal/zeolite filter, to protect the system from oil vapour coming from the compressor. The second is a Headline Filters microfibre filter, to protect the system from any residual oil droplets or dust particles (e.g. coming from filthy connection hoses). Another microfibre filter is placed at the low-pressure side of the compressor. This way, the PTR system and the rotary valve, which is particularly vulnerable to dust particles, is well protected at both the inlet and outlet. In principle, the microfibre filters are not necessary.

For the rotary valve, the so called 'no-contact' type is used. Figure 3-2 shows a schematic drawing of a no-contact type rotary valve. This type of valve has some major advantages:

- The power loss in this type of rotary valve is 12% of the total input power, instead of 28% for conventional rotary valves.
- The rotor makes no contact with the housing and the forces are balanced, which significantly decreases wear.

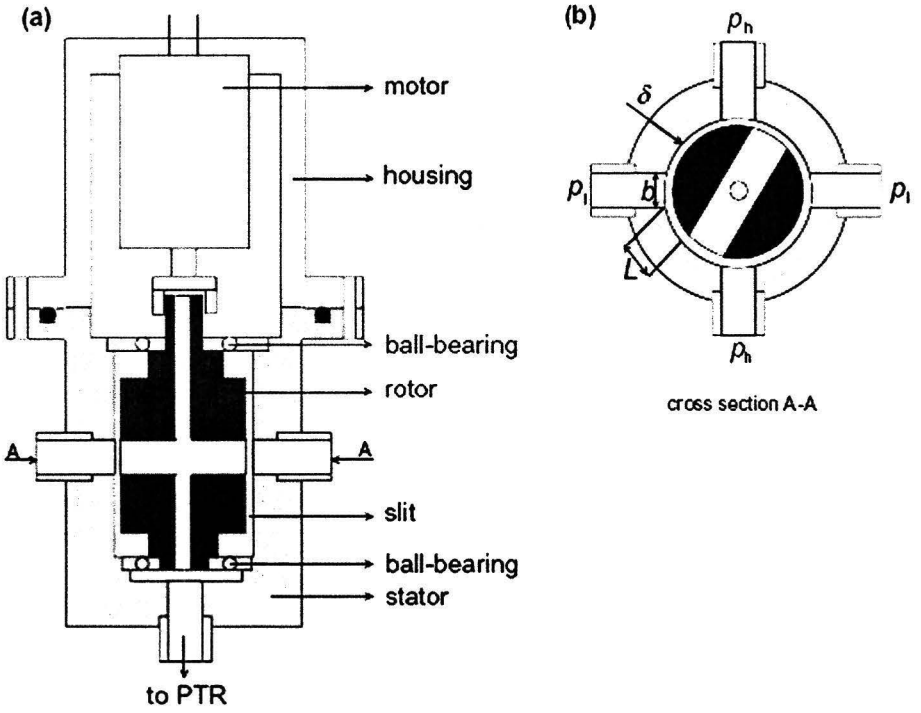

Figure 3-2. Side view (a) and top view (b) of a no-contact type rotary valve. The rotor is placed vertically in the stator, and is supported by two sets of ball-bearings. The slit δ between the rotor and the stator is typically 20 μm wide, so the rotor is not in contact with the stator. The rotor is driven by a motor placed in the top part of the rotary valve. In the housing, four connections are present for the low- and high-pressure side of the compressor. The connection to the PTR can be found at the bottom of the rotary valve.

The rotor is placed in the stator, separated by a gap δ of typically 20 μm wide, and supported by two sets of ball-bearings. While the rotor is rotating in the stator, it does not make contact with the stator. The width of the gap is small in order to prevent leaking. The stator has four connections; one pair going to the high-pressure side of the compressor, and one pair going to the low-pressure side. The two connections of the high-pressure side are on opposite sides of the stator. The same goes for the two connections to the low-pressure side, so the forces acting on the rotor are well balanced. At the bottom of the rotor is a connection to the PTR. In one revolution the rotor connects the PTR two times to the high pressure, and two times to the low pressure. So the frequency of the PTR is twice the rotating frequency of the rotary valve. The rotor is driven by a replaceable motor with a replaceable gear box. The system can be operated at frequencies ranging from 0.5 – 15 Hz, and possibly even higher. The system is designed to operate at low frequencies, typically 1 – 2 Hz. More information about the rotary valve can be found in [18].

The gas flows back from the system through the rotary valve, valve B, a filter, and the Bronkhorst Hi-Tec flow meter to the low-pressure side of the compressor (p_L). From the high- and the low-pressure side of the compressor, extra connections lead to the three minor orifices Mo1, Mo2, and Mo3, via valves E – J. The purpose of the minor orifices has been discussed in §2.2.7. For safety reasons, overpressure valves are added at the high- and low-pressure side of the rotary valves. Their threshold is set at 28 bar, which is well above the working pressure of the compressor, and low enough to protect the system from damage. The typical time-averaged pressure is 15 bar, with a pressure amplitude at the inlet of the system of 5.6 bar.

In Figure 3-1, one connection of the rotary valve branches to the left. This is the connection to the inlet of the PTR; the first-stage regenerator hot end. At this point, the pressure can be measured, and gas can be added or released. From the inlet of the system, the gas runs through the first-stage regenerator, where it is precooled to the first-stage cold-end temperature T_{L1}. This temperature is measured using a platinum resistor. At this point, the gas can either go to the first-stage pulse tube, or continue into the second-stage regenerator. The temperature in the second-stage regenerator is measured at three different locations; two calibrated diode thermometers at 1/3 and 2/3 of the regenerator's length, and one at the second-stage cold end (T_{L2}). Here, the gas flow branches again, going either to the second-stage pulse tube or to the third-stage regenerator. The temperature in the third-stage regenerator is again measured at three different locations. The cold-end temperature of the third-stage T_{L3} and the two remaining intermediate temperatures are measured using calibrated diode thermometers. From the third-stage regenerator, the gas flows into the third-stage pulse tube. The regenerator is designed in such a way that it can be disassembled relatively easily in order to change the material.

Thermal radiation shields are connected to the first- and the second-stage cold end, blocking the thermal radiation coming from warmer parts in the cryostat. The pressure in the pulse tubes is measured after the heat is rejected to the hot-end heat exchangers. The temperatures T_{p1H}, T_{p2H}, and T_{p3H} at the hot ends of the pulse tubes are measured also. The hot ends of the pulse tubes are connected to buffers at constant pressure via the first orifices. The double-inlet valves connect the hot ends to the inlet of the PTR. Figure 3-3 shows a picture of the actual PTR and its components. Only the low-temperature part is shown. It corresponds to the components in the 'shaded' part of Figure 3-1. Before the cooler can be run, the two heat shields are added and covered with isolation material, and the vacuum chamber is sealed and pumped. The total volume of the low-temperature part is approximately 280 cm^3.

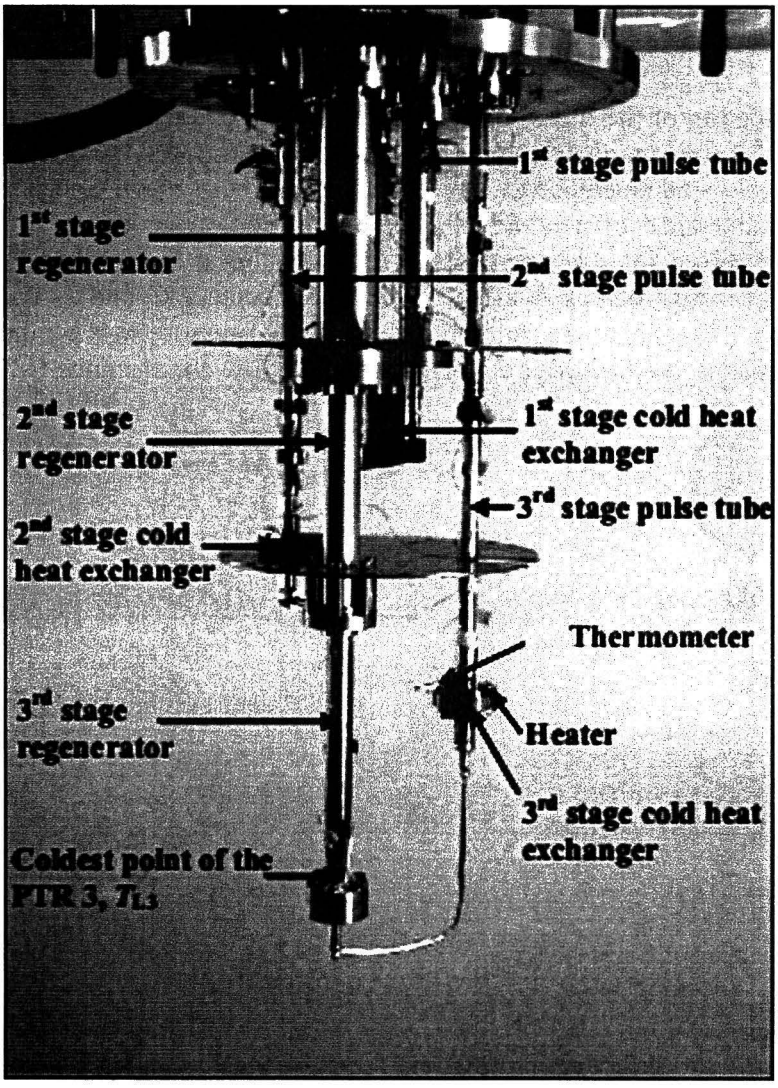

Figure 3-3. Picture of the three-stage PTR, showing its regenerators, pulse tubes, and heat exchangers.

3.2 Generation of pressure oscillations

By adjusting the speed of the rotary valve, the frequency of the pressure oscillation at the inlet of the system can be changed. Given an arbitrary system (consisting of volumes and impedances) connected to the rotary valve, increasing the rotation frequency of the rotary valve changes the dynamics of the whole system. This subject is treated in this section.

The goal is to obtain a simple model that can be used to describe the frequency dependent behavior of the pressure amplitude and the volume flow at the inlet of the PTR (the hot end of the first-stage regenerator). It is not intended to generate accurate predictions of the pressure and flow rate throughout the system. Therefore, the PTR system and compressor are greatly simplified. A single-stage PTR without double-inlet valve and minor orifice is considered, much like the PTR shown in Figure 2-1. Also, an ideal gas is assumed.

The dynamics of the combination of the tubes, filters, the rotary valve, and the GM-type compressor are approximated by an ideal[3] pressure oscillation generator, generating pressure p_c, in series with a flow conductance C_i. From the PTR point of view, C_i can be regarded as an internal conductance of a nonideal pressure oscillation generator. The volumes of the supply- and return lines are neglected. The pressure at the inlet of the system is p_{in}. The regenerator is regarded as an effective flow conductance C_r and its void volume is neglected ($f_f = 1$). The pulse-tube volume is V_p and the pressure in the pulse tube is p_t. The first orifice, leading to the buffer at pressure p_b, has flow conductance C_1.

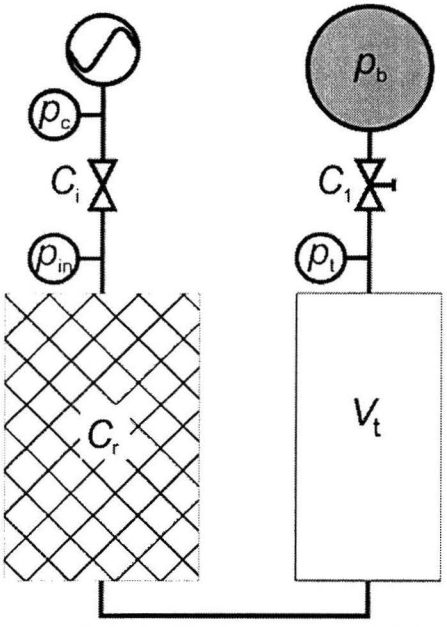

Figure 3-4. An ideal pressure oscillation generator (top left) with flow conductance C_i, connected to a single-stage PTR with regenerator flow conductance C_r and pulse-tube volume V_t. The flow conductance of the first orifice is C_1. Pressures are defined at the compressor (p_c), at the PTR inlet (p_{in}), in the pulse tube (p_t), and in the buffer (p_b).

[3] The amplitude of the pressure oscillations is independent of the amount of gas that is transported.

The pressure oscillation generated by the compressor is assumed to be harmonic

$$p_c = p_0 + p_{c1}\cos(\omega t), \tag{3-1}$$

with p_0 the average pressure, p_{c1} the amplitude of the small pressure oscillations ($p_{c1} \ll p_0$). The flow rate through an orifice is given by equation 2-17. The speeds of the gas at the low- and high-temperature side of the pulse tube are given by

$$v_L = \frac{C_r}{A_t}(p_{in} - p_t), \text{ and} \tag{3-2}$$

$$v_H = \frac{C_i}{A_t}(p_t - p_b). \tag{3-3}$$

Pressure p_{in} can be eliminated by applying conservation of mass and assuming an ideal gas. The average pressure p_0 is used in the ideal-gas law to obtain the molar volume.

$$\dot{n}_r = \dot{n}_i \text{ so } \frac{p_0}{RT_L}C_r(p_{in} - p_t) = \frac{p_0}{RT_H}C_i(p_c - p_{in}) \tag{3-4}$$

Here, $\dot{n}_r$ and $\dot{n}_i$ the molar flow rate through the regenerator and flow conductance C_i. Now,

$$p_{in} = \frac{p_c - p_t}{\frac{T_H}{T_L}\frac{C_r}{C_i} + 1} + p_t, \tag{3-5}$$

so v_L can be written as

$$v_L = \frac{1}{A_t}\frac{p_c - p_t}{\frac{T_H}{T_L}\frac{1}{C_i} + \frac{1}{C_r}}. \tag{3-6}$$

Using equation 2-16

$$\frac{p_c - p_t}{\frac{T_H}{T_L}\frac{1}{C_i} + \frac{1}{C_r}} = C_l(p_t - p_b) + \frac{V_{te}}{p_0}\frac{dp_t}{dt}, \tag{3-7}$$

with the effective pulse tube volume V_{te} given by

$$V_{te} = \frac{C_v}{C_p}V_t. \tag{3-8}$$

Using the harmonic approximation, pressures p_t and p_{in} can be calculated. The buffer pressure p_b is assumed constant and equal to the time-averaged pressure p_0. It can be shown that p_t is given by

$$p_t = p_0 + p_{c1}\frac{\left(1+\frac{C_1}{C_r}+\frac{T_H}{T_L}\frac{C_1}{C_i}\right)\cos(\omega t)+\alpha\left(\frac{C_1}{C_r}+\frac{T_H}{T_L}\frac{C_1}{C_i}\right)\sin(\omega t)}{\left(1+\frac{C_1}{C_r}+\frac{T_H}{T_L}\frac{C_1}{C_i}\right)^2+\alpha^2\left(\frac{C_1}{C_r}+\frac{T_H}{T_L}\frac{C_1}{C_i}\right)^2}, \tag{3-9}$$

with α given by equation 2-22. Pressure p_{in} can be calculated using equation 3-5. The values used in the model in order to obtain an example for the frequency dependent behavior of the system are given in Table 1. The theoretical (frequency-dependent) optimal value for the conductance of the first orifice, given by equation 2-36, is used.

Table 1. Values used for an example of the frequency dependent behavior of the system, based on experimental results of the three-stage PTR. Some values are adjusted to give a better example. Later, in a three-stage model, more accurate values are used.

Variable	Value
T_H	280 K
T_L	80 K
p_0	1.7 MPa
p_1	0.5 MPa
V_t	200 cm^3
C_r	10 (mm^3 s^{-1} Pa^{-1})
C_i	10 (mm^3 s^{-1} Pa^{-1})

The amplitudes of the pressure oscillations in the pulse tube and at the inlet, divided by the compressor pressure-oscillation amplitude, is shown in Figure 3-5.

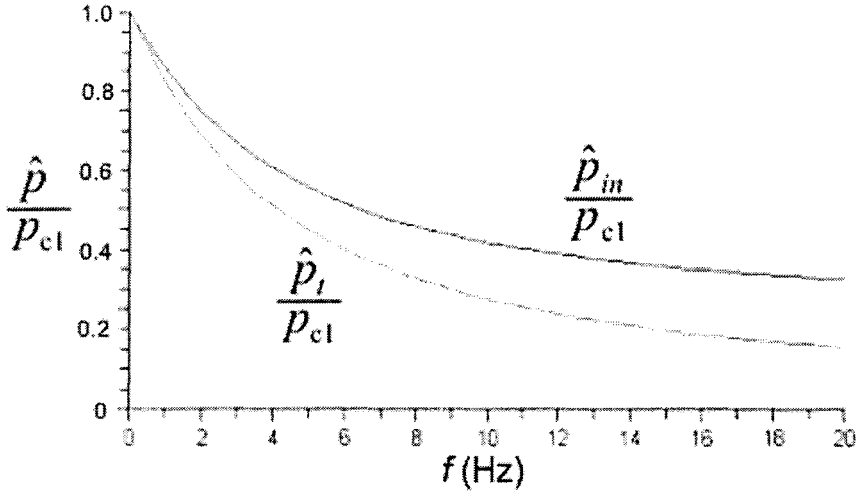

Figure 3-5. The frequency dependencies of the dimensionless amplitude of the inlet pressure p_{in} and pulse-tube pressure p_t for a simple model, represented by equation 3-7.

In this figure, the pressure ratio goes to one as the frequency approaches zero. At f=0 the first orifice is closed and the pulse tube gets time to fill-up completely. Therefore, the pressure amplitude is equal to p_{c1} in the entire system. As the frequency increases, the first orifice is opened gradually, and the pulse tube no longer gets time to fill-up completely. This results in a decreasing pressure amplitude, as can be seen in the figure. It can be shown that for $f \rightarrow \infty$, the pressure amplitude decreases with $1/f^2$.

Next, the time-averaged flow rate is considered. This flow rate should also go to zero if the frequency goes to zero. In a practical situation only the leak rate through the rotary valve and the flow rate through the minor orifices is present, which is not included in this model.

In order to obtain the molar flow rate through the compressor, the molar flow rate in the regenerator $\dot{n}_r$ can be integrated over one cycle, and multiplied by the frequency to get the time-averaged flow rate $\bar{\dot{n}}_r$. The flow through the regenerator is oscillating, so the absolute value of the flow rate is integrated. Furthermore, the gas that is going in during the first half of the cycle is flowing back during the second half. Therefore, the time-averaged absolute flow rate is divided by two, so the gas flow is not double-counted. This results in the time-averaged flow rate through the compressor $\bar{\dot{n}}_c$, indicated in Figure 3-6 (a detail of Figure 2-3).

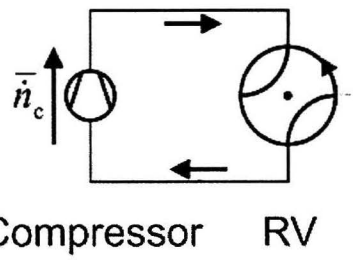

Figure 3-6. Time-averaged compressor molar flow rate $\bar{\dot{n}}_c$.

Using equation 3-4 and 3-5, the time-averaged molar flow rate through the compressor is

$$\bar{\dot{n}}_c = \frac{1}{2}\frac{p_0}{Rt_c}\int_0^{t_c}\left|\frac{p_c - p_t}{\frac{T_H}{C_i}+\frac{T_L}{C_r}}\right| dt, \qquad (3\text{-}10)$$

which can be measured experimentally. Figure 3-7 shows a plot of this flow rate as a function of the frequency. The gas flow per cycle n_c (mol), equal to $\bar{\dot{n}}_c$ divided by the frequency, is shown also.

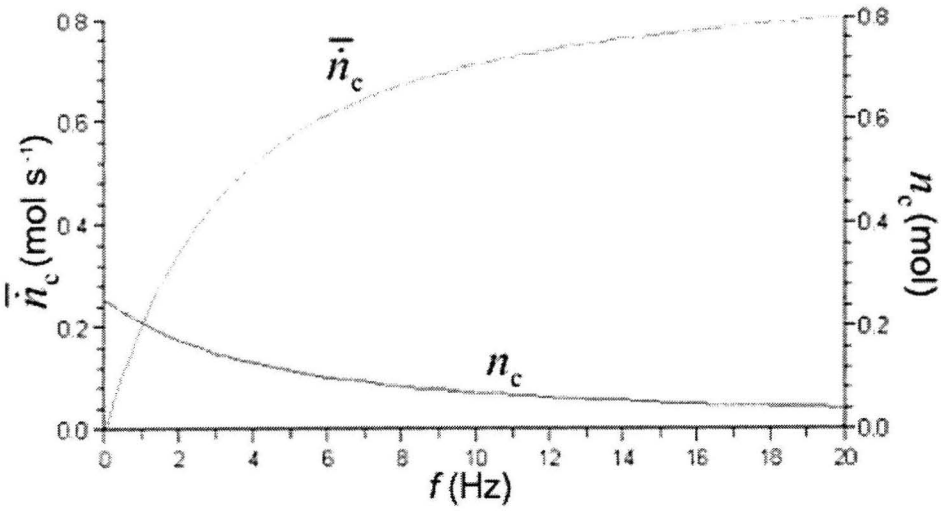

Figure 3-7. The frequency dependency of $\dot{\bar{n}}_c$ and n_c.

It can be seen that the simple model proposed above can give an idea about the frequency dependent behavior of p_{in} and p_t. Due to the decreasing effective impedance of the PTR (caused by the pulse-tube volume in series with a flow conductance) it can be expected that the inlet pressure amplitude decreases when the frequency is increased, as shown in Figure 3-5. On the other hand, the average flow rate will increase when the frequency is increased, as shown in Figure 3-7.

The gas flow per cycle decreases with increasing frequencies. As already mentioned, the Stirling compressor is not suitable for compressing/expanding large volumes, i.e. operating the PTR at low frequencies which requires a large piston displacement. Figure 3-7 shows that this problem may no longer occur for high frequencies.

In this paragraph, the behavior of a three-stage PTR was approximated by a single-stage model. It was not shown that this is a valid approximation. However, it is not difficult to imagine the situation for a three-stage model. In the three-stage case, the pulse-tube pressure oscillations p_t resulting from this model has to be used as p_c for the second stage, where $1/C_i$ for the second stage is taken zero. The same thing can be done for the third stage. It can be expected that the frequency dependent effects become stronger. The three-stage analysis is done in §3.3.3.

3.3 Optimization with increasing frequencies

When the operation frequency of the PTR is increased, various properties of the setup can be optimized in order to obtain optimal cooling power and/or reach the minimum no-load temperature. In this section the methods with which the setup can be optimized are discussed.

3.3.1 Optimizing orifices

As already mentioned, the buffer – first orifice combination determines the phase shift between the gas flow at the hot and cold end of the pulse tube. Optimizing the first orifice boils down to optimizing the phase shift. In §2.3, the equations for the optimal first orifice and double-inlet valve conductances were derived. All orifices are adjustable needle valves. Equation 2-36 shows that the flow conductance of the first orifice should be increased proportional with the frequency, i.e. opening the orifice. For the double-inlet valve, the expression that is found for the optimal flow conductance is not as clear as for the first orifice. However, by filling in equation 2-36 in equation 2-37, it can be seen that the optimal conductivity of the double inlet increases with the frequency (*ceteris paribus*). In practice, the cold-end temperature is highly sensitive to changes in the double-inlet flow conductance. If the cold-end temperature changes, also COP_C changes, which on its turn changes the optimal flow conductance of the double inlet.

In order to estimate the optimal setting of the minor orifice with increasing frequencies, the 'behavior' of the DC flow should be estimated. However, it is difficult to predict which asymmetries are more important than others when the frequency increases. Therefore, the minor orifice is regarded as a 'fine tuning' instrument, the effect of which can be derived from experiments.

The PTR can be optimized for a maximal cooling power, or for a minimum no-load cold-end temperature. When cooling power is required, the cold-end temperature is higher than the no-load temperature. This changes the temperature, and therefore the density and the viscosity of the gas flowing through the cold-end of the regenerator and the pulse tube. As a result, the flow rate at the cold end is different, which means that the optimal settings for the first orifice, double-inlet valve, and minor orifice are different.

3.3.2 Optimizing the regenerator

In §2.2.3 the general requirements of a regenerator were discussed. This section will focus on the consequences for the regenerator when the frequency is increased. Three important aspects of the regenerator are discussed: the heat capacity, the thermal penetration depth and the entropy production.

3.3.2.1 Regenerator: heat capacity

It this section, the volumetric heat capacity of the regenerator material and helium are compared. A correction factor is introduced, which takes into account the amount of helium that flows through the regenerator in a half cycle. This way, the heat capacities of various materials are compared to the heat capacity of the amount of helium that flows

through the regenerator in a half cycle ([13], [16]). The volumetric heat capacity of helium C_{He}^{V} is calculated using the molar heat capacity at constant pressure C_p, the molar weight m_m (4 g/mol) and the density ρ. Superscript V distinguishes the *volumetric* heat capacity from the molar heat capacity.

$$C_{He}^{V} = \frac{\rho}{m_m} C_p \tag{3-11}$$

The first-stage regenerator works in the temperature range of 90 – 300 K. Stainless steel and lead are common materials with a high heat capacity in this temperature range, as can be seen in Figure 3-8.

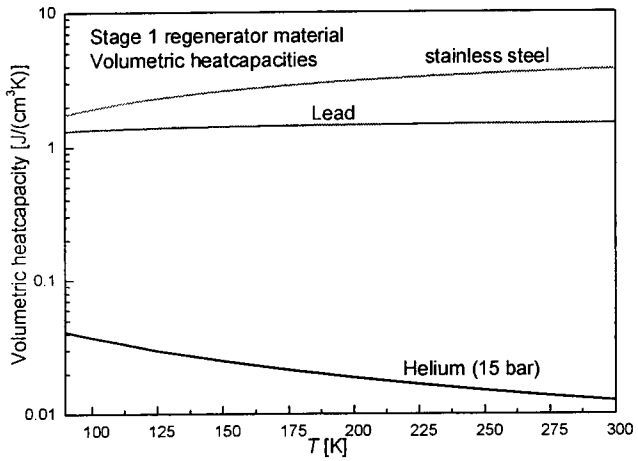

Figure 3-8. The volumetric heat capacity of stainless steel and lead compared to the volumetric heat capacity of helium.

The volumetric heat capacity of stainless steel is approximately 40 times higher (at 90 K) than the volumetric heat capacity of the helium. However, this ratio should be corrected for the amount of helium flowing through the regenerator in a half[4] cycle. Therefore, the volumetric heat capacity ratio should be multiplied by χ, given by

$$\chi = \frac{f_f V_r}{\int_0^{t_c/2} \dot{V} dt}, \tag{3-12}$$

where f_f is the filling factor of the regenerator, and V_r the volume of the regenerator. The (time dependent) flow rate $\dot{V}$ in the regenerator is integrated over a half cycle, representing the displaced volume inside the regenerator.

[4] Half because the gas rejects heat to the regenerator during the first half of the cycle, and takes up heat from the regenerator during the second half. This should not be counted double.

In this work the flow rate, measured using a flow meter, is divided by the frequency in order to get the displaced volume per cycle. Using conservation of mass and the pressure oscillations in the pulse tubes, the displaced volume at the second and the third stage can also be estimated. The heat capacity ratio R_C is defined as χ multiplied by the volumetric heat capacity of the regenerator C_r^V divided by the volumetric heat capacity of helium C_{He}^V.

$$R_C = \chi \frac{C_r^V}{C_{He}^V}. \tag{3-13}$$

If χ is small, a relatively large amount of gas flows through the regenerator, which decreases the heat capacity ratio. A good regenerator has a much higher heat capacity than the gas that is flowing through the regenerator, i.e. when $R_C >> 1$. Table 2 summarizes the values used to calculate χ.

Table 2. Values used to determine the correction factor χ in equation 3-12. A filling factor f_f of 0.35 is used for the first stage. For stages two and three, f_f is 0.6.

Stage	V_r (cm^3)	T (K)	Displaced volume (cm^3)	Correction factor χ
1	128	280	530	0.06
		90	180	0.2
2	40.8	90	160	0.2
		20	34	0.7
3	23.8	20	27	0.5
		2.2	6	2

At the first-stage regenerator hot-end temperature (280 K), the heat capacity ratio of the stainless steel regenerator is 35. At the regenerator's cold end (90 K) this ratio is 12. Because $R_C >> 1$ in both cases, stainless steel has a sufficiently high heat capacity and is suitable as the first-stage regenerator material.

The second-stage regenerator works in the temperature range of 20 – 90 K. The volumetric heat capacity of various materials is compared to helium in Figure 3-9. For temperatures below 70 K, stainless steel no longer has the highest volumetric heat capacity. For temperatures below 70 K, ErPr ([5]) has the highest volumetric heat capacity. For a regenerator at 20 K filled with ErPr, R_C is approximately 3. At 90 K, this ratio is approximately 6. Therefore, based on the heat capacity, ErPr is a suitable material for the temperature range of 20 – 90 K.

[5] Erbium Praseodymium (ErPr) is a magnetic alloy with a volumetric heat capacity 20 – 185 % higher than lead in the temperature range of 10 – 80 K. More information can be found in ref. [20] and [21].

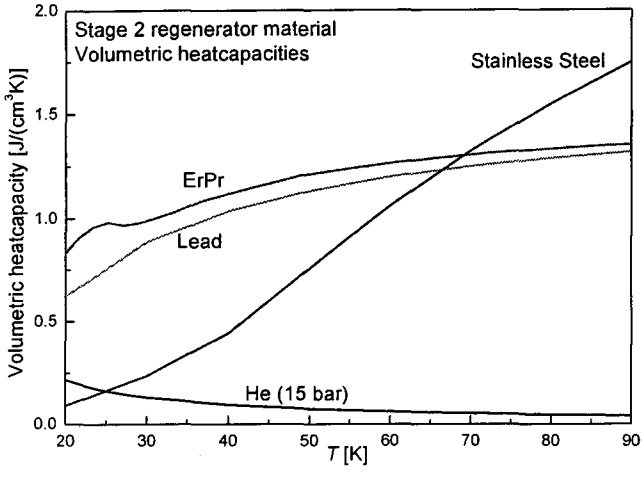

Figure 3-9. The volumetric heat capacity of ErPr, lead, and stainless steel compared to the volumetric heat capacity of helium.

The third-stage regenerator works at temperatures as low as 2 – 20 K. For this temperature range, it becomes increasingly difficult to find materials that have a high volumetric heat capacity compared to helium, as can be seen in Figure 3-10. The best choice would be to use a regenerator consisting of layers of $ErNi_{0.9}Co_{0.1}$, ErNi and ErPr. However, the material in this three-layer configuration must be separated and fixed very well, in order to ensure that the material does not mix or move (causing dissipation). In principle this can be done, but it can severely complicate the regenerator geometry, making it elaborate to produce and increasing its susceptibility to failure. In this work a two-layer configuration is used.

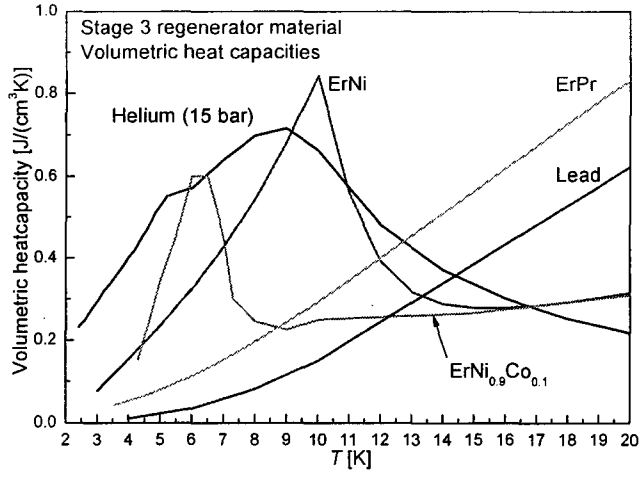

Figure 3-10. The volumetric heat capacity of several materials compared to the volumetric heat capacity of helium.

Because the temperatures in the third stage are so low, the density of helium is high and the displaced volume is low. Therefore, based on a displaced volume of ~6 cm^3 at the third-stage cold end, the correction factor $\chi > 1$. A two-layer regenerator consisting of $ErNi_{0.9}Co_{0.1}$ and ErNi is taken as an example. At 20 K, an ErNi regenerator has a heat capacity which is approximately equal to the heat capacity of the displaced helium. For an $ErNi_{0.9}Co_{0.1}$ regenerator at 4 K ([6]) this ratio is also approximately one.

An overview of the materials and dimensions of the first-, the second-, and the third-stage regenerator, used in this work, is shown in Table 3 and Table 4, respectively. It can be seen that in the first- and the third stage, a two-layer configuration has been chosen.

Table 3. Materials used for the regenerators. A detailed description of the first-stage regenerator is given in Appendix A.

Stage	Material	Size or amount	Filling factor f_f
1 (hot end)	Stainless steel	957 screens of mesh 200	0.33
1 (cold end)	Stainless steel	2 Sintered blocks of 19.7 mm	0.51
2	ErPr	0.25 – 0.30 mm grain size	0.61
3 (hot end)	ErNi	0.20 – 0.24 mm grain size	0.61
3 (cold end)	$ErNi_{0.9}Co_{0.1}$	0.20 – 0.50 mm grain size	0.59

Table 4. Regenerator housing dimensions (material: stainless steel).

Stage	1	2	3
Inner diameter (mm)	34	20	14
Wall thickness (mm)	0.6	0.5	0.4
Length (mm)	141	130	155
Volume (cm^3)	128	40.8	23.8

So far, the consequences of increasing the frequency have not been considered. In §3.2 it was found that the flow, passing through the regenerator per cycle (or displaced volume), decreases with increasing frequencies. This means that for high frequencies, the regenerator material comes in thermal contact with less helium than for low frequencies. Consequently, less regenerator material is needed to store heat, and the regenerator can be made smaller.

3.3.2.2 Regenerator: thermal penetration depth

In §2.2.3 it was discussed that the thermal penetration depth is a measure up to which extent (depth) a material is capable of exchanging heat with its surroundings within a certain time. Therefore, it is an important parameter in determining the (optimal) feature size (e.g. grain radius, mesh number) of the regenerator material. Generally, the thermal penetration depth of the regenerator material should be larger than the feature size of the regenerator material in order to ensure maximum heat exchange. The thermal penetration depth of the working gas should be larger than the size of the pores in the regenerator.

[6] Unfortunately, no volumetric heat capacity data for $ErNi_{0.9}Co_{0.1}$ below 4 K is available.

In this chapter, the thermal penetration depths of various regenerator materials and helium are shown. Next, a model is presented that describes the thermal behavior of particles (spheres) inside a regenerator. This model is used to find a relation between the regenerator's ability to store heat, the oscillation frequency, and the particle size.

Figure 3-11 shows the thermal penetration depth of helium, stainless steel, and lead for the first-stage regenerator temperature range for a frequency of 1.8 Hz. This frequency is typical for the three-stage PTR used in this work. The thermal penetration depth of helium is calculated based on the properties of helium at 15 bar. However, the pressure in the setup ranges from 12 – 21 bar, which results in 15 % increase or decrease of the thermal penetration depth.

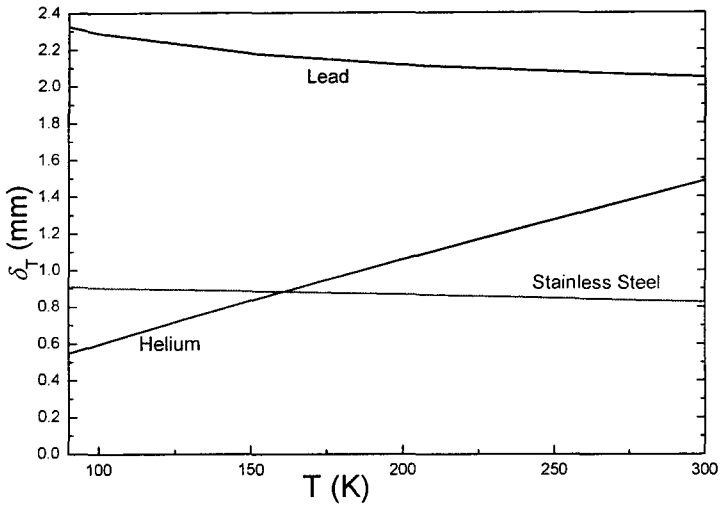

Figure 3-11. The thermal penetration depth of lead, stainless steel, and helium for 1.8 Hz.

The stainless-steel mesh 200 screens in the first-stage regenerator consist of wires of 50 μm thick. The thermal penetration depth is nearly 20 times larger. Figure 3-12 and Figure 3-13 show δ_T for the second- and the third-stage regenerator temperature range for various materials. It should be noted that the values for the δ_T of lead is based on *pure* lead. If an alloy is used instead, the mean free path of the electrons can significantly be reduced (especially at low temperatures, where electron – phonon scattering plays a minor role) [17]. In this case the thermal conductivity can be two orders of magnitude lower than for a pure material. This decreases δ_T by one order of magnitude. The size of the ErPr particles in the second stage is 0.25 – 0.3 mm. The thermal penetration depth is approximately 5 times larger, which is also the case for the ErNi particles in the third stage. Unfortunately, no data on the thermal penetration depth of $ErNi_{0.9}Co_{0.1}$ is available.

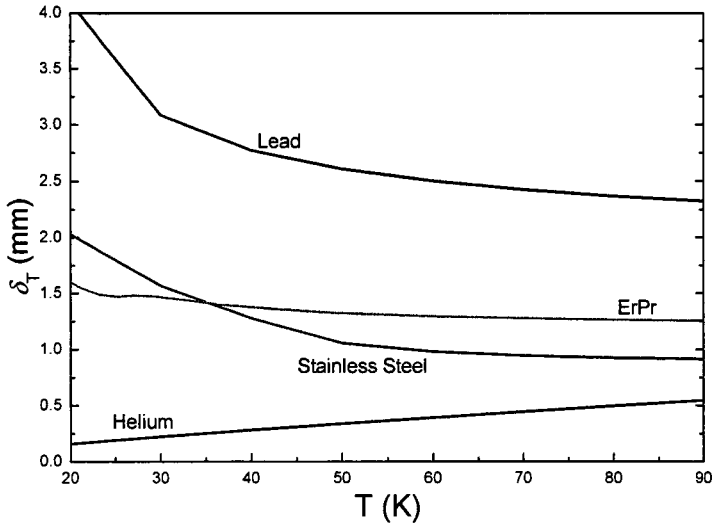

Figure 3-12. The thermal penetration depth of lead, ErPr, stainless steel, and helium for 1.8 Hz.

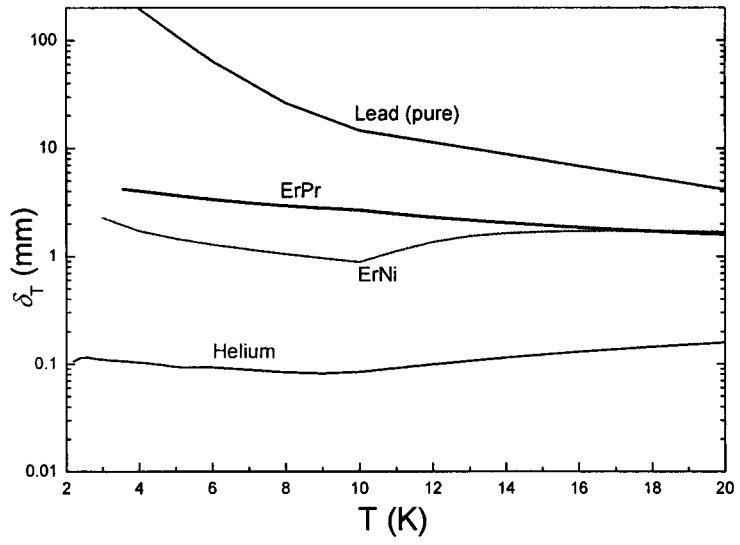

Figure 3-13. The thermal penetration depth of several materials and helium for 1.8 Hz. Values for lead are based on pure lead material properties.

So far it has been assumed that the thermal penetration depth of the regenerator materials can be taken as a guide for the regenerator mesh- or grain size. However, also the thermal penetration depth of helium should match the size of the pores between the regenerator grains. It can be shown that in a tetrahedral structure, the holes are 4 – 5 times smaller than the grains. Consequently, the smaller pore size compensates for the smaller thermal penetration depth in helium compared to the regenerator material (see Figure 3-11, Figure 3-12, and Figure 3-13).

In this work, an attempt has been made to make the relation between the grain size and the regenerator's ability to store heat more precise. Here, also the spherical geometry and 'wet' surface area per unit volume (as a function of the particle size) is taken into account. Furthermore, the frequency dependency is examined.

The model

In order to examine the relation between the grain size and the amount of heat stored in the material, a model can be constructed. This model is based on three equations.

In the regenerator material is a heat flow $\dot{Q}$ (J s^{-1}) and an internal energy U (J). By the first law of thermodynamics, a heat flow leads to a change of internal energy (in the absence of work).

$$\dot{Q} = \dot{U} \tag{3-14}$$

In a thin shell of the sphere of thickness Δr, a temperature change leads to a change of internal energy.

$$\Delta \dot{U} = \rho c 4\pi r^2 \frac{\partial T(r,t)}{\partial t} \Delta r, \tag{3-15}$$

where c is the specific heat capacity, ρ the material density and T the temperature being dependent on radius r and time t. For ρc the volumetric heat capacity C is used from now on. The heat flow through the shell surface at radius r is dependent on the local temperature gradient.

$$\dot{Q} = -4\pi r^2 \kappa \frac{\partial T(r,t)}{\partial r}, \tag{3-16}$$

where κ is the thermal conductivity of the material.

By combining the three equations given above, the following second order homogeneous partial differential equation can be derived.

$$\frac{C}{\kappa} \frac{\partial T(r,t)}{\partial t} = \frac{2}{r} \frac{\partial T(r,t)}{\partial r} + \frac{\partial^2 T(r,t)}{\partial r^2} \tag{3-17}$$

This equation can be simplified by substituting

$$T(r,t) = \frac{F(r,t)}{r}. \tag{3-18}$$

Now equation 3-17 can be written as

$$\frac{C}{\kappa}\frac{\partial T(r,t)}{\partial t}=\frac{\partial^2 F(r,t)}{\partial r^2}. \tag{3-19}$$

The time dependency of the temperature inside the regenerating is assumed harmonic due to the oscillating flow.

$$T(r,t)=\frac{F(r,t)}{r}=T_0+\frac{F_x(r)}{r}\cos(\omega t)+\frac{F_y(r)}{r}\sin(\omega t), \tag{3-20}$$

with T_0 the mean temperature which is independent of time and location. Substituting this equation into equation 3-17 gives

$$F_x(r)=-\frac{\delta_T^2}{2}\frac{\partial^2 F_y(r)}{\partial r^2} \text{ and } F_y(r)=\frac{\delta_T^2}{2}\frac{\partial^2 F_x(r)}{\partial r^2}, \tag{3-21}$$

so

$$F_x(r)=-\frac{\delta_T^4}{4}\frac{\partial^4 F_x(r)}{\partial r^4}, \tag{3-22}$$

where δ_T is given by equation 2-12. This is a fourth order linear homogeneous differential equation with constant coefficients in quadrature format. It can be shown that the general solution of this differential equation is a linear combination of four independent solutions (ref. [22] §17.7)

$$F_x(r)=C_1 e^x \sin x+C_2 e^x \cos x+C_3 e^{-x}\sin x+C_4 e^{-x}\cos x, \tag{3-23a}$$

and

$$F_y(r)=C_1 e^x \cos x-C_2 e^x \sin x-C_3 e^{-x}\cos x+C_4 e^{-x}\sin x, \tag{3-23b}$$

with $x=r/\delta_T$ the dimensionless radius. Here, δ_T (and hence C and κ) is constant and independent of r. Making C and κ time dependent would lead to second order corrections, which are neglected in this harmonic approximation. Values for C_1, C_2, C_3, and C_4 follow from boundary conditions. One of these conditions is that the temperature does not become infinite in the core of the grain. If $\lim_{r\to 0} T(r) < \infty$ it follows that for $F_x(r)/r$ and for $F_y(r)/r$ the cosine terms have to cancel: $C_2 = -C_4$ and $C_1 = C_3$. Equation 3-23 can now be written as

$$F_x(r)=C_1\left(e^x+e^{-x}\right)\sin x+C_2\left(e^x-e^{-x}\right)\cos x, \tag{3-24a}$$

and

$$F_y(r) = C_1\left(e^{x} - e^{-x}\right)\cos x - C_2\left(e^{x} + e^{-x}\right)\sin x. \tag{3-24b}$$

It is interesting to examine the temperature profile and heat transport in the sphere if a sinusoidal temperature variation (which was already assumed in equation 3-20) is imposed on the boundary of the sphere. This assumption is only valid if the gas is in good thermal contact with the grain surface, otherwise the temperature of the gas at the grain surface will drop/raise when heat is transported to/from the grain.

$$T(r=a) = T_0 + T_1\cos(\omega t), \tag{3-25}$$

where a is the radius of the spheres and T_1 the amplitude of the temperature oscillation. With this boundary condition, C_1 and C_2 are fixed and given by

$$C_1 = aT_1\frac{\sin\left(\frac{a}{\delta_T}\right)\left(e^{\frac{a}{\delta_T}} + e^{-\frac{a}{\delta_T}}\right)}{\left[2\cos\left(\frac{a}{\delta_T}\right)\right]^2 - \left(e^{\frac{a}{\delta_T}} + e^{-\frac{a}{\delta_T}}\right)^2}, \tag{3-26a}$$

and

$$C_2 = aT_1\frac{\cos\left(\frac{a}{\delta_T}\right)\left(e^{\frac{a}{\delta_T}} - e^{-\frac{a}{\delta_T}}\right)}{\left[2\cos\left(\frac{a}{\delta_T}\right)\right]^2 - \left(e^{\frac{a}{\delta_T}} + e^{-\frac{a}{\delta_T}}\right)^2}. \tag{3-26b}$$

It is now possible to calculate the temperature profiles and (with equation 3-16) the thermal conduction profiles in the grains. It is also interesting to calculate the amount of energy stored per unit volume in half a cycle. This can be seen as an effective heat capacity of the regenerator, taking into account the frequency of the oscillating gas flow, the grain size, the filling factor, and the material properties.

$$C_{reg} = \frac{f_f}{\frac{4}{3}\pi a^3}\frac{4\pi a^2}{T_1}\frac{1}{2}\int_{t=0}^{t=2\pi/\omega}\left|\left[\kappa\frac{\partial T(r,t)}{\partial r}\right]_{r=a}\right| dt \tag{3-27}$$

Here, the first term on the right hand side is the amount of grains in one cubic meter of regenerator, also taking into account the filling factor. The second term is the surface area of a grain divided by the temperature oscillation amplitude. The last term is the integration over the heat flux at the grain boundary over one cycle. Because the heat flux changes sign every half cycle, the absolute value is taken. The factor ½ corrects the integration for the heat that is going in *and* out the grain, effectively turning the full cycle integration into a half cycle integration.

A complicating factor is the phase shift between $T(a,t)$ and $\dot{Q}(a,t)$. Generally, $\dot{Q}(a,t)$ is maximal if the temperature changes fastest because the regenerator material has not had enough time to adjust to the new temperature. This means that $\dot{Q}(a,t)$ is in phase with the time derivative of the temperature $\dot{T}(a,t)$. In the example shown next, it has indeed been found that this phase difference is smaller than 1 %.

Heat capacity C_{reg} versus the grain size a can be plotted for various values of κ, C and ω. In Figure 3-14 the effective volumetric heat capacity C_{reg} is divided by the maximum volumetric heat capacity C_{max} ($= f_f \cdot C$) and plotted versus the dimensionless grain size a/δ_T (δ_T given by 2-12). This results in a frequency-independent characteristic plot for the effective heat capacity of the regenerator as a function of the grain size. For this example the material properties of ErPr at 30 K have been used.

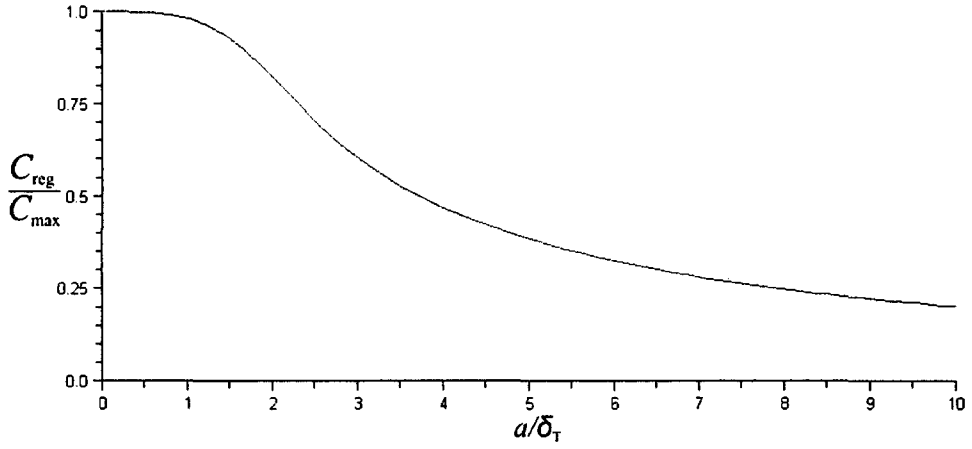

Figure 3-14. The dimensionless heat capacity of ErPr versus the dimensionless grain size.

As can be seen in Figure 3-14, the grain size where the effective volumetric heat capacity starts decreasing coincides with δ_T. At this particle size the heat exchange takes place all the way into the core of the grains. Further decreasing the size does not increase the effective heat capacity of the regenerator, as can be seen. However, in this model perfect thermal contact between the gas and the grain surface was assumed. In reality this is not the case, i.e. when δ_T of the gas is smaller than the size of the pores between the grains. In this case it may be necessary to further decrease the regenerator grain size in order to improve the heat exchange. *Increasing* the particle size decreases the heat capacity because the core of the grains does no longer participate in the heat exchange between the regenerator material and the gas. When the heat exchange between the gas and the regenerator material is optimal, increasing the particle size may be beneficial in terms of decreasing losses due to flow resistance. As can be seen in Figure 3-14, going from δ_T to $2\delta_T$ decreases the effective heat capacity only by 16 %.

In conclusion, this model can be useful when comparing different regenerator materials and grain sizes for different frequencies and filling factors. However, there are limitations which can be addressed in future work. The limited heat capacity and thermal penetration depth of the surrounding gas can be taken into account in order to obtain a more realistic result for the amount of heat that is exchanged. This can be accomplished by adding an extra shell of a different material, with different values for κ and C, around the initial grain (for $r > a$). Extra boundary conditions are necessary: both the temperature and $\dot{Q}$ must be continuous on $r=a$.

3.3.2.3 Regenerator: losses

The losses inside the regenerator consist of four contributions. The first two are caused by thermal conduction through the regenerator material and the working gas. This way, heat from the hot end of the regenerator can be transported to the cold end. Furthermore, entropy is produced due to heat exchange between the working gas and the regenerator material. Finally, entropy is produced due to the nonzero flow resistance of the regenerator material.

Entropy production due to thermal conduction

In ref. [15] measurements of the thermal conduction through regenerators with a similar composition as used in this work are published. In this work a conduction degradation factor f_{CD} is introduced. This is the correction factor for the thermal conduction through a regenerator packed with spheres (or screens) instead of a solid bar of the same amount of material and with the same cross-sectional surface area. Factor f_{CD} is a geometrical factor, not a correction for the porosity (which is f_f). The heat flow through a regenerator with length L_r, surface area A_r, matrix material thermal conductivity κ, filling factor f_f, cold-end temperature T_L, and hot end temperature T_H, is given by

$$\dot{Q}_c = \frac{A_r}{L_r} f_{CD} f_f \int_{T_L}^{T_H} \kappa \, dT . \tag{3-28}$$

It should be noted that this is the contribution of the thermal conduction through the regenerator material only, and not the conduction through the working gas. With ref. [13] the total entropy production in the regenerator due to axial conduction losses through the gas and the regenerator material are respectively

$$\dot{S}_{cg} = A_r f_{f,g} f_{CD,g} \int_0^{L_r} \frac{\kappa_g}{T_g^2} \left(\frac{\partial T_g}{\partial l} \right)^2 dl , \tag{3-29a}$$

and

$$\dot{S}_{cr} = A_r f_{f,r} f_{CD,r} \int_0^{L_r} \frac{\kappa_r}{T_r^2} \left(\frac{\partial T_r}{\partial l} \right)^2 dl , \tag{3-29b}$$

with $f_{f,g} + f_{f,r} = 1$, and subscript c indicating the loss due to conduction, and subscript g and r indicating the contributions of the gas and regenerator material, respectively.

Generally, the conduction degradation factors of the regenerator material and the working gas are different. Note that κ_g and κ_r are the real thermal conductivities instead of the effective thermal conductivity used in [13]. In practice $f_{f,g} \approx f_{f,r}$ and $\kappa_g << \kappa_r$, so the conduction through the working gas can be neglected. With a smooth temperature profile in the regenerator, and $T_L << T_H$ equation 3-29 can be approximated roughly by

$$\dot{S}_c \approx S_{cr} \approx f_{f,r} f_{CD,r} \kappa_r \frac{A_r}{L_r} \frac{T_H^2}{T_L^2}, \tag{3-30}$$

where κ_r is evaluated at T_L. It is now interesting to investigate what happens to the axial thermal conductivity (losses) if the system frequency is increased. The equations above do not show a direct relation between the frequency and the thermal conduction losses. If the temperature distribution, the dimensions, and the material properties remain constant, the conduction losses will not change. However, when the frequency increases, it may be necessary to change the dimensions or the material of the regenerator. Also, it may be necessary to increase the average pressure of the working gas in order to maintain a certain pressure amplitude in the pulse tubes. So even though the frequency is not directly related to the thermal conduction losses, it can still be meaningful to investigate the indirect consequences.

Increasing mean pressure
In [15] it is concluded that, even though the thermal conduction through the helium itself, helium plays an important role in the axial thermal conduction through the regenerator material. The sphere to sphere contact area is very small. The presence of helium near these contacts can enhance the axial thermal conductivity of the regenerator by two orders of magnitude compared to vacuum conditions. However, above 5 bar, the thermal conductivity no longer increases with increasing pressure. Therefore, it can be assumed that above 5 bar, the conduction losses through the regenerator material $\dot{S}_{cr}$ are constant.

For the conduction through the working gas only, a similar analysis can be done. It can be shown that this contribution is much smaller than $\dot{S}_{cr}$ ($\kappa_g << \kappa_r$). Furthermore, the thermal conductivity of helium does not change more than 5 % if the pressure is changed from 10 to 20 bar. Therefore, it can be concluded that increasing the average system pressure does not change the losses due to axial thermal conductivity.

Decreasing the particle size
The thermal penetration depth decreases with the square root of the frequency. In order to maintain optimal heat exchange, it may be necessary to decrease the regenerator particle or mesh size. Because this changes the amount of contacts and the size of the contacts of the regenerator grains or screens, this may change the conductivity degradation factor f_{CD} of the regenerator. In equation 3-29 it can be seen that this has consequences for the losses due to axial conductivity.

The filling factor of stacked screens is given by [16]:

$$f_{f,r} = \frac{\pi}{4} n d, \tag{3-31}$$

with n the mesh density (m^{-1}) and d (m) the wire thickness. It is clear that if nd remains constant, the filling factor (and therefore, also the losses due to axial conduction) will not change. A typical filling factor for stacked screens is 0.3.

When spheres are used, the theoretical maximum filling factor for hexagonal close packing is 0.74. However, since the regenerator is not filled manually grain-by-grain, it is better to use the filling factor of randomly packed spheres, which is 0.64. In practice, even a filling factor of 0.64 is hard to reach. Typically, values of 0.55 – 0.63 are obtained.

From [15], no clear relation was found between the conductivity degradation factor f_{CD} and the particle size, the mesh size, or the porosity. Therefore, f_{CD} is assumed constant in the relevant range of material dimensions. Obviously, this will have no effect on the losses due to thermal conductivity. A typical value for f_{CD} for stainless steel screens and spheres is 0.11.

Changing aspect ratio A_r/L_r
There can be several reasons why the area A_r over length L_r ratio (aspect ratio) of the regenerators should be changed if the frequency is increased. As discussed earlier in §3.2, the amount of gas flowing through the regenerator per cycle decreases. Therefore, less material is needed for heat storage, and the regenerator can be made smaller. It may also be necessary to decrease the pressure drop in the regenerators in order to maintain a certain pressure amplitude in the pulse tubes. This can be done by increasing the aspect ration A_r/L_r.

If the surface area is increased the axial conduction losses are increased proportionally, as can bee seen from equation 3-29. Changing the length of the regenerator is somewhat more complicated, because the solution for equation 3-29 depends on the axial temperature profile. Assuming a smooth (e.g. linear) temperature profile, it can be seen from equation 3-30 that decreasing the length of the regenerator increases the axial conduction losses proportionally.

When the dimensions of the housing are changed the thermal conduction through the housing wall may also change. This effect can be treated in a similar way to the axial conduction through the regenerator material. If the aspect ratio is varied, but the wall-thickness δ to radius r ratio is constant, the thermal conduction area of the housing A_h scales proportionally with the regenerator housing inner surface area A_r.

It is possible to compare the losses due to thermal conduction through the housing with the losses due to conduction through the regenerator itself. The surface area of the wall is typically 3 – 6 % of the inner surface area A_r. However, the parameters f_f and f_{CD} are equal to 1 for the wall (bulk material), while they are typically 0.5 and 0.1, respectively,

for the regenerator itself. Therefore, the losses due to thermal conduction through the housing can be of the same order as the losses due to thermal conduction through the regenerator itself.

Entropy production due to irreversible heat exchange

Due to irreversible heat exchange between the regenerator material and the gas, entropy is produced. In ref. [13] this contribution has been treated thoroughly. The following steps, up to equation 3-38, are all taken or derived from this article. An expression for the entropy production was derived

$$\dot{S}_e = A_r \int_0^{L_r} \frac{\beta (T_r - T_g)^2}{T_r T_g} dl, \tag{3-32}$$

where β (J s^{-1} K^{-1} m^{-3}) can be written as

$$\beta = g_\beta \frac{\kappa_g}{\delta^2}, \tag{3-33}$$

with g_β a geometrical factor of order one and δ the grain size. The next step is to make some rigorous assumptions in order to find a solution for equation 3-32.

An expression for $\beta(T_r - T_g)$ can be derived using the energy balance for the gas inside the regenerator

$$\frac{(1-f_f)C_p}{V_m}\frac{\partial T_g}{\partial t} - \frac{(1-f_f)T_g}{V_m}\left(\frac{\partial V_m}{\partial T_g}\right)_p \frac{\partial p}{\partial t} + jC_p \frac{\partial T_g}{\partial l} + j\left[V_m - T_g\left(\frac{\partial V_m}{\partial T_g}\right)_p\right]\frac{\partial p}{\partial l} = \beta(T_r - T_g) + \frac{\partial}{\partial l}\left(\kappa_g \frac{\partial T_g}{\partial l}\right), \tag{3-34}$$

which takes into account the variation of the molar enthalpy flow in time and in location (left hand side of the equation), the heat flow to the gas due to heat exchange with the regenerator material per unit volume (= $A_t \partial l$) (first leg on the right hand side of the equation), and the thermal conduction per unit volume (second leg on the right hand side of the equation). Here, j is the molar flow rate density (mol s^{-1} m^{-2}), and V_m the molar volume. For details on the derivation of this equation, see ref. [13]. For an ideal gas,

$$T_g\left(\frac{\partial V_m}{\partial T_g}\right)_p = V_m, \tag{3-35}$$

which simplifies the $\partial p/\partial t$ prefactor, and cancels the $\partial p/\partial l$ term. Assuming a sufficiently large filling factor, so $(1\text{-}f_f)\approx 0$, the first and the second term on the left hand side of the equation can be neglected. Also, the thermal conduction through the gas is neglected.

Finally, a 'smooth' temperature distribution in the regenerator is assumed

$$\frac{\partial T_g}{\partial l} \approx \frac{T_H}{L}. \tag{3-36}$$

Now, the simplified energy balance is given by

$$\beta\left(T_r - T_g\right) \approx \frac{n_c C_p}{t_c A_r} \frac{T_H}{L_r}, \tag{3-37}$$

with n_c ($=j\, t_c\, A_r$) the amount of moles of gas participating in one cooling cycle, and t_c (s) the cycle time ($=2\pi/\omega$). With $T_g = T_r = T_L$, the entropy production in the regenerator (equation 3-32) becomes

$$\dot{S}_e \approx \frac{C_{m,p}^2 \delta^2}{\kappa_g g_\beta V_r} \frac{T_H^2}{T_L^2} \frac{n_c^2}{t_c^2}. \tag{3-38}$$

This equation can be used to derive the frequency dependent behavior of the losses due to irreversible heat exchange in the regenerator. For the last term $(n_c/t_c)^2$ the following can be shown

$$\frac{n_c^2}{t_c^2} \propto \left(n_c f\right)^2 = \left(\bar{\dot{n}}_c\right)^2, \tag{3-39}$$

which is the square of the time-averaged molar flow rate in the compressor. From §3.2 (Figure 3-7) it can be seen that for system used for this example, the total flow rate increases with increasing frequencies for frequencies lower than ~10 Hz. For higher frequencies the flow rate stabilizes. The same frequency dependent behavior can be expected for the losses due to irreversible heat exchange, albeit that these losses increase with the square of the flow rate.

As discussed in §3.3.2 it is necessary to decrease the particle size at a certain frequency when the thermal penetration depth becomes too small. From equation 3-38 it can be seen that decreasing the particle size δ can significantly decrease the entropy production.

The aspect ratio can be found in V_r. The aspect ratio can be changed without changing the regenerator volume. However, in §3.3.2 it was noted that it may be possible to decrease the size of the regenerator because less heat capacity is required at higher frequencies. Decreasing the regenerator volume will increase the heat exchange losses.

Entropy production due to flow resistance

In ref. 73[13] also the viscous contribution can be found. It is expected that the viscous dissipation is high at the high temperature region of the regenerator. The first reason for this is that the viscosity of helium is higher at higher temperatures, as can be seen in

Figure 3-15. The second reason is that the volumetric flow rate is higher. This is caused by the high temperature, and hence the small helium density. Moreover, all the gas that goes to the second and the third stage must pass through stage one (and two).

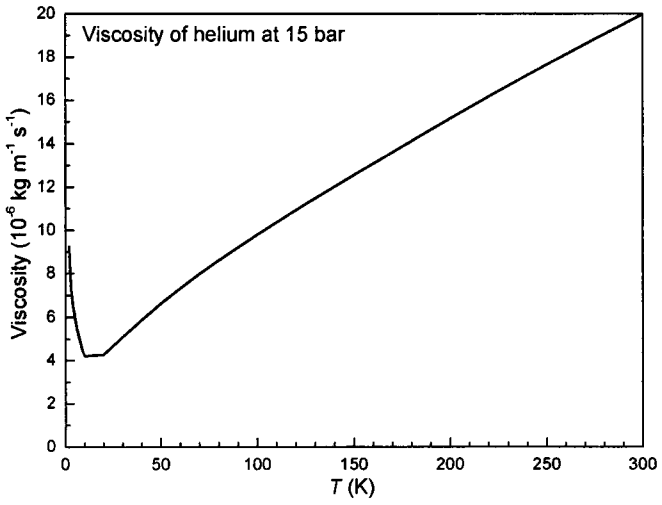

Figure 3-15. Viscosity of helium at 15 bar as a function of the temperature.

The general equation for the viscous losses is

$$\dot{S}_z = A_r \int_0^{L_r} \frac{\eta z_r (jV_m)^2}{T_g} dl . \tag{3-40}$$

Because the viscous dissipation primarily takes place in the high temperature region, the ideal gas law can be used to find V_m. Furthermore, T_H is taken as a measure for T_g and the value for η is taken at T_H. In order to calculate the flow resistance, the regenerator is approximated by a matrix of channels. For a laminar flow[7] running through a number of channels proportional to δ^{-2}, with δ the diameter of the channels, the flow resistance is given by

$$z_r = \frac{g_z}{\delta^2},$$

with g_z a geometrical factor of order 10. The entropy production is now given by

$$\dot{S}_z \approx \frac{\eta\, g_z\, R^2 T_H L_r}{\delta^2 p^2 A_r} \frac{n_c^2}{t_c^2} . \tag{3-41}$$

[7] Typical Reynolds numbers are in the order of one [13].

Again equation 3-39 and Figure 3-7 can be used to predict the frequency dependent behavior. For the system used for this example, the viscous losses increase for $f < \sim 10$ Hz, and remain constant higher frequencies.

As expected, decreasing the particle size δ increases the viscous losses quadratically. If conduction losses can be limited, it may be possible to counter-act the viscous losses by increasing the aspect ratio A_r/L_r. This way, the flow can be divided over more and shorter channels while keeping the total heat capacity of the regenerator constant.

Finally, the average pressure also plays an important role in the viscous losses. Increasing the pressure from 10 to 20 bar will slightly increase the viscosity, which will slightly increase the viscous losses. However, because the molar volume decreases proportionally with increasing pressure, and the viscous losses are dependent on the square of the molar volume (equation 3-40), the viscous losses will decrease with the square of the pressure.

Combining equations 3-30, 3-38, and 3-41 the total entropy production in the regenerator $\dot{S}_r$ due to axial conduction, irreversible heat exchange, and viscous dissipation can be calculated. The axial conduction losses of the gas are neglected.

$$\dot{S}_r \approx f_{f,r} f_{CD,r} \kappa_r \frac{A_r}{L_r}\frac{T_H^2}{T_L^2} + \frac{C_{im,p}^2 \delta^2}{\kappa_g g_\beta V_r}\frac{T_H^2}{T_L^2}\frac{n_c^2}{t_c^2} + \frac{\eta g_z R^2 T_H L_r}{\delta^2 p^2 A_r}\frac{n_c^2}{t_c^2} \tag{3-42}$$

3.3.3 Optimizing the pulse tubes

The main design properties of the pulse tubes are its dimensions (aspect ratio) and flow straighteners. When the gas enters or leaves the pulse tube it encounters an abrupt change in the tube cross-section, which generates turbulence. The surface area changes from the pulse-tube surface area A_p to the surface area of the connection tubes, which is much smaller, or *vice versa*. Also, turbulent losses occur at high Reynolds numbers *Re*. Generally, *Re* is in the order of one for characteristic parameters [14], which is well below the critical Reynolds number of ~2000. Turbulence causes hot and cold gas to mix, which generates entropy. The flow straighteners can significantly reduce the turbulent losses.

The losses due to irreversible heat exchange between the gas and the tube walls, and the losses due to axial heat conduction can be treated similarly to the losses described in §3.3.2. The flow resistance and the consequent losses in the pulse tube are assumed negligible.

3.3.3.1 Shuttle heat loss

An effect playing an important role in the pulse tubes is the heat exchange between the gas and the tube wall, often called 'shuttle heat loss' or 'surface heat pumping' [23], [24]. As already mentioned, gas warms up or cools down when it is compressed or expanded adiabatically (equation 2-3). At the same time, the gas in the pulse tube moves back and forth in the pulse tube (Figure 2-5). The tube wall is assumed to have a cycle-averaged temperature, which decreases approximately linearly from the pulse-tube hot end to the

cold end. Figure 3-16 shows the movement of gas elements that are being compressed at various positions in the pulse tube, and the temperature of the gas elements. Also shown are the linear temperature profiles of the tube wall. A similar plot can be made for the expansion of the gas.

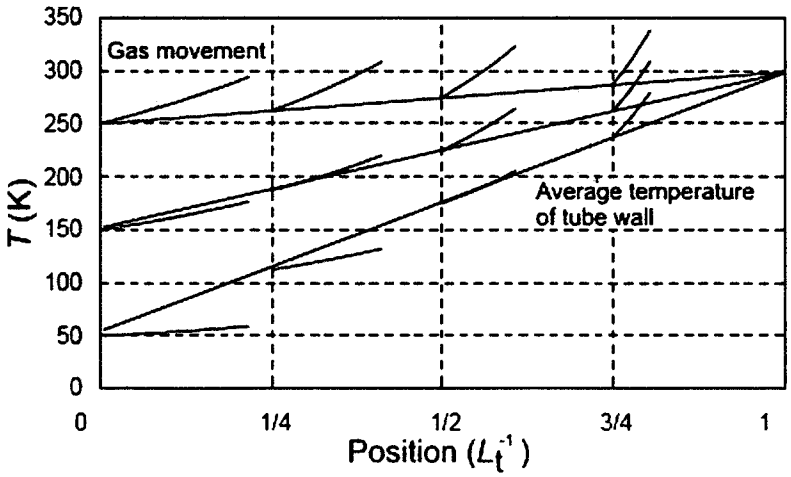

Figure 3-16. Temperature and movement of gas elements at various positions in the pulse tube, due to compression, for cold-end temperatures of 250, 150 and 50 K (Picture courtesy ref. [23]).

Focus on the 250 K cold-end temperature line. During compression the gas moves towards the hot end (right). The gas is warmer than the tube's wall and consequently heat is released to the tube's wall. During expansion, when the gas moves towards the cold end (left), the gas is colder than the tube walls and heat is transported from the wall to the gas. By transferring heat between the gas and the wall, heat is pumped from the cold end towards the hot end. The cooling of the basic PTR is based on this effect.

For the 150 K cold-end temperature line, this effect is still present when the gas element is further than ¼ L_t inside the tube. However, near the cold end the effect reverses. This reversed effect is stronger for a cold-end temperature of 50 K. In this case the gas still heats up during compression (causing the temperature to rise with ΔT), and moves towards the right over a distance Δx. However, $\Delta T/\Delta x$ is smaller than the temperature gradient in the tube wall. Consequently, heat is taken from the tube wall when the gas moves towards the hot end, and heat is released when gas moves towards the cold end. This causes heat to be 'pumped' from the pulse-tube hot end to the cold end, increasing the heat load on the cold end.

The shuttle heat effect can only take place near the wall of the tube, within the thermal boundary layer. For pulse tubes with a large surface area the amount of gas within the thermal boundary layer of the wall is small compared to the amount of gas that is isolated from the wall and can be considered adiabatic. If the radius of the pulse tube is large compared to the thermal penetration depth, the shuttle heat loss is relatively small. The thermal boundary layer has a thickness equal to the thermal penetration depth given by equation 2-12, which means that the shuttle heat effect is largest for high temperatures and decreases with the square root of the frequency.

In the PTR used in this work, the pulse tubes are made of stainless steel. The dimensions and typical cold-end temperatures are given in Table 5. Using equation 3-28 the heat flow through the wall can easily be calculated. It can be shown that the temperature gradient (0.8 K/mm), the tube diameter and wall thickness are smallest for the third stage. Therefore, the heat load due to thermal conduction is smallest in the third stage. Unfortunately, no data on enthalpy flow due to the shuttle heat effect and a DC flow are available for comparison. However, in all cases the radius of the pulse tubes is at least three times larger than the thermal penetration depth of helium at room temperature (shown in Figure 3-11).

Table 5. Properties of the pulse tubes.

Stage	1	2	3
Inner diameter (mm)	20	12.1	9
Wall thickness (mm)	0.5	0.3	0.25
Length (mm)	141	204	342
Volume (cm^3)	45.2	23.5	21.8
Typical cold end temperature (K)	90	30	3
Thermal conduction through wall (W)	0.53	0.15	0.06

3.3.3.2 Pressure oscillations

In §2.3 it was derived that the cooling power is proportional to the amplitude of the pressure oscillations in the pulse tube squared (equation 2-30). Therefore, it is interesting to establish a relation between frequency and the amplitude of the pressure oscillations in the first, the second, and the third stage of the PTR. A simple model similar to the one used in §3.2 is constructed. Again, the flow through the double-inlet valve and the minor orifice are neglected. Figure 3-17 shows the configuration of this three-stage model. The flow rate through a flow conductance is given by equation 2-17 and the effective pulse-tube volumes V_{te1}, V_{te2}, and V_{te3} for the three stages is given by equation 3-8. The buffer pressure p_b is assumed constant and equal to the time-averaged pressure p_0. Again, the compressor pressure p_c is given by

$$p_c = p_0 + p_{c1}\cos(\omega t). \tag{3-43}$$

The regenerator conductances should be regarded as effective conductances.

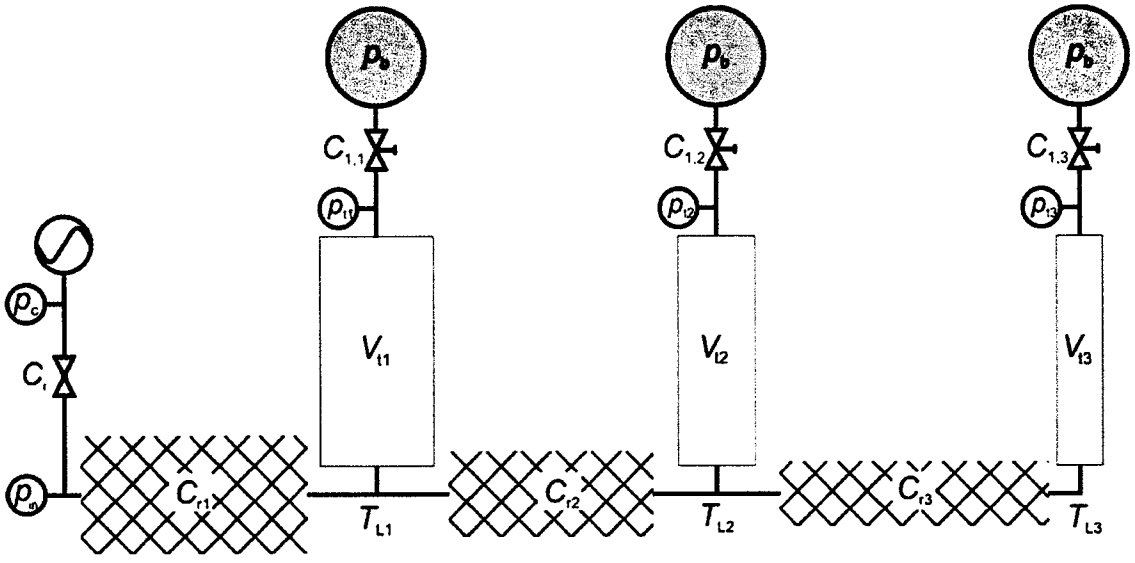

Figure 3-17. An ideal pressure oscillation generator (left) with flow conductance C_i, connected to a three-stage PTR with regenerator flow conductances C_{r1}, C_{r2}, and C_{r3}, and pulse-tube volumes V_{t1}, V_{t2}, and V_{t3}. The flow conductances of the first orifices are $C_{1,1}$, $C_{1,2}$, and $C_{1,3}$. Pressures are defined at the compressor (p_c), at the PTR inlet (p_{in}), in the pulse tubes (p_{t1}, p_{t2}, and p_{t3}), and in the buffers (p_b).

The velocity at the cold end of the first-stage pulse tube v_{L1} is given by

$$A_{t1}v_{L1} = C_{r1}(p_{in} - p_{t1}) - \frac{T_{L1}}{T_{L2}}C_{r2}(p_{t1} - p_{t2}), \tag{3-44}$$

where A_{t1} is the surface area of the first-stage pulse tube, and T_{L1} and T_{L2} are the temperatures at the cold end of the first- and the second-stage regenerator. Equation 3-5 can be used to calculate the inlet pressure p_{in}. It can be seen that the flow rate that is going to the second-stage regenerator is subtracted from the flow rate coming through the first-stage regenerator. Likewise, the velocity at the cold end of the second- (v_{L2}) and the third- stage (v_{L3}) are given by

$$A_{t2}v_{L2} = C_{r2}(p_{t1} - p_{t2}) - \frac{T_{L2}}{T_{L3}}C_{r3}(p_{t2} - p_{t3}), \tag{3-45}$$

and

$$A_{t3}v_{L3} = C_{r3}(p_{t2} - p_{t3}). \tag{3-46}$$

The velocity at the hot end of the pulse tube is given by

$$v_{H(i)} = \frac{C_{1,(i)}}{A_{t(i)}}(p_{t(i)} - p_0), \tag{3-47}$$

for all three stages, where (i) is the number of the corresponding stage.

Applying equation 2-16 for all stages gives

$$C_{r1}(p_{in}-p_{t1})-\frac{T_{L1}}{T_{L2}}C_{r2}(p_{t1}-p_{t2})=C_{1,1}(p_{t1}-p_0)+\frac{V_{te1}}{p_0}\frac{dp_{t1}}{dt}, \tag{3-48a}$$

$$C_{r2}(p_{t1}-p_{t2})-\frac{T_{L2}}{T_{L3}}C_{r3}(p_{t2}-p_{t3})=C_{1,2}(p_{t2}-p_0)+\frac{V_{te2}}{p_0}\frac{dp_{t2}}{dt}, \tag{3-48b}$$

and

$$C_{r3}(p_{t2}-p_{t3})=C_{1,3}(p_{t3}-p_0)+\frac{V_{te3}}{p_0}\frac{dp_{t3}}{dt}. \tag{3-48c}$$

Here, V_{te} is given by equation 3-8 for all three stages. It should be noted that these equations are based on the assumption of an ideal gas. This is a valid assumption for the first and the second stage, but is problematic for the third stage. However, only a small fraction of the helium in the third-stage pulse tube is too cold to be approximated by an ideal gas. A subsequent (small) deviation in the third stage dynamics, resulting from this model, can be expected.

Equation 3-1 is used for the compressor pressure p_c. The values used for the flow conductances of the regenerators and C_i are estimations based on measurements at 1.8 Hz. The optimal flow conductance given by equation 2-36 is taken as a measure for the flow conductances of the first orifices. In practice, the first-orifice conductance may deviate from the theoretical optimum because the theory is based on a *single*-stage PTR. The hot-end temperature T_H is 280 K. The mean pressure p_0 is 1.5 MPa. The compressor pressure amplitude p_1 is 0.5 MPa. For the volumes of the pulse tubes, the real values are used, given in Table 5. The flow conductance C_i is 20 (mm^3 s^{-1} Pa^{-1}). In the following table, the remaining parameters and their values are given for the three stages.

Table 6. Values used in the three-stage PTR model.

Variable	Stage 1	Stage 2	Stage 3
T_L (K)	80	30	2
C_r (mm^3 s^{-1} Pa^{-1})	25	25	15

In order to compare the result of this model, the normalized pressure amplitude at the inlet of the system is shown as a function of the frequency. This is done in Figure 3-18. In this context, the ^ indicates that the amplitude of a parameter is used. The result is similar to the result that has been obtained in §3.2.

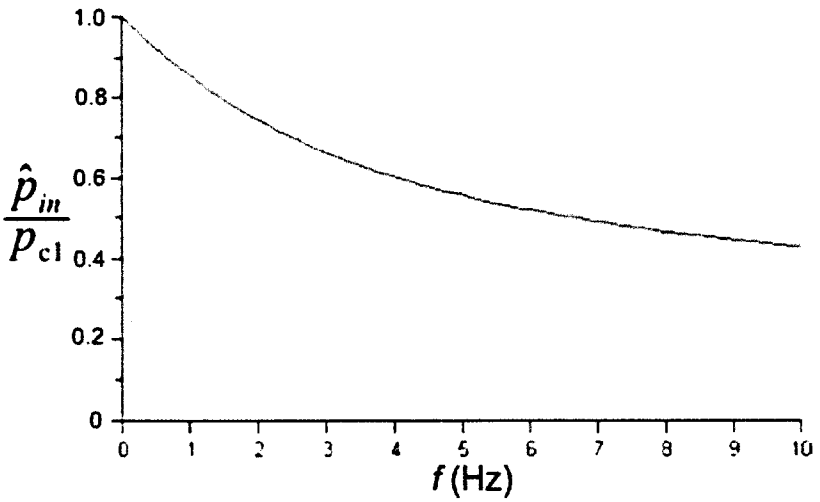

Figure 3-18. The pressure amplitude at the inlet of the system, divided by the compressor pressure amplitude, shown as a function of the frequency.

It can be seen that for high frequencies, a large fraction (~50 %) of the initial pressure amplitude is already lost when the flow reaches the inlet. Even though C_i is an estimated value, it can be concluded that it is important to minimize not only the pressure drop in the pulse tubes, but also in the system generating the pressure oscillations.

The calculated amplitudes of the pressure oscillations in the three pulse tubes, divided by the *inlet* pressure amplitude, are shown in Figure 3-19. The inlet pressure amplitude is used because there is no experimental data on the compressor pressure amplitude available. By using the inlet pressure amplitude, the results of this model can be compared to the measurements.

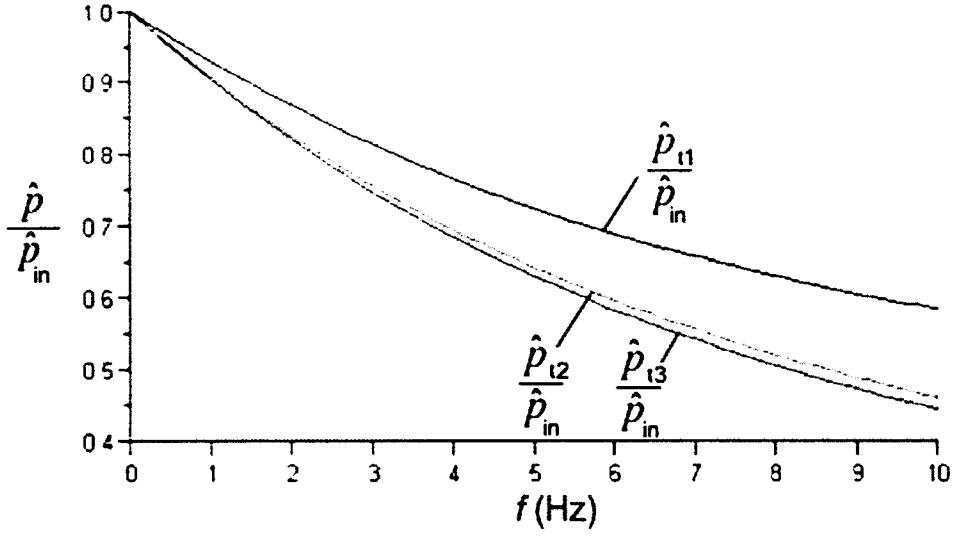

Figure 3-19. The frequency dependency of the dimensionless amplitude of the pulse-tube pressure amplitudes for a simplified model, represented by equation 3-48.

Again, a significant part of the initial pressure amplitude is lost if the frequency is increased. The largest decrease of the pressure amplitude takes place in the first-stage regenerator, where the flow rate and the viscosity are highest. Equation 2-30 (where p_1 is the pressure amplitude in the pulse tube) shows that the cooling power decreases significantly. If the flow conductances of the regenerators are kept constant, the pressure amplitudes in the pulse tubes decreases by a factor of approximately two, and the cooling power decreases by a factor of approximately four, when the frequency is increased from 1.8 to 9 Hz.

Using equation 3-10, the time-averaged molar flow rate through the compressor can be calculated and plotted as a function of the frequency. This is shown in Figure 3-20. Again, the same trend can be seen as was found in §3.2, Figure 3-7

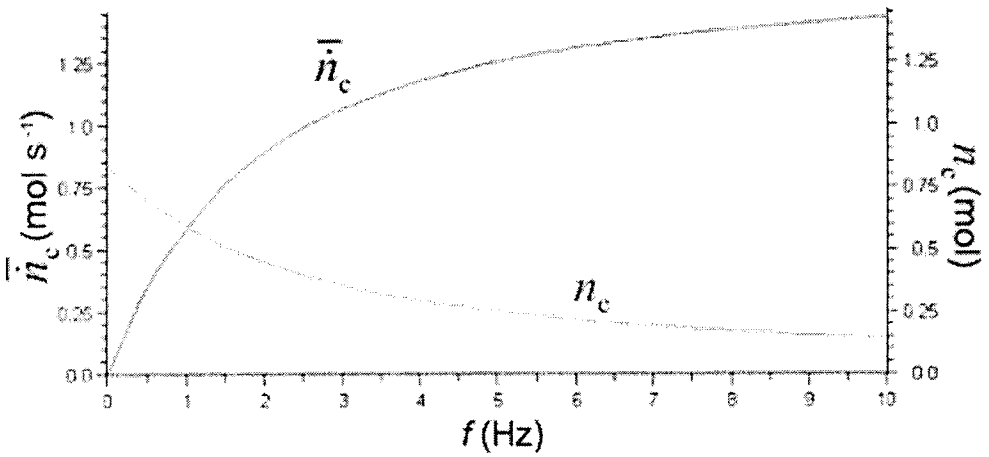

Figure 3-20. The frequency dependency of $\dot{\bar{n}}_c$ and n_c for the three-stage model described above.

In the next chapter, measurement results are shown and compared to the results of this model.

4 Results and discussion

In this chapter, the results of increasing the frequency of the PTR are given and discussed. The first part treats the optimization that was done using the needle valves only. In the second part the setup is modified in order to improve its high-frequency performance. The setup is optimized for a minimum no-load third-stage cold-end temperature.

4.1 Optimization using the orifices

In the first part of this work, the frequency was increased without modifying the setup physically. The system is optimized by fine-tuning the first orifices, then the double-inlet valves and finally the minor orifices. After changing a particular setting, the setup is left to stabilize for at least one hour. Full optimization may require two or more iterations of fine tuning all nine orifices.

4.1.1 Lowest cold-end temperature

In Figure 4-1 the lowest third-stage cold-end temperature (T_{L3}) is shown as a function of the frequency. It can be seen that below 5 Hz, the system is relatively insensitive to the frequency changes. Above 7 Hz, T_{L3} crosses the 4 K line and increases steeply to 8.5 K at 11 Hz. Here, and from now on, the lines connecting the actual data points are there to show the general trend of the data, and to help to distinguish between different data sets.

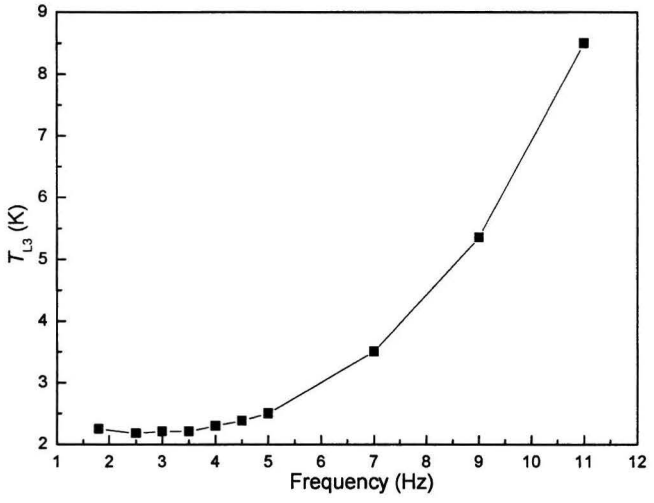

Figure 4-1. Lowest third-stage temperature as a function of the frequency.

It is remarkable that the PTR, originally designed and optimized for operation at ~1.8 Hz, can still perform so well at a frequency of ~5 Hz. Only at a frequency as high as five times the original operating frequency the performance of the system starts to decrease significantly. The minimum temperature is obtained at 1.8 – 2.5 Hz and has a value of 2.2 K. This temperature is close to the λ-point of helium at 15 bar, which is at 2.0 K. The λ-

line separates the normal fluid from the superfluid phase of helium. The phase diagram of ^{4}He is shown in Figure 4-2. The critical point of ^{4}He is at a temperature of 5.2 K and a pressure of 0.23 MPa. This means the helium is a fluid throughout the PTR. Near the λ-line, α_V becomes zero. At α_V=0 the adiabatic compression and expansion no longer has an effect on the temperature of the gas (equation 2-3) [25]. Therefore, it is impossible to reach temperatures below 2 K with ^{4}He. The lighter isotope of helium, ^{3}He, has its α_V=0 line near 1 K. Therefore, temperatures below 2 K can be obtained using ^{3}He instead of ^{4}He. In fact, this has been done in previous work on this PTR, and a minimum no-load temperature of 1.73 K was reached [26].

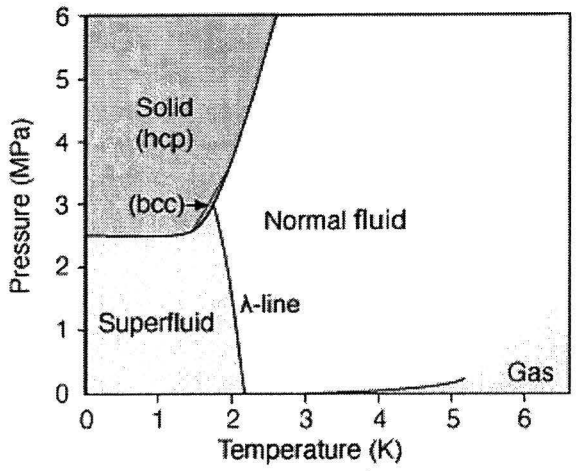

Figure 4-2. The phase diagram of ^{4}He.

4.1.2 Pressure amplitude and flow rate

Part of the explanation of the increasing cold-end temperature, discussed in the previous section, can be found in the pressure amplitude. As already mentioned, the system's cooling power (equation 2-30) is closely related to the pressure amplitudes in the pulse tubes. Based on the three-stage model, introduced in §3.3.3, it is expected that the pressure amplitudes at the inlet and in the pulse tubes decrease with the frequency as shown in Figure 3-18 and Figure 3-19, respectively. To give an idea of how the pressure oscillations at the inlet and in the pulse tubes change when the frequency is increased, Figure 4-3 shows the time-dependent pressures for 1.8 and 11 Hz.

At 1.8 Hz, the frequency is low enough to distinguish the different phases of a cycle. The arrows indicate the times when the system is neither connected to the high- nor to the low-pressure side of the compressor. After the first arrow at ~0.2 s, the system is at high pressure p_H and the rotary valve connects the system to the low-pressure side of the compressor (at p_L). This is the expansion step. Around 0.3 s the flow rate through the regenerators is highest because the difference between the inlet pressure and the first-stage pulse-tube pressure is largest. Around 0.45 s the pressure no longer decreases, which means that the pulse tubes have had time enough to reach p_L. From 0.46 – 0.52 s the rotary valve is closed. After that, the compression step takes place, and the cycle starts over again.

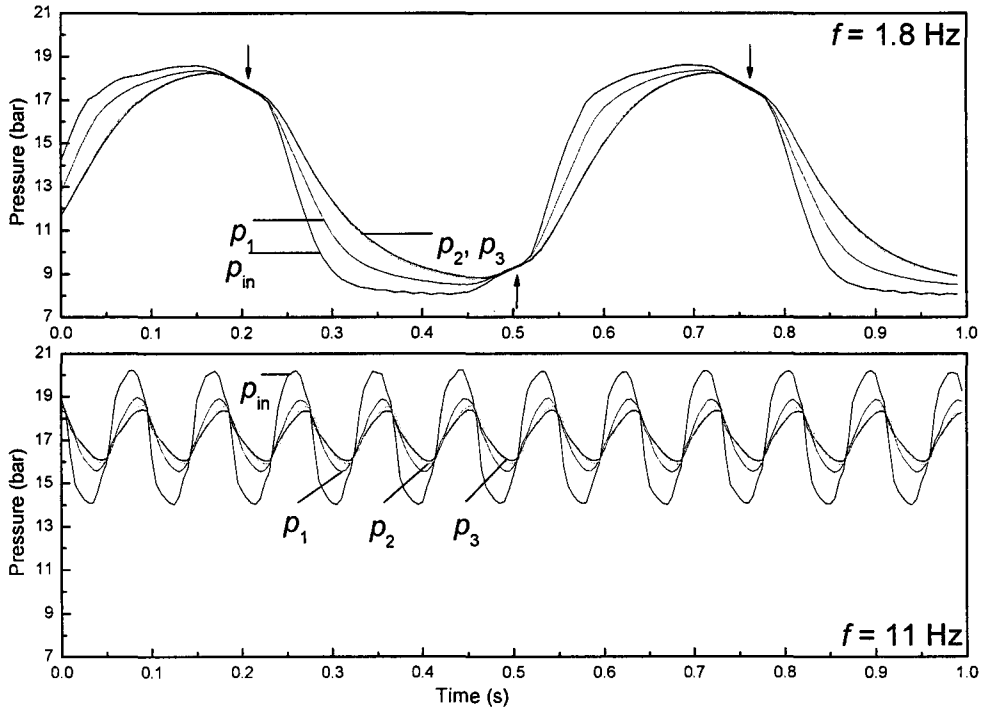

Figure 4-3. The pressures at the inlet and in the pulse tubes as functions of the time for 1.8 and 11 Hz. The arrows indicate the short intervals during which the rotary valve is closed. The scales of both graphs are equal to give a better impression of the changes.

As can be seen, the pressure amplitudes are much larger for 1.8 Hz than for 11 Hz. The inlet pressure amplitude as a function of the frequency is shown in Figure 4-4.

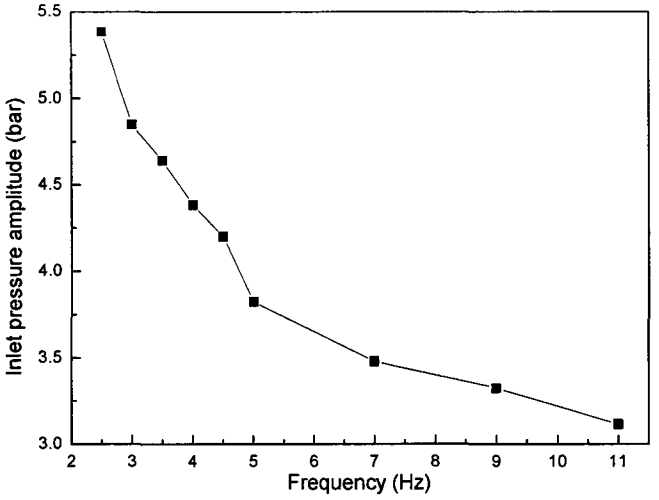

Figure 4-4. The inlet pressure amplitude as a function of the frequency.

Unfortunately, no data on the pressure amplitude of the compressor is available, so the measured inlet pressure amplitude cannot be normalized using the compressor pressure amplitude (as opposed to the modeled pressure amplitude shown in Figure 3-18). At low frequencies (~3 Hz), the inlet pressure amplitude decreases steeper than for higher frequencies. The pressure amplitude decreases from 5.4 to 3.1 bar when the frequency is increased from 2 to 11 Hz. This decrease of the pressure amplitude is approximately 40 % of the initial pressure amplitude. This is in agreement with the results of the model (Figure 3-18).

Figure 4-5 shows the pressure amplitude in the pulse tubes divided by the inlet pressure amplitude. This results in the normalized pressure amplitude, and corresponds to the results from the model, shown in Figure 3-19. Based on the model, it was expected that the largest pressure drop occurs in the first stage regenerator, where the viscous losses are highest. This can also be seen in the measurements. If the frequency is increased from 2 to 11 Hz, the pressure amplitude in the first stage regenerator decreases from 93 to 56 % of the initial (inlet) pressure amplitude. In the second stage, another 5 – 10 % is lost. The pressure drop in the third stage is smallest: 6 % of the inlet pressure amplitude at a frequency of 11 Hz. The effect of the regenerator and the pulse tube can be compared to a 'low-pass filter'.

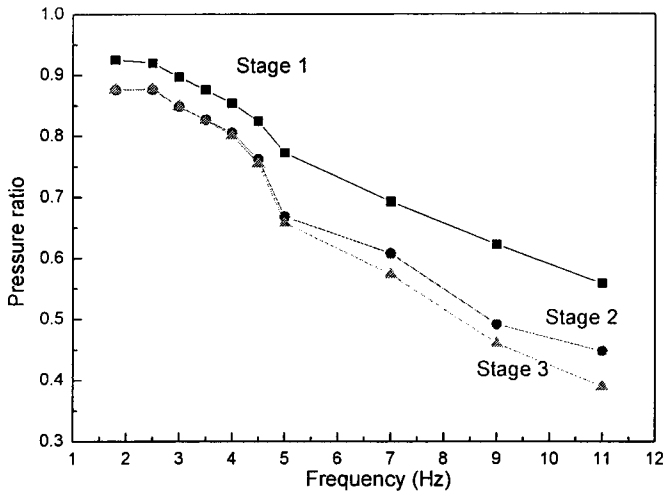

Figure 4-5. The pressure amplitudes in the pulse tubes divided by the inlet pressure amplitude, as functions of the frequency. The difference between a pressure ratio of one and the first-stage pressure ratio corresponds to the pressure drop in the first stage. The difference between the first- and the second-stage pressure ratios corresponds to the decrease of the pressure amplitude in the second stage. The decrease of the pressure amplitude in the third-stage is represented by the difference between the second- and the third stage pressure ratio.

The flow rate through the compressor ($\dot{\bar{n}}_c$ or n_c/t_c) has been measured using a flow meter at the low-pressure side of the compressor (see Figure 3-1). The time-averaged molar flow rate as a function of the frequency is shown in Figure 4-6. Also, the molar flow per cycle n_c (which is the flow rate divided by the frequency) is shown.

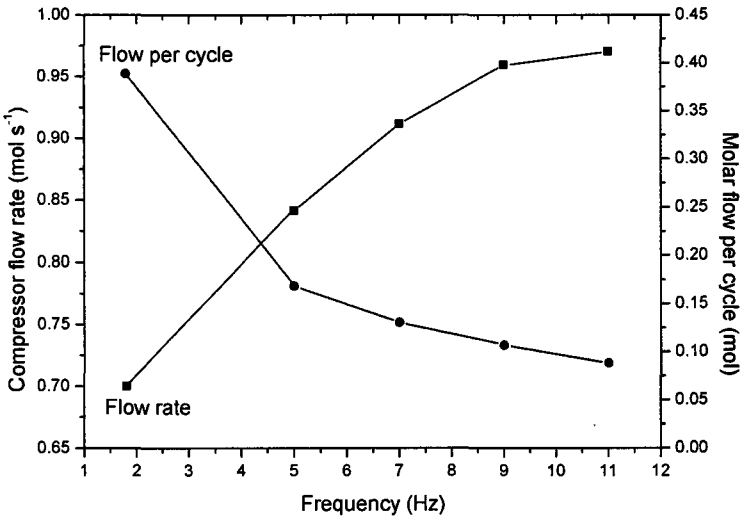

Figure 4-6. Molar flow rate through the compressor (see Figure 3-6), and the molar flow per cycle, as functions of the frequency.

The flow rate can be compared to the results that were obtained with the three-stage model (Figure 3-20). The modeled values are approximately 30 % higher than the measured flow rates, which can be addressed to the fact that the first-orifice flow conductances were based on the optimal single-stage theoretical values that were too high (see §4.1.4). Regardless of this difference, the overall shape is similar. The flow rate increases steeply at low frequencies, and flattens out at higher frequencies (~9 Hz). As has been mentioned earlier, the effective resistance of the combination 'flow conductance of the regenerator' and the 'volume of the pulse tube' decreases with increasing frequencies, which explains the increasing flow rate. In short: the volumes of the PTR can be filled (and emptied) more often in a second if the frequency increases.

In §2.3 it was derived that the cooling power is dependent on the pressure amplitude and the flow rate through the regenerator[8]. At 11 Hz, the pressure amplitude in the third stage is only 1.2 bar, while at ~2 Hz the pressure amplitude was nearly 5 bar. This decrease in the pressure amplitude, taking place in all three stages, can explain the increasing cold-end temperature. However, not only the pressure amplitude should be taken into consideration. As said, the time-averaged molar flow rate increases steeply between 1.8 and 7 Hz, and flattens out for higher frequencies. Figure 4-3 shows that the time-averaged pressure was increased from 13 bar to 17 bar, while the frequency was increased from 1.8 to 11 Hz. In fact, already at 4.5 Hz the time-averaged pressure was nearly 17 bar. Equation 3-41 shows that the viscous losses increase with the square of the time-averaged flow rate, but can be decreased by increasing the time-averaged pressure. Unfortunately, increasing the time-averaged pressure any further would exceed the compressor's maximum pressure. It is likely that the increasing molar flow rate and the reduction of the

[8] In this section it was also assumed that the flow rate through the regenerator is proportional to the pressure amplitude. As a consequence, the cooling power is dependent on the pressure amplitude squared. However, in this argumentation the flow rate and the pressure amplitude are kept separate.

viscous losses (due to the increased time-averaged pressure) compensate for the decreasing pressure amplitude in the 1.8 to 5 Hz frequency range. Therefore, the cold-end temperature remained approximately constant. For frequencies above 7 Hz, the molar flow rate did not increase much and the viscous losses could no longer be reduced by increasing the average pressure. However, the pressure amplitudes continued to decrease. This led to a significant increase of the cold-end temperature, as can be seen in Figure 4-1. In §4.2 the modifications of the PTR components in order to increase the pressure amplitudes are discussed.

4.1.3 Stirling compressor

Figure 4-6 shows that the amount of gas being displaced every cycle decreases from 0.39 to 0.09 mol. At room temperature and a time-averaged pressure of 15 bar, this means that the volume that is displaced per cycle at the inlet of the PTR decreases from 0.60 to 0.14 liters. For a piston compressor, i.e. a Stirling-type compressor, this is an important design parameter. A reliable and efficient Stirling-type compressor with a displaced volume of 0.60 liters operating at 1.8 Hz is practically not feasible. However, given the trend of the flow per cycle shown in Figure 4-6, it is likely that the flow per cycle is approximately 70 cm^3 at a frequency of 15 – 20 Hz. At this frequency and displaced volume, a Stirling compressor is suitable for generating the pressure oscillations, as shown below. The properties of a Stirling-type compressor suitable for this PTR can be estimated. The following assumptions are made:

1. The PTR can be operated successfully at f_{PTR} = 20 Hz.
2. The time-averaged pressure p_0 is 17 bar.
3. The pressure amplitude at the inlet of the PTR p_{c1} is 4 bar.
4. The gas flow in one cycle is 70 cm^3 at 280 K and p_0 (n = 0.05 mol).
5. The compression-space volume V_{c0} is 150 cm^3.
6. For stability reasons the Stirling compressor has two pistons.
7. The piston stroke amplitude Δx is 1.5 cm.

Assumptions 2 – 4 are estimated using actual measurements of the PTR. Assumptions 5 – 7 are based on the properties of actual Stirling-type compressors [27]. Using equation 2-9, the amount of helium required to generate a pressure amplitude of 4 bar (adiabatically) in the compression space is approximately 22 cm^3. The volume flow *amplitude* required for the PTR, attached to the compression space, is 35 cm^3. The phase-shift between the pressure in the compression space and the flow rate to the PTR is neglected for this estimation. The displaced volume of the two pistons is ~57 cm^3 going from their equilibrium positions x_0 to $x_0 + \Delta x$, or $2\pi r_p^2 \Delta x$ = 57 cm^3. Consequently, the piston radius r_p is 2.5 cm. The pressure in the compression space is equal to the pressure at the inlet of the PTR:

$$p_c = p_0 + p_{c1}\cos(\omega t). \tag{4-1}$$

With this compression space pressure, the equation for the resonance frequency is

$$f_r \approx \frac{1}{2\pi}\sqrt{\frac{k_s}{m_p}+\left(\frac{p_{c1}}{\Delta x}+\frac{\gamma p_0 \pi r_p^2}{V_{b0}}\right)\frac{\pi r_p^2}{m_p}}. \qquad (4\text{-}2)$$

A buffer volume V_{b0} of 2 liters is used. The mechanical spring k_s is taken very small because this spring only increases the resonance frequency. It turns out that a piston mass of approximately 3.5 kg results in a resonance frequency of ~20 Hz. A summary of all parameters is given in Table 7.

Table 7. Estimation of the design parameters of a 20 Hz Stirling-type compressor suitable for the three-stage PTR.

PTR parameters		**Stirling-compressor parameters**	
p_0 (bar)	17	V_{c0} (cm^3)	150
p_{c1} (bar)	4	Pistons	2
n (mol)	0.05	Δx (cm)	1.5
f_{PTR}	20	r_p (cm)	2.5
		V_{b0} (cm^3)	2000
		k_s (N/cm)	0
		m_p (kg)	3.5

4.1.4 Orifice settings

The measured optimal flow conductances of the three stages are shown as functions of the frequency in Figure 4-7.

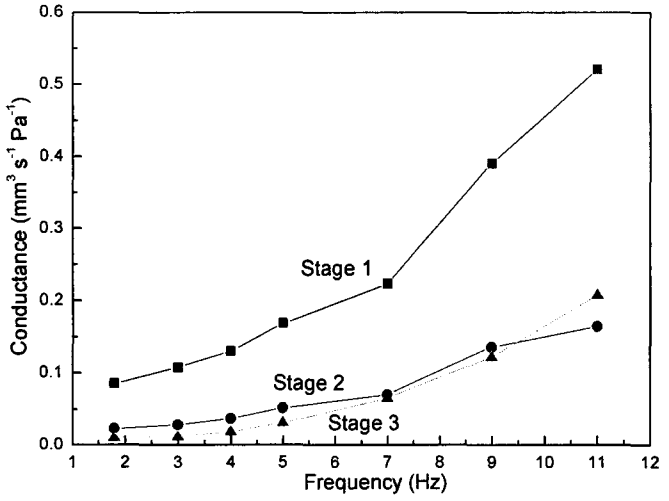

Figure 4-7. The flow conductances of the first-, the second-, and the third-stage first orifices. The error in the conductances is approximately 10 %.

The flow conductance is calculated using the manufacturer's data on the flow characteristics of the needle valves, and the pressure difference $p_t - p_b$, for all three stages. The flow conductance of the first stage is highest, and the flow conductances of the second and the third stage are comparable. This was expected because the volume of the first-stage pulse tube (45 cm^3) is much larger than the volume of the second- and the third stage. A larger pulse-tube volume requires a larger hot-end flow rate to optimize the out-of-phase term of the gas velocity at the hot end. The volume of the third stage (22 cm^3) is slightly lower than the volume of the second stage (24 cm^3). Moreover, the optimum phase-shift for each stage can be different. This can explain the small difference in the flow conductance of the second and the third stage. The flow conductances of the first- and the second stage are approximately linear. A linear increase of the optimal flow conductance was expected based on equation 2-36. The flow conductance of the third-stage first orifice increases steeper as the frequency increases. A possible explanation is that the compressibility of the (nonideal) gas in the third stage increases due to the increase of the cold-end temperature from 2.2 to 8.5 K. This means that at higher temperatures, larger hot-end volume flows are required in order to adjust the out-of-phase component of the gas flow at the cold end. A larger volume flow is obtained by opening the orifice, i.e. increasing its conductivity.

However, an important difference between the predicted optimal flow conductances (based on normal flow conditions) and the measured values can be found. Generally, the predicted values are approximately four times higher. The first orifice flow conductance C_1 calculated using the manufacturer's flow characteristics can be compared with the flow conductance calculated using the time derivative of the pressure in the buffer;

$$\frac{dp_b}{dt} = \frac{C_p}{C_v}\frac{p_0}{V_b}C_1(p_t - p_b) \tag{4-3}$$

where V_b is the buffer volume, p_t the pulse tube pressure, p_b the buffer pressure, and the pressure changes in the buffer are assumed small. Pressures p_b and p_t and the buffer volumes are known for all three stages, so C_1 can be calculated for all three stages. The manufacturer's flow characteristics turned out to be in agreement with the flow conductances calculated using equation 4-3.

The explanation for the difference with the theoretical values can be found in the derivation of the ideal first-orifice conductance. In equation 2-24 the velocity of the gas at the cold end is calculated for a single-stage PTR. For a three-stage PTR this equation should be

$$v_{L1} = \frac{C_{r1}}{A_{t1}}(p_c - p_{t1}) - \frac{\rho_{L2}}{\rho_{L1}}\frac{C_{r2}}{A_{t2}}(p_{t1} - p_{t2}), \tag{4-4}$$

with ρ_{L1} and ρ_{L2} the density of the gas at the cold end of the first- and the second stage. A similar equation is valid for the second-stage cold-end velocity. These equations show that in the three-stage case all pressures and cold-end velocities are related. Changing the

first-orifice conductance of one stage not only changes the out-of-phase component in that stage, but also in the two other stages. In fact, this mechanism has been observed during the optimization of the PTR. Moreover, the possibility of various DC-flow circuits through the minor orifices and double-inlet valves across multiple stages further complicates a quantitative explanation. A qualitative explanation for the difference is that the actual cold-end velocity is much lower than what would have been the case for a single-stage PTR. The reason for this is that the gas flow through the first-stage regenerator is divided over three stages. A lower cold-end velocity requires a smaller hot-end velocity to optimize the out-of-phase component; hence the first-orifice conductance should be smaller.

Figure 4-8 shows the double-inlet valve conductances for the three stages.

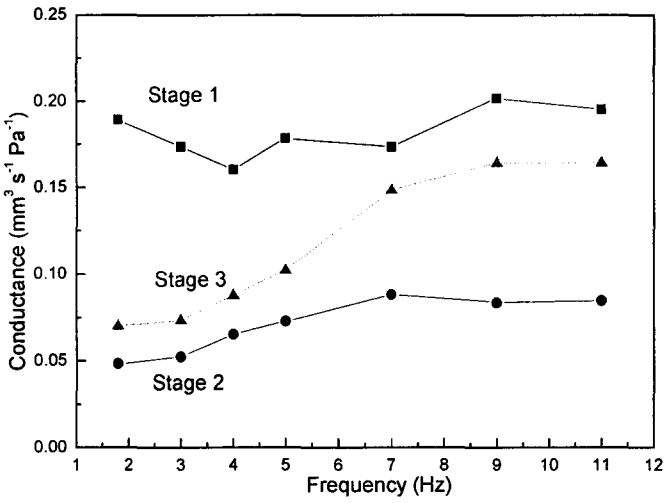

Figure 4-8. The flow conductances of the first-, the second-, and the third-stage double-inlet valves. The error in the conductances is approximately 10 %.

As was concluded in §3.3.2.3, the volumetric flow rate and, therefore, the viscous losses due to the regenerator flow resistance are highest in the first stage. The double-inlet valve by-passes the regenerator, and reduces the viscous losses in the regenerator. As a result, the optimal first stage double-inlet flow conductance is largest. In the second stage the flow rate and viscosity are smaller; hence the viscous losses are smaller. Therefore, the flow conductance of the second-stage double-inlet valve is smaller. In the third stage, the viscous losses are smallest. However, the flow conductance of the double-inlet valve is higher than it is for the second stage. It is possible that due to the high density of the gas flow at the cold end of the third-stage a large volumetric flow rate is required at the hot end. This would significantly increase the viscous losses in the first- and the second-stage regenerator. Therefore it is beneficial to have a relatively large double-inlet flow conductance in the third stage.

The benefits of the double-inlet valves can be demonstrated best by operating the PTR in the 'single-orifice mode'. In this mode, all double-inlet valves and minor orifices are closed. Figure 4-9 shows the pressures in the PTR as functions of the time during normal operation (top) and single-orifice mode operation (bottom). It can be seen that by closing the double-inlet valves, the pressure amplitudes in all stages, and the third stage in particular, decrease significantly. Table 8 shows the pressure amplitudes in the first-, the second-, and the third-stage pulse tubes divided by the pressure amplitude at the inlet of the PTR, for the single-orifice mode and 'normal' mode. While the pressure amplitudes in the first- and the second stage decreased by 12 and 16 %, respectively, the third-stage pressure amplitude decreased by 56 %. What's more, the cold-end temperature of the third stage increased from 2.5 K during normal operation to 38 K in the single-orifice mode (at 5 Hz). Due to the absence of the double-inlet and the increased T_{L3}, the volumetric flow rate through the third-stage regenerator has increased significantly. This explains the large decrease of the pressure amplitude in the third-stage pulse tube.

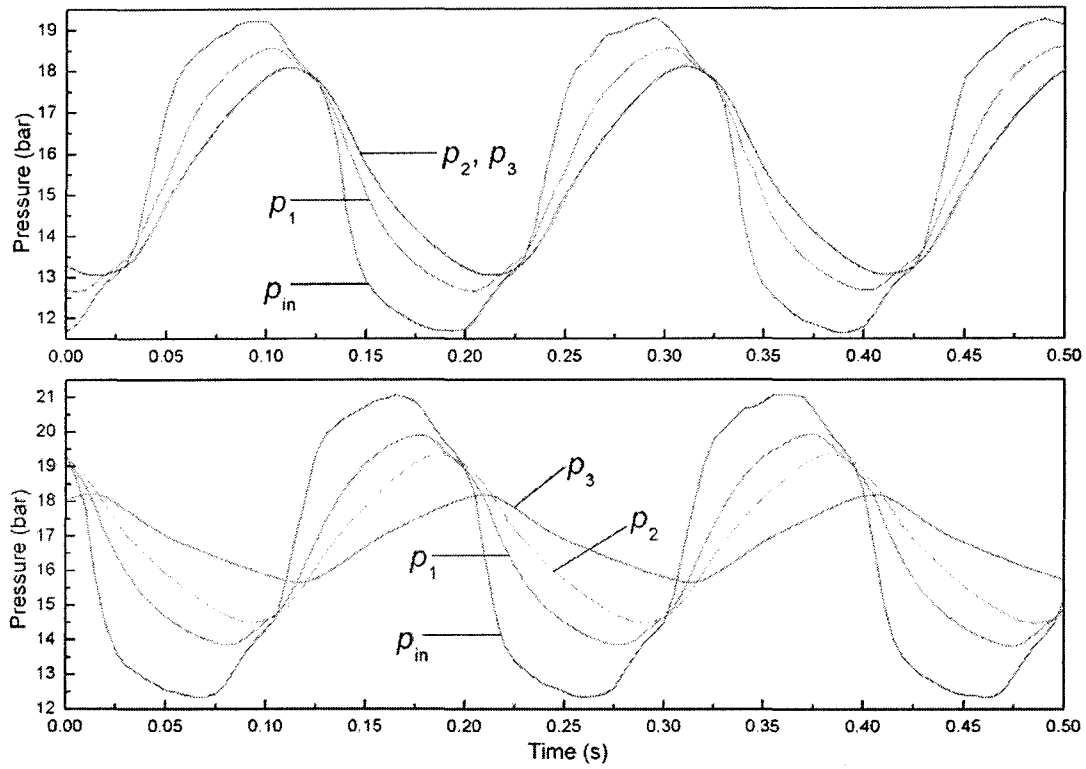

Figure 4-9. Pressures at the inlet of the PTR and in the pulse tubes as functions of the time, with the double-inlet valves open (top), and the double-inlet valves closed (bottom). The frequency is 5 Hz.

Table 8. Pressure amplitudes in the pulse tubes divided by the pressure amplitude at the inlet, for the single-orifice mode and double-inlet mode operating at 5 Hz.

	Double-inlet closed	**Double-inlet open**
Stage 1	0.69	0.78
Stage 2	0.56	0.67
Stage 3	0.29	0.66

By opening the double-inlet valve of the third stage, the phase shift between cold-end velocity v_{L3} and hot-end velocity v_{H3} can be optimized. This decreases T_{L3}. Moreover, less gas has to pass through the first- and the second-stage regenerator, which decreases the viscous losses and enhances the overall performance of the PTR even further.

The minor orifices are used for fine-tuning of the DC-flow. During the experiments conducted in this research, they were connected with the low-pressure side of the compressor. This means that a small DC-flow running from the pulse-tube hot end towards the cold end is counter-acted.

4.1.5 Temperature profile

Figure 4-10 shows the temperature distributions for various frequencies in the second- and the third-stage regenerator. While the temperature of the cold end of the first stage remained approximately constant, the temperature of the cold end of the second stage increased from 30 K to 41 K. The fact that the first-stage cold-end temperature has remained virtually constant means that the heat exchange and heat storage conditions are optimal even up to 11 Hz. At 11 Hz, the thermal penetration depth in the first stage regenerator material is still approximately 10 times higher than the diameter of the wires in the mesh 200 screens. Also the heat capacity of the first-stage regenerator material is much higher than the heat capacity of the helium flowing through the regenerator in one cycle. It may be possible that the pressure amplitudes in the pulse tubes, discussed in §4.1.2, can be increased by decreasing the resistance of the first-stage regenerator. This can be done by removing some of the first-stage regenerator material, or replacing it by a coarser material. This has been done, and the results are shown in §4.2.1.

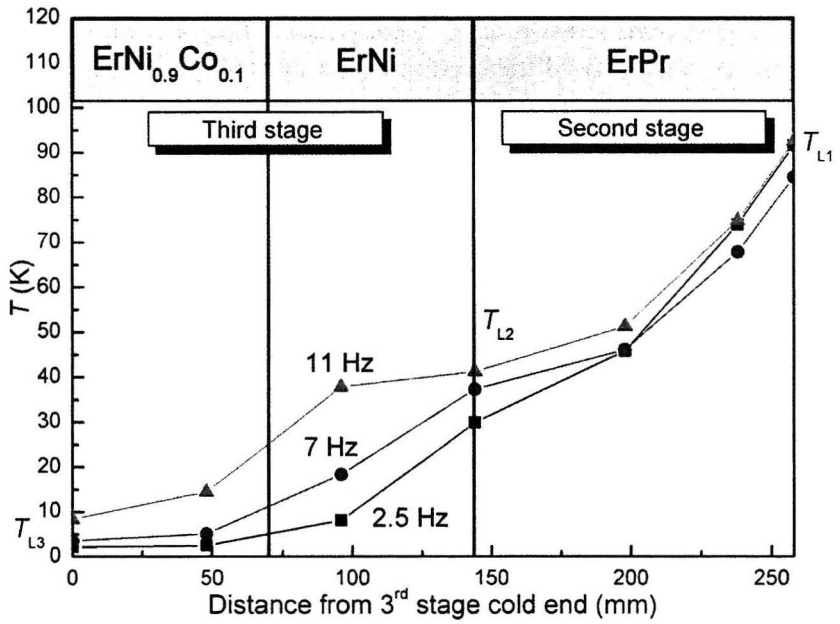

Figure 4-10. Temperature distributions for 2.5 Hz, 7 Hz, and 11 Hz, for the second- and the third-stage regenerator. The horizontal axis is the location in the regenerator, measured from the cold end (left).

If the temperature drop in each stage is a measure for the stage's performance, the performance of the second stage has deteriorated significantly. A possible explanation is that the thermal penetration depth in the second-stage regenerator has become smaller than the grain size due to the increased frequency. The grain size of the ErPr is 0.25 – 0.30 mm. The thermal penetration depth of ErPr at 10 Hz ranges from 0.6 mm at 40 K to 0.7 mm at 20 K. The thermal penetration depth is still at least twice as large as the grain size (while it was at least five times higher, at 1.8 Hz). It is also important that the thermal penetration depth in helium is large compared to the size of the holes between the regenerator grains. At 10 Hz, δ_T has decreased to 0.1 mm. The size of the holes is expected to be in the order. Therefore, the heat contact between the regenerator material and the helium may be insufficient, so it is likely that the thermal penetration depth of helium is limiting the performance of the second-stage regenerator. In this case it would be beneficial to decrease the grain size of ErPr particles in the second stage. In fact, this has been done and the results of this experiment are shown in §4.2.1.

The performance of the third stage has decreased also. It is difficult to say whether this is caused by the decreased performance of the second stage, and hence the higher hot-end temperature of the third-stage regenerator. At 1.8 Hz, the thermal penetration depth of helium (0.1 mm) was already in the same order of magnitude as the size of the holes between the grains. However, the third-stage regenerator is relatively long and thin. Therefore, the helium has to travel further into the regenerator, passing by many regenerator grains on its path. This may enhance the thermal contact between the regenerator grains and the helium. However, at 10 Hz, δ_T of helium has decreased to ~0.04, which is significantly smaller than the size of the holes. Especially the $ErNi_{0.9}Co_{0.1}$ in the cold part of the regenerator is relatively coarse (0.2 – 0.5 mm). Changing this material to a finer grain size significantly enhances the thermal contact. Decreasing the particle size will probably not increase the viscous losses much because of the low volumetric flow rate and the low viscosity of the helium in the third stage. In §4.2.1 the results of changing the third-stage regenerator material are discussed.

4.1.6 The α-parameter

In §2.3 the α-parameter was said to be an important characteristic parameter for the PTR. It cannot be measured directly, but it can be derived from other known parameters [9]. The formalism used in §2.2.4 and §2.3 is also used here. The molar flow rate through the first orifice is given by equation 2-27 ($p_1 << p_0$ and $p_b \approx p_0$). The adiabatic pressure change in the buffer due to a molar flow through the first orifice is

$$\frac{dp_b}{dt} = \frac{C_p}{C_v}\frac{RT_H}{V_b}\dot{n}_1. \tag{4-5}$$

The pressure in the buffer can now be written as

$$p_b = p_0 + p_{b1}\sin(\omega t), \tag{4-6}$$

where the buffer pressure-oscillation amplitude p_{b1} is given by

$$p_{b1} = p_0 \frac{C_p}{C_v} \frac{C_1 p_1}{\omega V_b}. \tag{4-7}$$

The α-parameter, given by equation 2-22, can now be written in measurable quantities:

$$\alpha = \frac{p_{t1} V_t}{p_{b1} V_b} \tag{4-8}$$

Figure 4-11 shows the values for α calculated using equation 4-8. As concluded earlier, the theoretical optimum is one. Considering that this optimum is derived for an ideal single-stage PTR without minor orifice, the measured values are not far off. Apparently, the ratios of the pressure amplitudes in the pulse tubes and the buffers decrease with increasing frequencies. A possible explanation is that the first orifice is being opened. This levels-out the pulse-tube and buffer pressure, effectively decreasing the α-parameter given by equation 4-8.

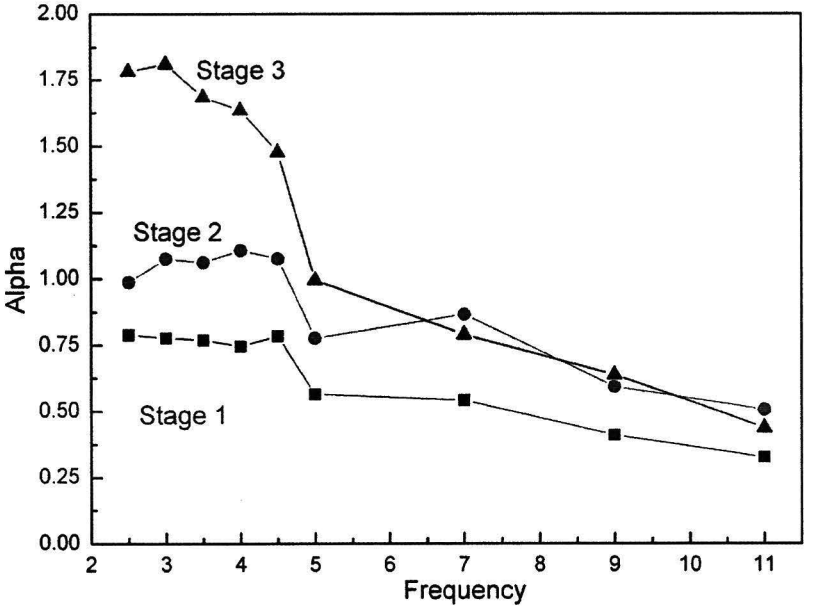

Figure 4-11. Values for α for all three stages as functions of the frequency.

4.2 Optimizing PTR components

In this section the modifications made to the PTR in order to improve its high-frequency performance are treated. First, the results of actual modifications to the regenerators are shown. Next, future optimization of the pulse tubes is discussed using the three-stage model for the pressure amplitudes in the pulse tubes. All modifications are tested at 9 Hz.

4.2.1 Regenerator optimization

4.2.1.1 First stage

In §3.3.2 it was concluded that both the heat capacity and the thermal contact (related to the thermal penetration depth) are good. Due to the decreased molar flow per cycle, the heat capacity ratio (equation 3-13) has improved even further. Therefore, some of the first-stage regenerator material was removed in an attempt to increase the pressure amplitudes in the pulse tubes. The two sintered steel blocks (see Table 3 and Appendix A) are replaced by one solid stainless steel plug of the same size with a central flow channel of 6 mm diameter, which is the same diameter as is used for tubes connecting the regenerator. In this way, approximately one third of the regenerator material is removed, and the regenerator now consists of 957 stacked mesh 200 screens. Using a plug is more convenient than resizing the regenerator itself. The placement of the plug is schematically shown in Figure 4-12 (case 2). The changes of the pressure amplitudes in the pulse tubes resulting from the changes made to the regenerators, described in this section, are summarized in Figure 4-13.

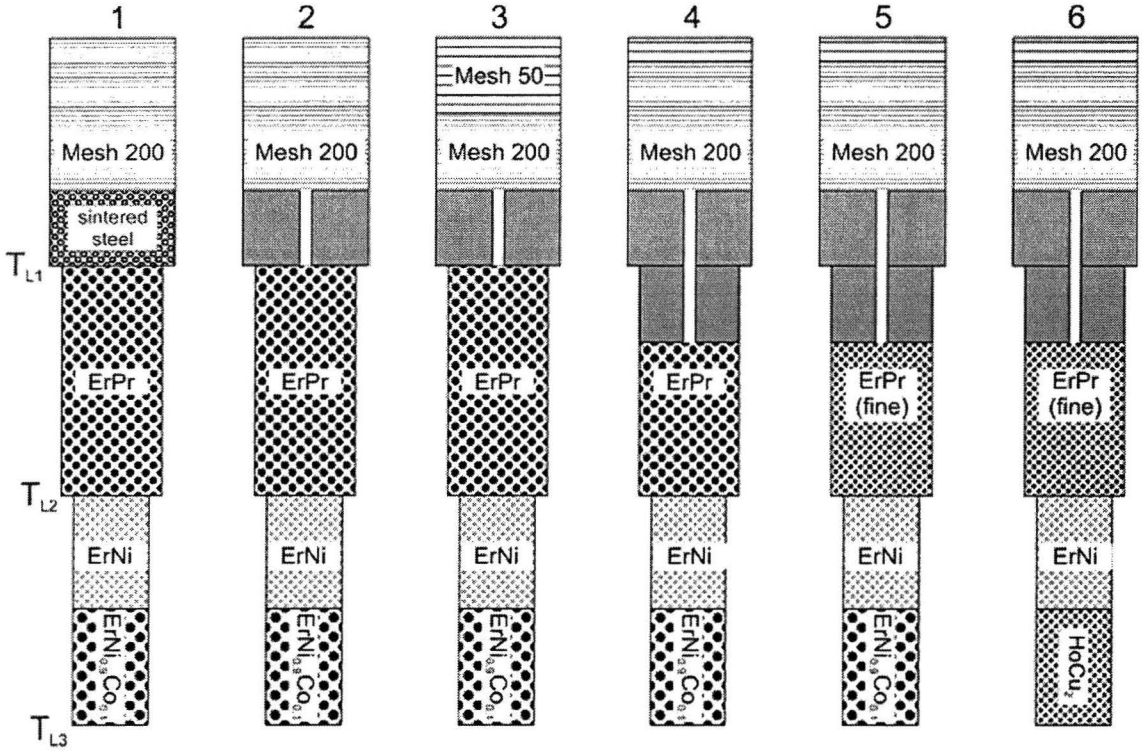

Figure 4-12. Subsequent regenerator layouts after the modifications.

The new first-stage regenerator configuration did not change the first-stage temperature at all. Apparently, the heat capacity of the first-stage regenerator material is still high enough. Also, the viscous losses may have decreased, which could have made up for the decreased heat capacity. However, this should have lead to an increase of the pressure amplitudes in the pulse tubes. Unfortunately, the pressure amplitudes remained approximately constant. An increase of only 3 – 6 % was observed in the pressure amplitudes in the pulse tubes. Later on, this result was supported by the three-stage model for the pressure amplitudes. It was checked whether a possible decrease of the flow resistance could have been undone by the sudden change in cross-sectional surface area of the flow channel, going from the mesh 200 screens to the plug, without distributing the flow. Therefore, a plug has been replaced with a plug with more holes, aligned with the holes at the bottom of the regenerator housing. However, this did not change the pressure amplitudes.

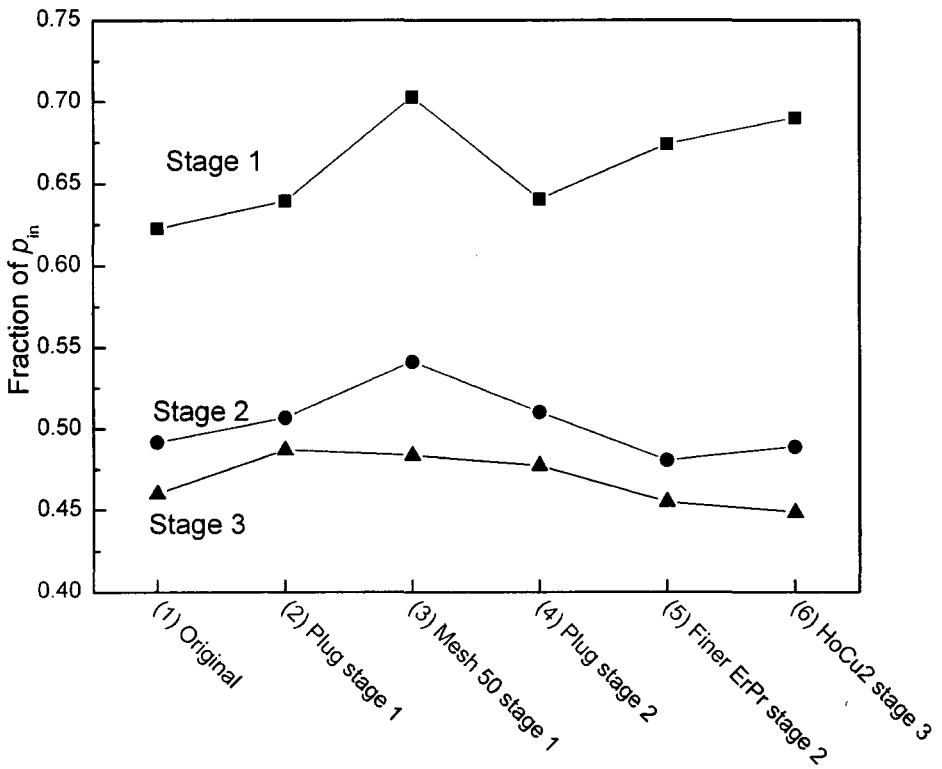

Figure 4-13. Summary of the changes made to the regenerators, and the effect on the pressure amplitudes in the pulse tubes at 9 Hz.

It may be possible that the flow resistance was taken out at the wrong end of the regenerator. The sintered steel blocks have a high flow resistance, but they are placed at the cold end, where the volumetric flow rate and the viscosity are low, so the effect of the flow resistance is relatively small. The regenerator has to be assembled starting at the cold-end. It turned out to be practically not possible to stack the mesh 200 screens, then the alternating mesh 50 screens / wires for flow distribution, and the plug on top of that, without deranging the underlying screens. Therefore, in addition to the plug at the cold end, 350 mesh 200 screens at the hot end of the regenerator have been replaced by 94 mesh 50 screens (case 3). The mesh 50 screens are much coarser and have a smaller flow

resistance, while they have the same filling factor as the mesh 200 screens. This time, the increase of the pressure amplitude in the first-stage pulse tube was larger: 10 %, which confirms that the largest pressure drop takes place at the high-temperature range. The pressure amplitudes in the second and the third stage increased with 3 and 2 %, respectively. The overall performance of the PTR decreased significantly due to this modification. The cause of this is the increase of T_{L1} from 83 to 98 K. Apparently, the heat storage conditions in the first stage have deteriorated too much by replacing the screens. The δ_T of stainless steel at 10 Hz (0.4 mm) is still relatively large compared to the diameter of the wires of the mesh 50 screens (0.2 mm). However, the size of the holes in the mesh 50 screens is 0.5 mm, while δ_T of helium at 10 Hz is approximately 0.4 mm. This is a possible explanation for the decrease of the first-stage performance. From the 94 mesh 50 screens, 30 were left at the hot end of the regenerator, and 64 were replaced by 264 mesh 200 screens.

It can be concluded that the amount of material in the first-stage regenerator has been decreased successfully by 30 %. This did not increase the pressure amplitudes in the pulse tubes significantly. Due to the decreased δ_T, it was not possible to use a coarser material in order to decrease the flow resistance at the hot end of the regenerator.

4.2.1.2 Second stage

The amount of material in the second stage was also reduced using a similar plug as was used in the first stage (case 4). This time, the plug was placed at the hot end of the regenerator, where the viscosity and volumetric flow rate are highest. Unfortunately, no significant increase in the pressure amplitudes of the second and the third stage was observed, as can be seen in Figure 4-13. Also, the first-stage pressure amplitude did not decrease, which signifies that no additional amount of gas is redistributed from the first-stage pulse tube to the second and the third stage due to a decreased flow resistance of the second stage. Later on, the three-stage pressure-amplitude model confirmed that the increase of the pressure amplitudes in the second- and the third-stage pulse tubes is small.

Surprisingly, the cold-end temperature of the second stage increased only by 2.3 K; from 38.3 to 40.6 K. In §4.1.5 it was concluded that the heat-storage conditions in the second-stage regenerator are not optimal. However, the heat-storage conditions are most likely limited by the thermal contact between the gas and the regenerator material, and not by the heat capacity of the regenerator material. This can explain why the reduction of the amount of regenerator material did not significantly decrease the performance of the second stage. Therefore, it was decided that the plug can stay in the regenerator, but the material should be changed.

The ErPr with a grain size of 250 – 300 μm has been replaced by ErPr with a grain size of 125 – 300 μm (case 5). Assuming a homogeneous distribution of the grain sizes, this is a reduction of the average grain size of nearly 25 %. In total, 118 g of the coarse ErPr has been replaced by 124 g of fine ErPr. Therefore, the filling factor increased from 0.61 to 0.64. The thermal penetration depth of helium is now at least two times larger than the holes between the grains, which means that the thermal contact between the helium and the regenerator material has improved significantly. Consequently, the performance of

the second-stage regenerator improved. Experiments confirmed this; T_{L2} decreased from 40.6 to 34.0 K. As a result, also the performance of the third-stage regenerator improved. The ErNi temperature (see Figure 4-10 at 96 mm from T_{L3}) dropped from 34.5 to 18.9 K, and the cold-end temperature of the third stage T_{L3} decreased from 5.4 to 4.3 K. The performance of the PTR operating at 11 Hz (instead of 9 Hz) has also been measured. Temperature T_{L3} decreased from 8.5 K for the unmodified PTR to 6.7 K for the PTR with the modified regenerators. The reduced grain size resulted also in an increase of the viscous losses, as can be expected based on the expression for the viscous losses (equation 3-40). The flow resistance of the second stage increased, changing the pressure amplitudes in the first-, the second-, and the third-stage pulse tubes. The pressure amplitudes in the second- and the third stage decreased approximately 5 %. On the other hand, more helium was redistributed to the first-stage pulse tube, and the pressure amplitude increased by 5 %. Apparently, the decrease of the cooling power, resulting from the reduction of the pressure amplitude, is small compared to the increased regenerator performance.

In conclusion, the heat capacity of the second-stage regenerator does not limit its performance, hence approximately 30 % of the material could be removed without any significant deterioration of the second-stage performance. However, the thermal contact did limit the performance. By decreasing the grain size, and particularly the size of the holes between the grains, the cold-end temperature of the second- and the third stage were decreased by 6.6 (16 %) and 1.1 K (20 %), respectively. It is likely that the performance of the regenerator can be further enhanced by decreasing the grain size. Increasing the frequency from 1.8 to 9 Hz, the thermal penetration depth decreased with 55 % while size of the grains was decreased by only 25 %. However, decreasing the grain size also decreases the pressure amplitude of the second- and the third stage, which eventually can reduce the overall performance of the PTR.

4.2.1.3 Third stage

In §4.1.5 it was concluded that the third-stage regenerator performance can be improved by decreasing the size of the $ErNi_{0.9}Co_{0.1}$ grains due to the limited thermal contact between the regenerator material and the helium. Furthermore, previous research [9] using the same material has raised doubts about the quality of the material. Therefore, also the type of material is changed (case 6). The alternative material that was chosen is $HoCu_2$. This is also a high heat capacity material in the 2 – 20 K temperature range, and was used successfully in previous research. The grain size of the new $HoCu_2$ material is 180 – 250 μm, instead of 200 – 500 μm diameter grains of $ErNi_{0.9}Co_{0.1}$. In total, 56 g of $ErNi_{0.9}Co_{0.1}$ was replaced by 60 g of $HoCu_2$. The densities of $ErNi_{0.9}Co_{0.1}$ and $HoCu_2$ are $9.5 \cdot 10^3$ kg m^{-3} and $9.0 \cdot 10^3$ kg m^{-3}, which means that the filling factor did not change.

Due to the increased thermal contact, the cold-end temperature decreased from 4.33 to 3.95 K. This is mostly caused by the increased performance of the hot-end third-stage regenerator material. It should be noted that 3.95 K was obtained without fully optimizing the setup. Half way the optimization the cold-end temperature started to increase gradually over time. Most likely the third-stage regenerator grains have been re-ordered into a denser structure during a week of nonstop operation, which allowed the

grains to start moving, generating additional losses. Tightening the third-stage regenerator material should solve this problem, which can be done in future work. Most likely, the third-stage performance is still limited by its hot-end temperature, which is still 36 K. This temperature was 25 – 30 K at lower frequencies. If a temperature this low cannot be reached, it may be beneficial to replace the third-stage hot-end regenerator material by ErPr, which performs better at higher temperatures. Whether the improved performance is caused by the change of the material, the change of the particle size, or both, can be determined by sieving out the $ErNi_{0.9}Co_{0.1}$ grains larger than 250 μm and using this as the regenerator material. The pressure amplitudes in the pulse tubes remained virtually constant, as can be seen in Figure 4-13. Apparently, the viscous losses in the third stage are small indeed, as opposed to the viscous losses in the second stage where a decrease in the pressure amplitude was observed after decreasing the grain size.

4.2.2 Pulse tube optimization

In §4.1.2 it has been concluded that the decreasing performance of the PTR when the frequency is increased, is most likely caused by the decreasing pressure amplitude in the pulse tubes. In §4.2.1 modifications which have increased the pressure amplitudes in the pulse tubes have been discussed. During this research the pulse tubes have been left unchanged, while the high-frequency optimization of the setup is most likely highly dependent on the pulse-tube volume. The three-stage model discussed in §3.3.3.2 will be used to explore the consequences of changing the flow conductances of the regenerators and the volumes of the pulse tubes.

In many cases, increasing the operating frequency of a PTR is accompanied by the down-scaling of its size [28]. The amount of gas participating in one cycle decreases (Figure 4-6) and the regenerator material can be reduced without loss of performance. Consider the down-scaling of the PTR at a certain frequency, with a certain scaling factor. This would decrease the amount of gas participating in one cycle, say also with the same scaling factor. Using equation 2-30, it can be shown that if the amount of gas participating in a cooling cycle is decreased by a certain factor and the pressure amplitudes in the pulse tubes are kept constant, the cooling power decreases proportionally. The losses due to irreversible heat exchange in the regenerator decrease proportionally (equation 3-38). In order to estimate the change of the other losses regenerator, it is important to know *how* the sizes of the components are decreased:

1) The lengths of the regenerators and pulse tubes are kept constant and the volume is scaled down by scaling down the surface area (decreasing the aspect ratio A_r/L_r). It can be shown that the losses due to axial conduction decrease proportionally (equation 3-30), and the viscous losses decrease proportionally (equation 3-41). In §3.3.3.1 it was discussed that the radius of the pulse tube r_t should be large compared to the thermal penetration depth of helium in order to minimize the shuttle-heat losses. The r_t/δ_T ratio can be kept constant if the volume of the pulse tube is scaled down proportionally to the frequency. The resistances of the regenerators increase proportionally, which makes it difficult to keep the pressure amplitude in the pulse tubes constant (even though the volumetric flow rate decreases proportionally).

2) The volume of the regenerators and the pulse tubes is scaled down while the aspect ratio is kept constant. In this case, the axial conduction losses remain constant, and the viscous losses decrease with the square of the scaling factor. The ratio r_t/δ_T increases if V_t is scaled down proportionally to the frequency, which enhances the adiabatic environment of the helium in the pulse tube. The resistances of the regenerators remain constant while the volumetric flow rate decreases. This makes it easier to maintain high pressure amplitudes in the pulse tubes. In principle, the regenerators can be decreased with a constant aspect ratio, while the pulse tubes maintain their length and are made thinner. The shuttle-heat losses are small as long as $r_t >> \delta_T$. This option would minimize the axial conduction losses in the pulse tubes.
3) The surface area of the regenerators and pulse tubes are kept constant and the volume is scaled down by scaling down the length (increasing the aspect ratio A_r/L_r). The losses due to axial conduction increase proportionally, and the viscous losses decrease with the third power. The flow resistance of the regenerators decreases so it will be easier to maintain high pressure amplitudes in the pulse tubes.

Most likely, the third option is the worst. The axial conduction losses increase, while the cooling power decreases, which will significantly decrease the performance of the PTR. Furthermore, there is no need to decrease the viscous losses more than proportionally since there is no indication the viscous losses are limiting the PTR performance. E.g. the performance of the PTR increased when the grain sizes of the second- and the third-stage regenerator material were decreased.

Given the relatively large decrease of the pressure amplitude in the pulse tubes (Figure 4-5) it is most likely the best choice to keep the aspect ratio constant, and put up with the relative increase of the conduction losses. The significant decrease of the viscous losses and the possibility of higher pressure amplitude in the pulse tubes are likely to compensate for this increase.

A scaling factor of two is chosen as an example. In Table 9 the modeled pressure amplitudes in the pulse tubes and at the inlet are shown if there is no scaling, the first case (decreasing the aspect ratio), and the second case (aspect ratio constant).

Table 9. Results of the three-stage pressure-amplitude model. Pressure amplitudes at the inlet and in the pulse tubes divided by the compressor pressure amplitude, at a frequency of 10 Hz. The 'column' normal shows the unchanged situation (no scaling). Case 1 corresponds to decreasing the volume by decreasing the surface area, and case 2 corresponds to maintaining a constant aspect ratio.

Location	Normal	Case 1 (A/L = 0.5)	Case 2 (A/L = 1)
Inlet	0.36	0.53	0.45
Pulse tube 1	0.21	0.31	0.33
Pulse tube 2	0.17	0.25	0.29
Pulse tube 3	0.16	0.24	0.29

It can be seen that decreasing the volume of the pulse tubes by a factor two significantly increases the pressure amplitudes. In the third stage the pressure-amplitude increase is highest. As expected, by maintaining a constant aspect ratio the highest pressure amplitudes can be obtained. However, the difference with case one is not large. Furthermore, by decreasing the size of the regenerators, the void volume in the regenerators is decreased. This increases the pressure amplitudes in the pulse tubes because no additional gas flow is required to compress the helium in the void volume of the regenerators.

It must be noted that the flow conductances of the first orifices are still based on the single-stage optimal value. If the first-orifice flow conductances in the model are decreased in order to obtain a better agreement with the experimental results, the pressure amplitudes change. However, a similar trend can be found and, therefore, the principle explained above is still valid.

4.2.3 Heat shields

Depending on the orifice that is being changed, the temperatures of the PTR can take from a half hour to up to several hours to stabilize. Therefore, the heat capacities of the copper thermal radiation shields attached to the first- and the second-stage cold ends (2.6 and 1.7 kg) were reduced by replacing them by thinner versions of 1.1 and 0.7 kg, respectively. In this way, the mass has been reduced to 43 % of the original mass. Figure 4-14 shows the cool-down curves of the PTR with the old (top) and the new heat shields (bottom). The cool-down time has reduced from approximately 400 to 250 minutes; a reduction of 37 %. No changes in the steady-stage cold-end temperatures have been observed after installing the new heat shields. During experiments, the system's time of response to changes has significantly decreased.

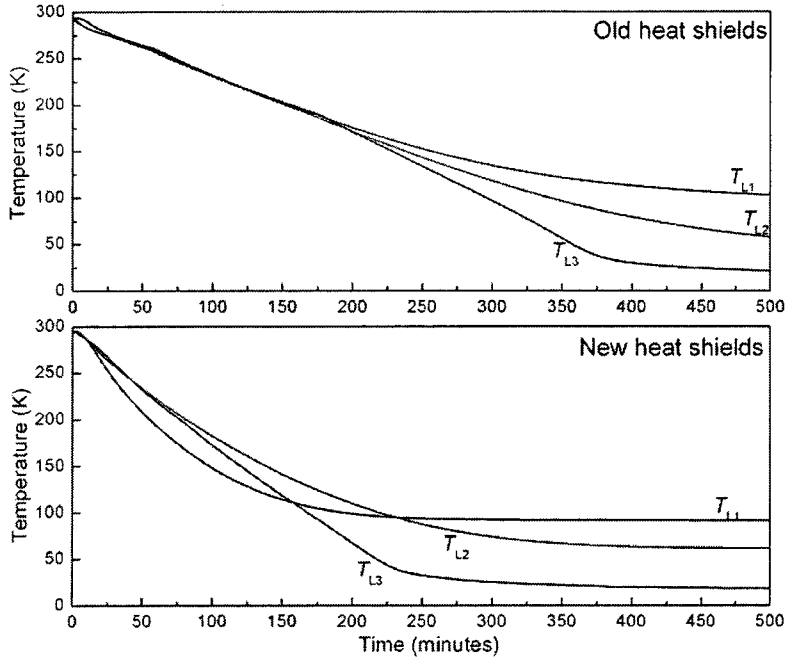

Figure 4-14. Cool-down curves for the PTR with the old (top) and the new heat shields (bottom).

5 Conclusions and recommendations

In this work the operating frequency of the three-stage GM-type PTR was increased from 1.8 to 11 Hz. Up to a frequency of 5 Hz the overall performance of the PTR, measured by its cold-end temperature, could be kept below a temperature of 2.5 K. This was accomplished by optimizing the first orifices, double-inlet valves, and the minor orifices. It is remarkable that the PTR performs so well even up to three times the frequency it was originally designed for. Above 5 Hz the cold-end temperature started to increase rapidly, to 8.5 K at 11 Hz. It was shown that the pressure amplitude at the inlet of the PTR decreased from 5.4 to 3.1 bar when the frequency was increased from 1.8 to 11 Hz. Also, the pressure amplitude in the first-stage pulse tube decreased from 93 to 56 % of the inlet pressure amplitude. The pressure-amplitude decreases in the second- and the third stage were smaller. The decreasing pressure amplitudes in the pulse-tubes were confirmed using a model for the pressure amplitudes in the three-stage PTR. The time-averaged flow rate increased from 0.70 to 0.97 mol s^{-1}, while the amount of gas participating in one cooling cycle decreased from 0.4 to 0.1 mol. The increase of the cold-end temperature can be explained by the interplay of the decreasing pressure amplitudes in the pulse tubes, the increasing time-averaged flow rate, and the increased viscous- and heat-exchange losses.

The temperature profile was compared for different frequencies. They were analyzed using the heat capacities of the regenerator material and helium, and the thermal penetration depths. This way, various modifications to the first-, the second-, and the third-stage regenerators were proposed. Different regenerator geometries and material sizes were tested at a frequency of 9 Hz.

At high frequencies, the amount of gas participating in a cycle decreases. Hence, less heat capacity in the regenerator is required to store/release heat. In the first stage, 30 % the cold-end material was replaced by a plug with a flow channel. This did not decrease the performance of the first stage, nor did it increase the pressure amplitudes in the subsequent stages. Replacing another 30 % of the regenerator's hot-end material by courser material resulted in increased pressure amplitudes in the pulse tubes due to the decreased flow resistance. However, also the heat exchange between the regenerator material and the helium decreased significantly. The net effect was an increase of the first-stage cold-end temperature from 83 to 98 K.

Replacing some of the material at the hot end of the second-stage regenerator by a plug led to similar results as were observed in the first stage. The performance did not decrease significantly, and the pressure amplitudes remained virtually constant. The thermal contact was enhanced by decreasing the particle size of the regenerator material. This decreased the second-stage cold-end temperature from 40.6 to 34.0 K. As a result, the performance of the third-stage improved also; T_{L3} decreased from 5.4 to 4.3 K. The flow resistance of the regenerator increased slightly. As a result, also the pressure amplitudes in the pulse tubes decreased. It is expected that further decreasing the particle size of the second-stage material by approximately 25 % can further decrease T_{L2}.

In the third stage the $ErNi_{0.9}Co_{0.1}$ was replaced by $HoCu_2$ with a smaller grain size. This improved the heat exchange between the helium and the regenerator material. As a result, the cold-end temperature T_{L3} decreased from 4.33 to 3.95 K. In order to decrease T_{L3} significantly, the second-stage cold-end temperature should be decreased.

Generally speaking, increasing the frequency leads to decreasing the size of the PTR. The cooling power decreases with the pressure amplitudes and the flow rate at the cold end of the pulse tubes. It was observed that it is difficult to maintain high pressure amplitudes in the pulse tubes at high frequencies. This can decrease the performance of the PTR. Using a three-stage model for the pressure amplitudes it was shown that the pulse-tube pressure amplitudes can be increased by decreasing the volumes of the pulse tubes. Decreasing the volume of the pulse tubes can be done by decreasing its radius as long as it is much larger than the thermal penetration depth. The regenerators should be made smaller by maintaining the same aspect ratio or by decreasing the radius only (hence, decreasing the aspect ratio). The pressure amplitudes can be maximized by maintaining the same aspect ratio. The axial thermal conduction losses can be minimized by decreasing the aspect ratio.

Estimated design parameters for a Stirling-type compressor were derived from the expected flow rate and pressure amplitudes at 20 Hz. Typical Stirling-type compressor values were used, and resulted in a two-piston compressor operating at a resonance frequency of approximately 20 Hz.

In future work the high-frequency performance of the second-stage should be improved further. The ErPr can be sieved to obtain a grain size of 125 – 200 μm. In preparation of the scaling-down of the PTR, a plug similar to the ones inserted in the first- and the second-stage regenerator can be used to replace some of the third-stage material. Eventually it is necessary to decrease the sizes of the pulse tubes and regenerators, and to switch to a Stirling-type compressor. In this work, guidelines for scaling-down of the PTR and for the requirements of a Stirling-type compressor were given. The requirements of a Stirling-type compressor can be determined more precisely. The extensive experience with modeling and designing Stirling-type compressors present in Stirling Cryogenics & Refrigeration B.V. can prove to be of great value for the project. In this context it is also interesting to optimize the PTR for operation without minor orifices since they are not present in a Stirling-type PTR. Therefore, the possibilities of the active buffer PTR should be explored.

The theoretical work can focus on the modeling and simulation of the high-frequency dynamics of the three-stage PTR, and the connection between the Stirling-type compressor and the three-stage PTR. This information is of great importance in the process of designing, optimizing, and fine-tuning of the cryocooler and its components.

6 Literature

[1] J.G. Weisend II, "Handbook of cryogenic engineering", Taylor & Francis, 1998.

[2] R. Radebaugh, "Pulse tube cryocoolers for cooling infrared sensors", Proceedings of SPIE, The International Society for Optical Engineering, Infrared Technology and Applications XXVI, Vol. 4130, 2000, pp. 363-379.

[3] E.I. Mikulin, A.A. Tarasov, and M.P. Shkrebyonock, "Low-temperature expansion tubes", Adv. In Cryogenic Eng. **29**, 1984, pp. 629-637.

[4] R. Radebaugh, J. Zimmerman, D.R. Smith, and B. Louie, "Comparison of three types of pulse tube refrigerators: New methods for reaching 60 K", Adv. In Cryogenic Eng. **31**, 1986, pp. 779-789.

[5] M.Y. Xu, A.T.A.M. de Waele, and Y.L. Ju, "A pulse tube refrigerator below 2 K", Cryogenics **39**, 1999, pp. 865-869.

[6] N. Jiang, U. Lindemann, F. Giebeler, and G. Thummes, "A ^{3}He pulse tube cooler operating down to 1.27 K", Cryogenics **44**, 2004, pp. 809-816.

[7] R. Radebaugh, "Recent developments in cryocoolers", Proc. 19th Int. Congress of Refrigeration, Vol. IIIb, The Hague, 1995, pp. 973-989.

[8] J. Olson, M. Moore, P. Champagne, E. Roth, B. Evtimov, J. Jensen, A. Collaço, and T. Nast, "Development of a space-type 4-stage pulse tube cryocooler for very low temperature", Lockheed Martin Advanced Techonology Center, CEC-ICMC 2005, paper C1-R-03.

[9] I. Tanaeva, "Low-temperature cryocooling", dissertation thesis, University Press TUE, Eindhoven, 2004.

[10] Deuk-Yong Koh, Yong-Ju Hong, Seong-Je Park, Hyo-Bong Kim, and Kwan-Soo Lee, "A study on the linear compressor characteristics of the Stirling cryocooler", Cryogenics **42**, 2001, pp. 427-432.

[11] A.T.A.M. de Waele, "Cryogenic technology", lecture notes of cryogenic technology courses, Eindhoven University of Technology, Physics department, LTE, 2004.

[12] A.T.A.M. de Waele, M.Y. Xu, and Y.L. Ju, "Nonideal-gas effect in regenerators", Cryogenics **39**, 1999, pp. 847-851.

[13] A.T.A.M. de Waele, P.P. Steijaert, and J. Gijzen, "Thermodynamical aspects of pulse tubes", Cryogenics **37**, 1997, pp. 313-324.

[14] A.T.A.M. de Waele, P.P. Steijaert, and J.J. Koning, "Thermodynamical aspects of pulse tubes II", Cryogenics **38**, 1998, pp. 329-335.

[15] M.A. Lewis, and R. Radebaugh, "Measurement of heat conduction through metal spheres", Cryocooloers **11**, 2001, pp. 419-425.

[16] R.A. Ackermann, "Cryogenic regenerative heat exchangers", Plenum Press, New York, 1997.

[17] F. Pobell, "Matter and methods at low temperatures", Springer-Verlag, Berlin Heidelberg, 1992.

[18] M.E. Will, I.A. Tanaeva, R. Li, and A.T.A.M. de Waele, "New rotary valves for pulse-tube refrigerators", Cryogenics **44**, 2004, pp. 793-800.

[19] Z. Shaowei, W. Peiyi, and C. Zhongqi, "Double inlet pulse tube refrigerators: an important improvement", Cryogenics **30**, 1990, pp. 514.

[20] K.A. Gschneidner Jr., A.O. Pecharsky, and V.K. Pecharsky, "Ductile, high heat

capacity, magnetic regenerator alloys for the 10 to 80 K temperature range", Cryocoolers **11**, 2001, pp. 433.
[21] T.W. Wysokinski, J.A. Barclay, K.A. Gschneidner, V.K. Pecharsky, and A.O. Pecharsky, "Comparative evaluation of erbium and lead regenerator materials for low temperature cryocoolers", Cryogenics **42**, 2002, pp. 463.
[22] R.A. Adams, "Calculus", fourth edition, Addison-Wesley, 1999.
[23] J.H. Baik, "Design methods in active valve pulse tube refrigerator", dissertation thesis, University of Wisconsin – Madison, 2003.
[24] M.E. Will, "Counterflow pulse-tube refrigerators", University Press TUE, Eindhoven, 2005.
[25] A.T.A.M. de Waele, M.Y. Xu, and Y.L. Ju, "Pulse-tube performance at very low temperatures", Physica B 284-288, 2000, pp. 218-2019.
[26] I.A. Tanaeva, A.T.A.M. de Waele, "A small helium-3 pulse-tube refrigerator", Cryogenics **45**, 2005, pp. 578-584.
[27] Stirling Cryogenics & Refrigeration B.V., internal report DW-20050154, 2005.
[28] R. Radebaugh, "Microscale heat transfer at low temperatures", S. Kakaç *et al.* (eds.), 2005.

7 Summary

The four-kelvin temperature range is of great importance for medical, military, environmental, and scientific purposes. The ideal cryocooler is highly reliable and maintenance free, efficient, free from interference with the cooling object, and low cost. None of the cryocoolers, currently available, meet all requirements. The pulse-tube refrigerator (PTR) is capable of reaching temperatures below four kelvin. It can be highly reliable with virtually no interference with the cooling object. However, the pressure oscillations are currently generated by a Gifford-McMahon (GM) compressor and a rotary valve combination. This decreases the efficiency and reliability significantly. The goal of this project is to substitute the GM-type compressor and the rotary valve by a Stirling compressor. The Stirling linear compressor generates the pressure oscillations using a resonating piston. Its reliability and efficiency are considerably higher than the GM-type compressor and rotary valve. However, the Stirling type compressor works at frequencies generally an order of magnitude higher than the PTRs driven by a GM-type compressor. In this work, an existing three-stage 2.2 K GM-type PTR, originally operating at 1.8 Hz, is optimized for high-frequency operation.

At 1.8 Hz, the minimum no-load temperature was 2.2 K using ^{4}He. This is close to λ-line; the theoretical minimum. For frequencies below 5 Hz this temperature could be kept below 2.5 K by optimizing the orifices. At higher frequencies the cold-end temperature started rising rapidly, up to 8.5 K at 11 Hz. The frequency increase led to a significant decrease of the pressure amplitudes in the pulse tubes. However, the time-averaged flow rate in the compressor increased. The increase of the cold-end temperature can be explained by the interplay of the decreasing pressure amplitudes in the pulse tubes, the increasing time-averaged flow rate, and the increased viscous- and heat-exchange losses. Based on the characteristics of the three-stage PTR, the properties of a Stirling-type compressor suitable to drive the PTR at 20 Hz were estimated.

By removing 30 % of the first- and the second-stage regenerator material it was shown that the heat capacity of the regenerator material is high compared to the heat capacity of the amount of helium involved in one cooling cycle. However, due to the decreasing thermal penetration depth, particularly in the helium, it was necessary to decrease the grain size in the second- and the third-stage regenerators. It was concluded that the PTR should be scaled down in order to improve its high-frequency performance. This was based on the positive results after removing part of the regenerator material, and a model predicting a significant increase of the pressure amplitudes in the pulse tubes. Guidelines regarding the scaling-down of the PTR were given.

At the moment the PTR is capable of reaching 4 K at a frequency of 9 Hz. Reducing the size of the PTR and using fine-grained materials for the regenerators should enable the PTR to reach 4 K operating at 20 Hz. At this frequency the PTR is suitable to be driven by a Stirling-type compressor.

Appendix A

Table 10. The first-stage regenerator configuration in detail

Material	Function
5x mesh 50 screens / 5x 0.4 mm wire	Divide flow to decrease flow resistance
6x mesh 50 screens	
957x mesh 200 screens	Heat storage
3x mesh 50 screens	Divide flow to decrease flow resistance
2 sintered stainless steel blocks (19.7 mm each) f_f of 0.5	Heat storage
7x mesh 50 screens / 5x 0.4 mm wire	Divide flow to decrease flow resistance
felt	Block particles coming going to the 2nd stage

The mesh 200 screens consist of 50 μm thick wires. The mesh 50 screens consist of 200 μm thick wires. The mesh number is the amount of holes per inch (2.54 cm). One mesh 50 screen weighs 0.82 g and one mesh 200 screen weighs 0.21 g.

The combination mesh 50 screens / 0.4 mm wires are stacked layers of screen – wire – screen. The wire is bent to separate the screens, creating space for an even flow distribution over the whole surface, as can be seen below.

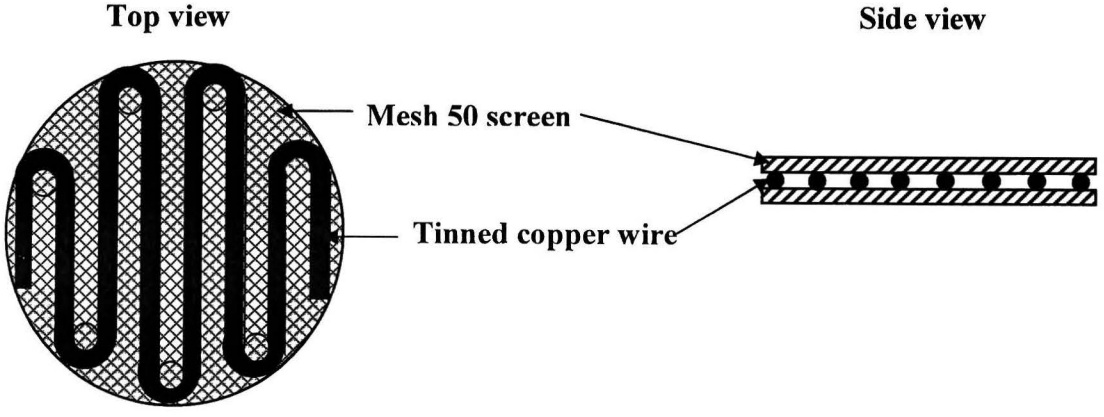

Later, the 2 sintered steel blocks were replaced by a plug. This was done in order to reduce the pressure drop.

8 Acknowledgements

Now, upon completion of this Master's thesis, it is good to take a moment to realize how many people contributed to it. While this year passed-by like it was a second, I have had the chance to work with the most skilled, friendliest, enthusiastic, and motivating people throughout my academic studies. Hereby, I would like to thank all of them for their help, enthusiasm, the nice working environment, and the countless pies we shared. However, some people deserve my special gratitude.

My supervisor Irina Tanaeva has shown me the best experimental mentorship I could have whished for. Her understanding of the PTR has enabled me to learn a lot in such a short period. From stacking a thousand regenerator screens manually, wallpapering, or soldering invisible thermometer wires, time flew thanks to the nice working atmosphere she created. For all this, and much more, I owe you my gratitude, Irina.
Special thanks also go to Fons de Waele, who has been a most motivating professor. Fons, you challenged me in many ways to exceed myself. I have learned a lot from you, from cryogenics in general, to writing a report, and the many places on earth I want to visit after seeing your pictures.
Furthermore, I would like to thank Manon Will for her down-to-earth advice and many lunch break discussions. Her personal interest made me feel welcome from the first day on.
I would also like to thank Marcel ter Brake and Jos Zeegers for their advices and fruitful discussions.
The technical skills of the technicians of the group and the faculty workshop also need special mentioning. In particular Leo van Hout, Loek Penders, and Jos van Amelsvoort contributed to the research by their outstanding technical support.
I thank Stirling Cryogenics & Refrigeration B.V. and Daniel Willems in particular, for allowing me to experience a small part of the process of creating a linear compressor.
To Isabelle I would need a lifetime to express my gratitude. Fortunately she allowed me to do that by giving the right answer to my proposal. I thank her for the many times I could find rest, understanding and support at her side.
Finally, I want to thank my friends, parents, and brothers for supporting me throughout my academic studies, making me feel at home here in Eindhoven, in Amstelveen, and in Lijnden.